Stratigraphy and Sedimentary Petrology of the Hillbank and Yalbac Formations, Corozal Basin, Belize

by

Karena K. Gill

A thesis submitted to the Graduate Faculty of
Auburn University
in partial fulfillment of the
requirements for the Degree of
Master of Science

Auburn, Alabama
May 7, 2017

Belize, Central America, Hillbank, stratigraphy, Yalbac

Approved by

David T. King Jr., Chair, Professor of Geology
Ronald Lewis, Professor of Geology
Ashraf Uddin, Professor of Geology

Abstract

The informal Hillbank and Yalbac formations are predominantly carbonate units that are found only in the subsurface of the Corozal basin in northern Belize. The 75 to 700 m-thick Hillbank and the 200 to 3000 m-thick Yalbac are economically important stratigraphic units. The Hillbank consists of two alternating sequences of genetically related facies: a carbonate sequence dominantly consisting of dolostone and a fluvial sequence dominantly consisting of coarse, clean sandstone. In stratigraphic order, there are a lower dolomitic facies package (Lower Hillbank Dolostone or LHBD), a lower clastic facies package (Lower Hillbank Sandstone or LHBS), a middle dolomitic facies package (Middle Hillbank Dolostone or MHBD), and an upper clastic facies package (Upper Hillbank Sandstone or UHBS). These packages are interpreted as shallow marine facies (LHBD), fluvial and alluvial plain facies (LHBS), sabkha and shallow marine facies (MHBD), and fluvial and alluvial plain facies (UHBS).

The Yalbac formation was deposited conformably above the Hillbank in a continuation of marine sedimentation. The Yalbac consists of three packages of genetically related facies, members Y1-Y3. The lower genetic package (Y3) consists of a basal transitional mixed siliclastic and dolomitic facies that grades into a dolomitic facies, which is interpreted as representing shallow marine, sabkha, and hypersaline environments. The middle genetic package (Y2) consists of thick-bedded dolomitic facies with rare anhydrite-rich layers that are interpreted as being shallow restricted lagoon and tidal flat environments transitioning to evaporites on sabkhas. The upper

genetic package (Y1) was not studied petrographically in the present research due to a lack of available samples, but historic accounts report a dolomitic and anhydritic facies, consistent with Y2, which is interpreted as shallow subtidal and sabkha environments.

Sr-isotope stratigraphy reveals an interpreted set of age dates for selected intervals within the Hillbank and Yalbac. Sr-values from these Corozal basin units indicate Upper Triassic to Lower Jurassic for the Hillbank and the lower beds of the Y3. There is a significant break in the Sr values between the lower beds and upper part of the Y3 member, specifically spanning 133-190 m.y. This indicates a substantial and previously unknown stratigraphic break within this member. The span from the base of the Barton Creek formation to the upper part of the Y3 member of the Yalbac displays sequential Sr-ages determinations suggesting that this rock section spans Lower to Upper Cretaceous. Comparison with the global sea-level cycle chart indicates that some Mesozoic sea-level drops may be related to this substantial unconformity and other breaks in the Hillbank-Yalbac section.

Acknowledgments

To the Almighty God, your love and grace abounds.

To my academic advisor, Dr. David King and his lovely wife, Lucille. Your gentle and kind demeanor has left a lasting impact on my scholastic and personal aspirations. My sincerest gratitude is extended for your guidance, constant support and unyielding supply of delicious meals that not only made me feel at home, but also fueled countless late nights in the office. Correspondingly, I would like to thank my committee members, Dr. Ronald Lewis and Dr. Ashraf Uddin who provided valuable input, acumen and prompt responses. To Dr. Haibo Zou, your passion and zest for geochemistry is unambiguous; thanks for allowing us to utilize your lab and for all the direction along the research. To my DAEE Apprentice, Sarah Asher, you have been a valuable asset and I look forward to seeing where research takes you.

This project is funded and supported by Belize Natural Energy Ltd. (BNE). I would like to extend my sincerest gratitude for the monetary support, access to data and supplies, and for the valued input from the staff. To the Geology team, Fay Smith, Eugene Ariola, and Gisele Nabet, I owe an insurmountable amount of gratitude for your patience, knowledge and unwavering willingness to help; I could not have completed this project without your vital input and making the resources available when needed.

Special thanks to the following organizations who secondarily funded this research and supported presentation at conferences: American Association of

Petroleum Geologist Grants-in-Aid Program, Donald R. Boyd Memorial Grant; On to the Future, Geological Society of America; Gulf Coast Association of Geological Societies Grants-in-Aid Program; Auburn Geosciences Advisory Board Travel Grant and the Spencer Water and Dan Folse Memorial Research Grant.

To my family and friends, I am who and where I am because of you. Thanks for the myriad of adventures, unremitting love and unequivocal support.

Table of Contents

List of Tables

List of Illustrations

List of Abbreviations

SLO	Spanish Lookout Oilfield	SR	Santa Rosa
ND	Never Delay Oilfield	MC	Margaret Creek
MU	Mike Usher		
AU	Auburn University		
BNE	Belize Natural Energy		
SIS	Strontium Isotope Stratigraphy		
Sr	Strontium		
PPL	Plane-polarized light		
XPL	Crossed-polarized light		
RB	Red Bank		
BC	Barton Creek		
Y#	Yalbac member		
UHBS	Upper Hillbank sandstone		
MHBD	Middle Hillbank dolostone		
LHBS	Lower Hillbank sandstone		
LHBD	Lower Hillbank dolostone		

1. INTRODUCTION

1.1. Geography

Belize is an English-speaking country located on the eastern flank of the coast of Central America (Figure 1), which is bordered on the north by México, on the west and south by Guatemala, and on the east by the Caribbean Sea. A working hydrocarbon system has been recognized for several decades and exploration was initiated in 1938 with a series of geophysical surveys carried out by Shell Oil. Subsequently, the first wells drilled in the early 1950s by Gulf Oil followed by the Phillips in the 1960s (Sherman, 1992). However, it was not until the last 10 years that Belize's petroleum exploration has become largely successful with Belize Natural Energy Ltd. (BNE) discovering the Spanish Lookout and Never Delay fields in 2005 and 2007, respectively. In addition, more recently, in 2012 Blue Creek Exploration Ltd. has discovered a working hydrocarbon system but with an insufficient amount of moveable hydrocarbons just 70 km to the north of the producing Spanish Lookout field in the Corozal basin (Figure 1, "New World Oil and Gas Plc," 2012).

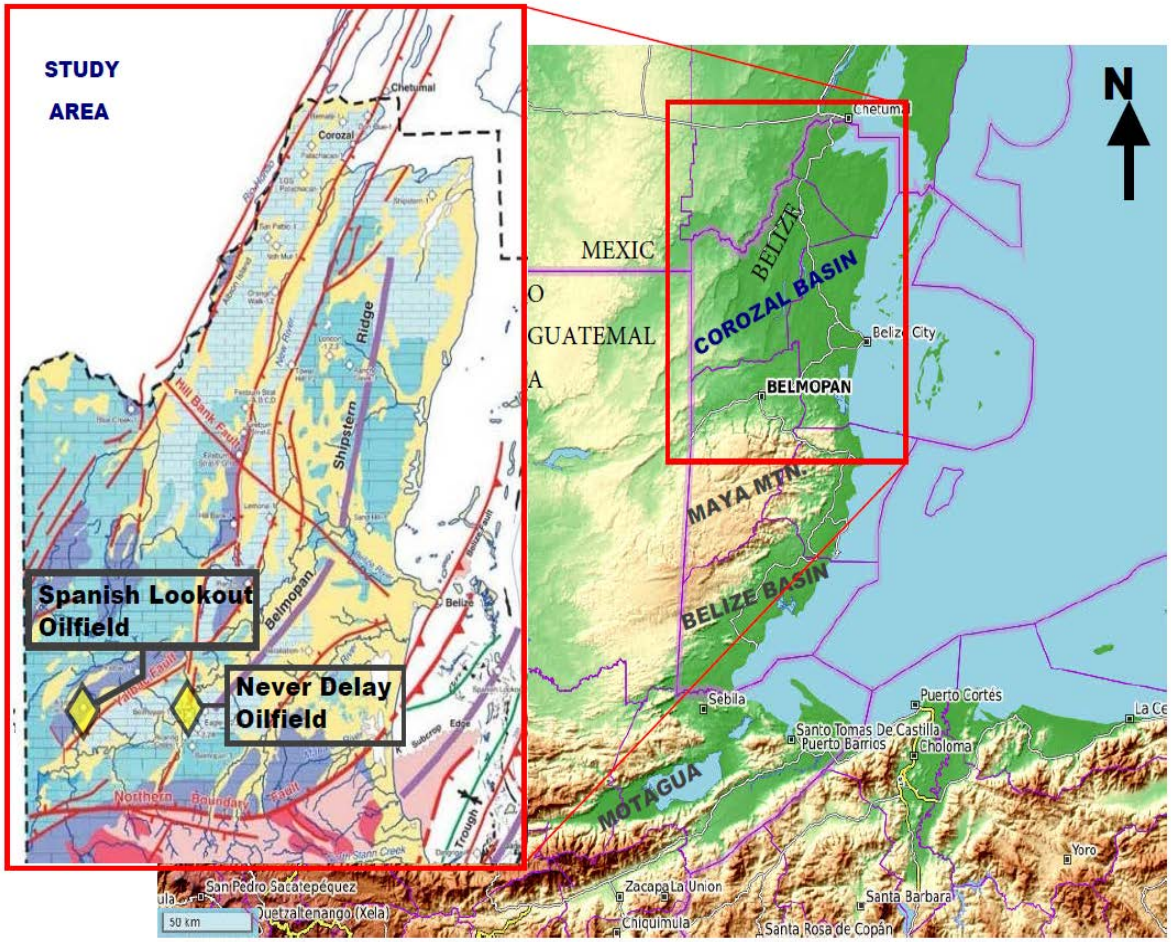

Figure 1. Regional Location Map. Edited from Erhardt et al. (2017). Inset showing the extent of the Corozal basin: from Purdy et al. (2003).

The informal[1] Hillbank (also written Hill Bank) and Yalbac formations are the oil producing formations of the Corozal basin in northern Belize (Figure 2). Considering the hydrocarbon potential of these units as well as the general lack of modern, published

[1] All stratigraphic units in Belize are informal. Both the International Stratigraphic Guide, 2nd ed. (Salvador, 1994) and the North American Stratigraphic Code (NACSN, 2005) stated that formal units must be published in a recognized scientific medium and must include a statement of intent to designate that formal unit. On both of these points, all stratigraphic units in Belize fail to qualify as formal units. The original descriptions of Belize stratigraphic units whose names are in informal use today trace back to hand-typed (and subsequently photocopied) documents (i.e., not recognized scientific media) and they do not include statements of intent to designate. Therefore, all stratigraphic units in Belize are "provisional informal names," as discussed in the International Stratigraphic Guide, 2nd ed. (Salvador, 1994). Subsequent publications in recognized scientific media (e.g., King et al., 2004) have referred to these units, their descriptions, and in some instances their informal 'type localities,' but these publications have not formalized the units. Owing to these esoteric issues, the lower case "f" on formations and "g" on groups are used to make clear the continued informal status of these units and to be consistent with previous work (e.g., King et al. [2004] and references therein).

research on their sedimentary facies, depositional environments, ages, and sequence stratigraphy, the need to conduct a formal geological investigation on these formations is important and essential. According to the Belize Geology and Petroleum Department, up to 2013, a total of 134 wells have been drilled in Belize. BNE drilled 60 of these recent wells, 18 of which were cored partially. Those cores and cuttings from the BNE wells were made available for use in this research. There are currently eight companies which hold exploration licenses in Belize and are carrying out seismic surveys and drilling exploration wells in the continuous search for commercial petroleum (Geology and Petroleum Department, 2013). Despite all this hydrocarbon exploration, presently little is known, and even less is publicly available in open scientific literature, about the sedimentary geology and age of the Hillbank and Yalbac.

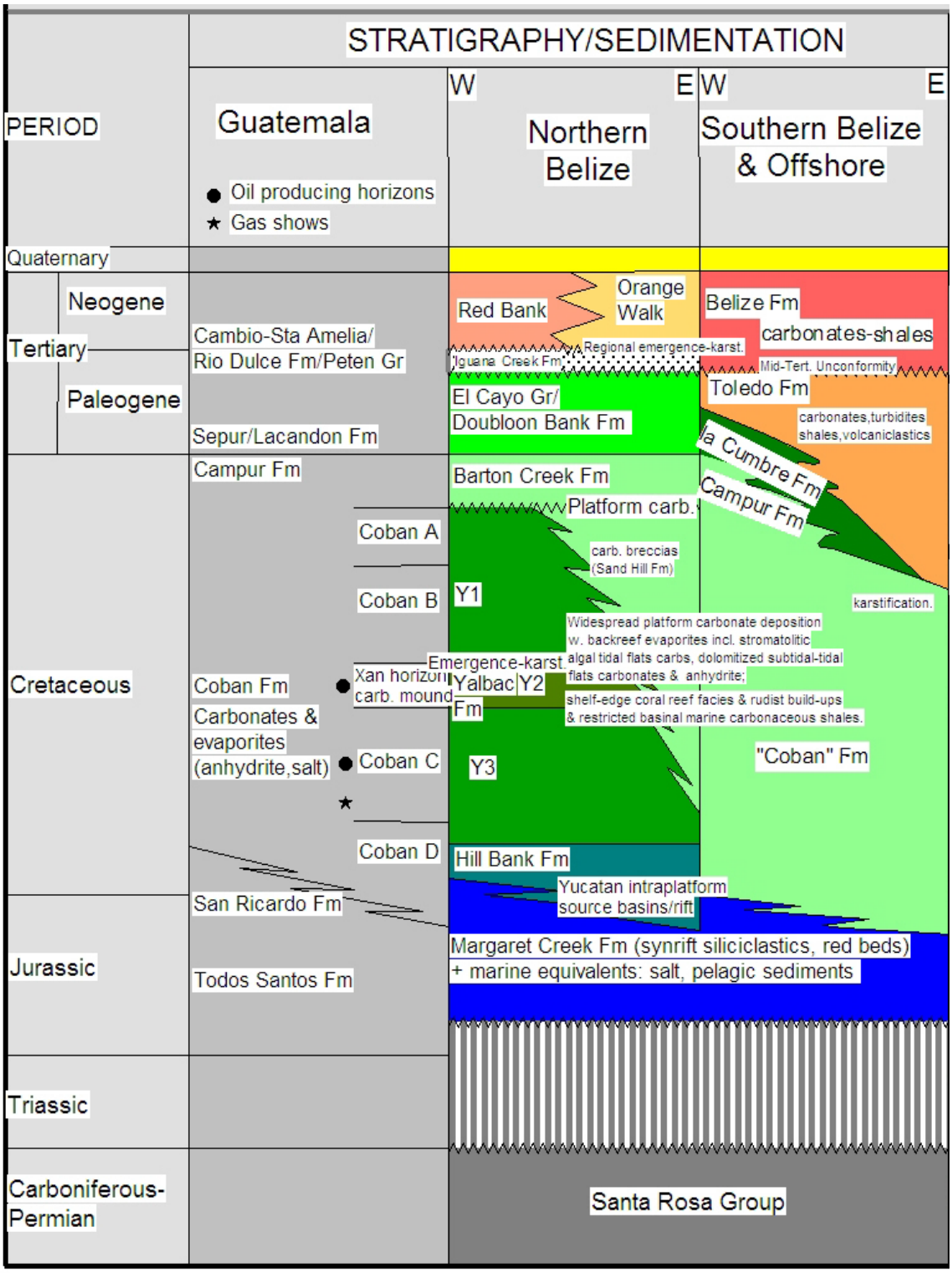

Figure 2. Stratigraphic sequence and general correlation of Belize and Guatemala. From Cornec (2003).

1.2. Geological Setting

The sedimentary strata of northern Belize were deposited in the Corozal basin, which is an eastward extension of the prolifically producing Chiapas-Petén Basin of southeast México and Guatemala (Limes, 1979). Northern Belize has four physiographic zones from west to east: (1) most westerly, a karst flat limestone plain; (2) more centrally, a zone of coastal swamp; (3) a well-developed lagoonal zone; and (4) a barrier reef zone (Limes, 1979).

Tectonically, the Corozal basin and the development of the geology of Belize have been most influenced by the Chiapas uplift in México, La Libertad uplift in Guatemala's Petén, and the Maya Mountain uplift in Belize (Limes, 1979; Hibbard, 1988; Morrice, 1988). The structural evolution of Belize can best be described as having resulted from two separate sets of plate movements: the opening of the Yucatán basin north of the Cayman Ridge during Mesozoic (Late Jurassic to Late Cretaceous), and secondly the movement of the Caribbean plate respectively eastwards and away from the North American plate (beginning during Late Cretaceous; Whittaker, 1983). The Polochic fault separates the Caribbean plate from the North American plate, passing along the Gulf of Honduras near the southern border of Belize (Whittaker, 1983). It was during Late Cretaceous (specifically Campanian and Maastrichtian), that the onset of Caribbean plate movement apparently induced uplift (likely the equivalent of the Laramide orogeny of North America; Whittaker, 1983; Limes, 1979; Hibbard, 1988; Morrice, 1988). These movements resulted in the north-northwest trending set of normal faults and a later, northeast trending left-lateral strike slip movement (Whittaker, 1983). This activity is likely what has influenced migration and accumulation of hydrocarbon in the area.

Normal faulting formed a rifted trailing edge plate boundary (Whittaker, 1983). Rifting and subsidence of the present continental margin began during Late Jurassic when terrestrial clastics (originally named Todos Santos, but now called the Margaret Creek) were deposited locally on an irregular faulted surface (Whittaker, 1983). As rifting continued during Cretaceous, the entire area, except possibly for the higher parts of the Maya Block, subsided below sea level, and thick carbonates were deposited (Coban and Campur in Guatemala, Hillbank and Yalbac in Belize; Whittaker, 1983). Regional dip of the Cretaceous and Cenozoic sediments over the northern Belize shelf is one to three degrees north and northwest, dipping towards the Mexican border (Hibbard, 1988).

The Spanish Lookout and Never Delay oil fields (Figure 1) are located on the southern margin of the Corozal basin within the Northern Boundary Fault Zone (Bateson and Hall, 1977; Petersen et al., 2012). This section of Mesozoic and Cenozoic sediments range greatly in thickness from 450 m in the south near the Maya Mountains to approximately 3500 m in the north (Hibbard, 1976). Studies of these formations, have led to the interpretation that they were deposited in a transgressive-regressive sequence across the northern Belize shelf in a marine embayment environment (Hibbard, 1976; Morrice, 1988). The Lower Cretaceous carbonate-evaporite sediments of northern Belize are stratigraphic and lithologic equivalents to highly productive Lower Cetaceous sediments of the Gulf Coast basin in the United States and México and Guatemala (Hibbard, 1976; Morrice, 1988; Hibbard, 1988). Dominant rock types include dolostones, limestones, and anhydrite-rich rocks which make up much of the Cretaceous section over this broad area (Hibbard, 1976). It was during Early Cretaceous, that an emerging welt separated the carbonate and evaporate sequence on the north from a possibly

equivalent deep-water, open-sea sequence (limestones, turbidites, volcanic, and volcaniclastic rocks; Bishop, 1980).

1.3. Structural Evolution/Paleo-geologic Timing

The structural evolution of the Yucatán, and by extension the Caribbean, has been a highly debated topic and several models for its evolution have been developed. In 2009, Pindell and Kennan proposed that the Yucatán Block was formed by detachment from North America, specifically the northeastern Mexican Gulf region, as a result of extension and rifting between the North and South American plate during Early to Middle Jurassic (Pindell and Kennan, 2009). This extension was followed by initial seafloor spreading during Late Jurassic, with a strong counterclockwise rotation that is related to curvilinear fracture zone trends in the Gulf of México (Pindell and Kennan, 2009). They suggested that earliest Cretaceous was the time of the end of significant movement of Yucatán with respect to North America. Subsequently, during Neocomian final separation and emplacement of the Yucatan occurred. This model is very complex and requires intricate geometry with major rotation.

Subsequent interpretations by Kim, et al. (2011) contradict this model and propose an alternate hypothesis. During the opening of the Gulf, an initial Jurassic episode involves a clockwise rotation of the Yucatán Block away from the northern Gulf of México coast (Kim et al., 2011). The key difference proposed is that this episode finished with the Yucatán Block being situated off the southwest coast of Florida (Kim et al., 2011). Then, a second stage, during the Miocene, involved the southwest migration of the Yucatán Block (<250 km, i.e. up to the inferred length of the Yucatán slab) into its current position (Kim et al., 2011). The later episode concluded with the collision of the

Yucatán Block with southeast México. This interpretation provides an explanation for the formation of the Chiapas Fold and Thrust Belt in southeast México (Kim et al., 2011).

1.4. Objectives

The Hillbank and Yalbac formations are the subject of the present research. The purpose of this research is to provide a modern, published report on these subsurface units, with a description of their depositional environments and evidence of relative change in sea level. Additionally, strontium-isotope stratigraphy was done on these formations to determine their ages and limits of their boundaries. The objective of this research is to conduct sedimentological investigations on these important oil-bearing formations (Hillbank and Yalbac) with the goal of better understanding their age, stratigraphy, and petrology.

1.5. Significance

The lack of extensive outcrops, significant road access, and dense vegetation has significantly hindered geological investigations within the borders of the country. There are, to date, no known outcrops of the Hillbank and Yalbac formations, so petrographic, core, and cuttings studies are extremely important. In addition, the scarcity of fossils and lack of well-preserved fossils is another hindrance in determining the ages and stratigraphic relationships. Foraminifera are extremely rare to absent in the Hillbank and Yalbac formations of the Corozal Basin (Ramanathan, 1990). Previous petrological studies have only been made with thin sections from well chippings (eg. Purrazzella, 1992; Nair, 1988). Therefore, core thin-section description of drill-core pieces (as in this study) is critical both for accurate depth placement and for understanding depositional environments and facies relationships.

The present study will help in the understanding of (a) where and when the Hillbank and Yalbac carbonates and their associated microfacies formed, (b) what diagenetic changes occurred within each carbonate facies, (c) the facies relationships, global correlation, and (d) basic sequence stratigraphy of this economically important subsurface stratigraphic section. This kind of information can help in prediction of (a) Hillbank and Yalbac facies distribution laterally and vertically, (b) thickness and porosity trends in the carbonates and clastics, and (c) coeval stratigraphic relationships in other parts of the basin. This research is the first openly available geological investigation of depositional environments, age estimations, and core thin-section descriptions of the Hillbank and Yalbac formations in the Corozal basin since the units were first drilled nearly a half century ago.

The research value of these age estimations is that they allows us for the first time to give supporting evidence about formation ages, which allows us to compare sedimentary facies changes with some parts of the global sea-level curve. Strontium-based age estimates in carbonates can help us detect stratigraphic breaks in the section as well. If we can better understand the connection, if any, with global eustasy, this may allow us to better interpret any link between the local stratigraphy and regional tectonic events.

2. PREVIOUS RESEARCH

Most of the early interpretation and reports on the geology of Belize were concentrated on the Maya Mountains in the quest for exploitable minerals. The geological recording of Belize largely began in 1921 when Belize was still a colony known as British Honduras. Government geologist Leslie H. Ower was chiefly the frontiersman who conducted a geological survey compiling the first geological map of the colony. Ower (1928) divided the geology in three main portions based almost entirely on changing topography. The low relief portion to the north of the latitude 17^0 10' (now known as the Corozal basin); the well-vegetated, mountainous central region known as the Maya Mountains; and the southernmost end of the colony, which was viewed as a complex area of mudstones and massive limestone hills (now called the Belize basin). Due to the nature of his investigation, Ower focused most of his efforts on the study of Paleozoic intrusives and provided a very loose description of the units. He did however recognize the relationship of Belize's geology with the geology of neighboring Guatemala and México.

Publications from Giovanni Flores, then a geologist with Bahamas Exploration Co. Ltd., succeeded Ower's work. Flores (1952) conducted geological studies on the Corozal basin dominantly using aerial photography and fossil assemblages. He added an Upper Cretaceous to Pleistocene sedimentary series lying uncomfortably above the Paleozoic intrusive basement. Early exploration wells (Hillbank 1; Wrestling, 1956) revealed a cyclical succession of limestone/dolostone and anhydrite Cretaceous

sequence in the Corozal basin. Well reports dating as far back as 1972 named this sequence as the Hillbank formation with the overlying Yalbac formation (Harr, 1972). Subsequently, Bryson (1975) examined the relationship between the stratigraphy of Belize and neighboring regions to find that northern Belize forms the eastern margin of the Chiapas-Petén evaporite basin, with the Yalbac formation forming the marginal facies of that basin. Bryson (1975) built on the previously established stratigraphy and was the first to provide a formal description of the of the Cretaceous units, recognizing the Yalbac and Hillbank formations. He described the Hillbank as consisting of porous, tan to light grey limestones and dolostones that may be slightly anhydritic and lie above the Margaret Creek (MC) formation. No fossils were observed and therefore the age was indiscriminately determined only by relative age dating using its stratigraphic position. Bryson (1975) also noted that the Hillbank transitions into the Yalbac formation, which consists of interbedded limestone, dolostone, anhydrite, and minor shales, and that the Yalbac is separated from the overlying Barton Creek (BC) by an unconformity. No fossils of note were found and the age was estimated by relative position to be Lower Cretaceous. Hibbard (1976) recognized the changing environments represented within the Yalbac and divided it into upper, middle, and lower members.

Cornec (1985; 1986) then made use of this groundwork and adapted Flores' work to later on produce provisional geological maps of Belize and supplemental documents. Cornec later updated his work to form a modern geological map and corresponding cross-sections (Cornec, 2003). Assessments of the petroleum system and hydrocarbon potential of the Corozal basin have been conducted by (Bishop, 1980; Nair, 1988; King and Petruny, 2012b; Petersen et al., 2012). More recent stratigraphic

descriptions of the Corozal basin stratigraphy have been given by King et al. (2003; 2004) as well as King and Petruny (2012a, 2013, 2014).

3. METHODOLOGY

3.1. Graphics and Correlation

A small-scale data set of 62 wells located solely in the Corozal basin were used for this study. The software IHS Petra was used to organize most of the well data. Formation tops, where available, were uploaded into the software and zones were created in order to generate isopach maps of the Yalbac and Hillbank formations. Because of the well locations, these isopach maps were clipped to the southwestern part of the basin to remain true to data and limit interpolation. Core from twelve wells was made into petrographic thin sections, and seven wells were separately sampled for strontium isotope analysis. The depth location of the strontium samples as well as the thin section depth locations are both plotted in Figure 3. As part of the basin analysis and to gain a better understanding of the depositional system, a one-dimensional (1D) basin model of the Corozal basin burial history (based on previous work only) was created using the BasinMod program.

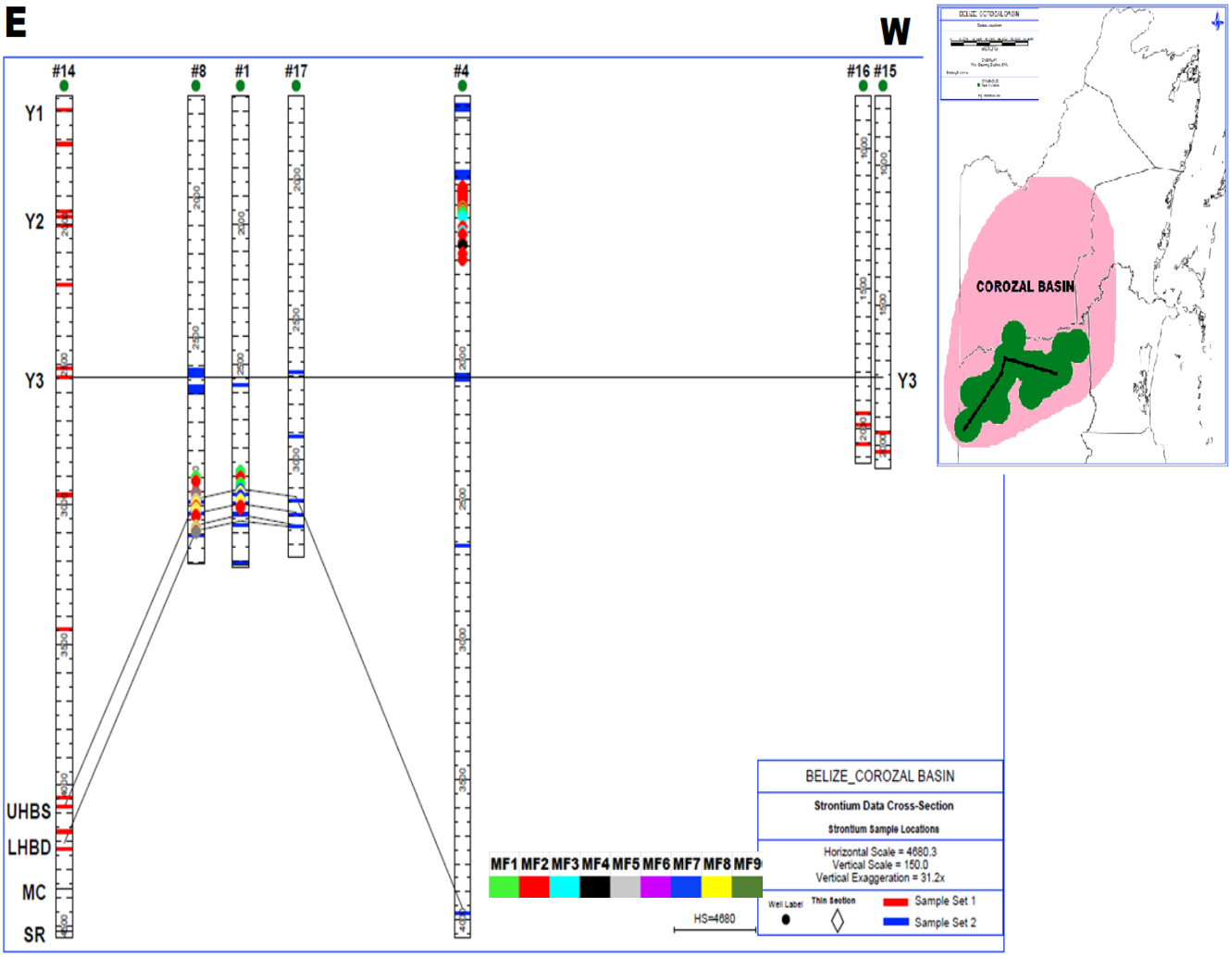

Figure 3. Panel diagram of the wells used for strontium isotope analysis, showing the sample locations as well as respective thin section locations. Seven wells were sampled in order to complete strontium isotope stratigraphy. The red bars represent the first sample set. A second sample set (blue bars) was also taken to get a wider range within the formations as well as to get a complete extent of the basin. This cross-section intersects the basin in a general E-W direction and the datum is set on the top of Y3 member of the Yalbac formation. Thin section locations are also posted

3.2. Sample Selection

Thin sections were received directly from BNE and used for this study; therefore, there was no thin-section sample selection or preparation protocol for the present report. BNE's thin section collection represented all available core samples from the area studied.

For the strontium analyses, a total of 47 samples were collected from well chippings from 7 wells throughout the Corozal basin for strontium analysis. Due to the proprietary nature of the dataset, well names had to be aliased and locations obscured. Samples were collected from throughout the well, with special consideration at the boundary of the stratigraphic subdivisions, e.g. the Y1-Y2 boundary or the Y3-Hillbank boundary. This was done in order to get constraints on the uppermost and lowermost possible ages of the main stratigraphic subdivisions in the study area. The wells studied transect the Corozal basin in a general east-west direction and their correlation and interpretation allow for consideration of lateral variation and continuity in part of the basin. The samples were collected from the formations and members as follows (Table 1): 4 samples from the BC; 4 samples from Y1; 1 sample from Y1/Y2 contact; 4 samples from Y2; 1 sample from Y2/Y3 contact; 14 samples from Y3; 1 sample from Y3/UHBS contact; 4 samples from UHBS; 4 samples from UHBD; 3 samples from MHBS; 6 samples from LHBD; and 1 sample from MC.

Table 1. Strontium samples per stratigraphic subdivision. Stratigraphic abbreviations are in the text above.

Formation/Member	# Samples
BC	4
Y1	4
Y1/Y2	1
Y2	4
Y2/Y3	1
Y3	14
Y3/UHBS	1
UHBS	4
UHBD	4
MHBS	3
LHBD	6
MC	1
Total	47

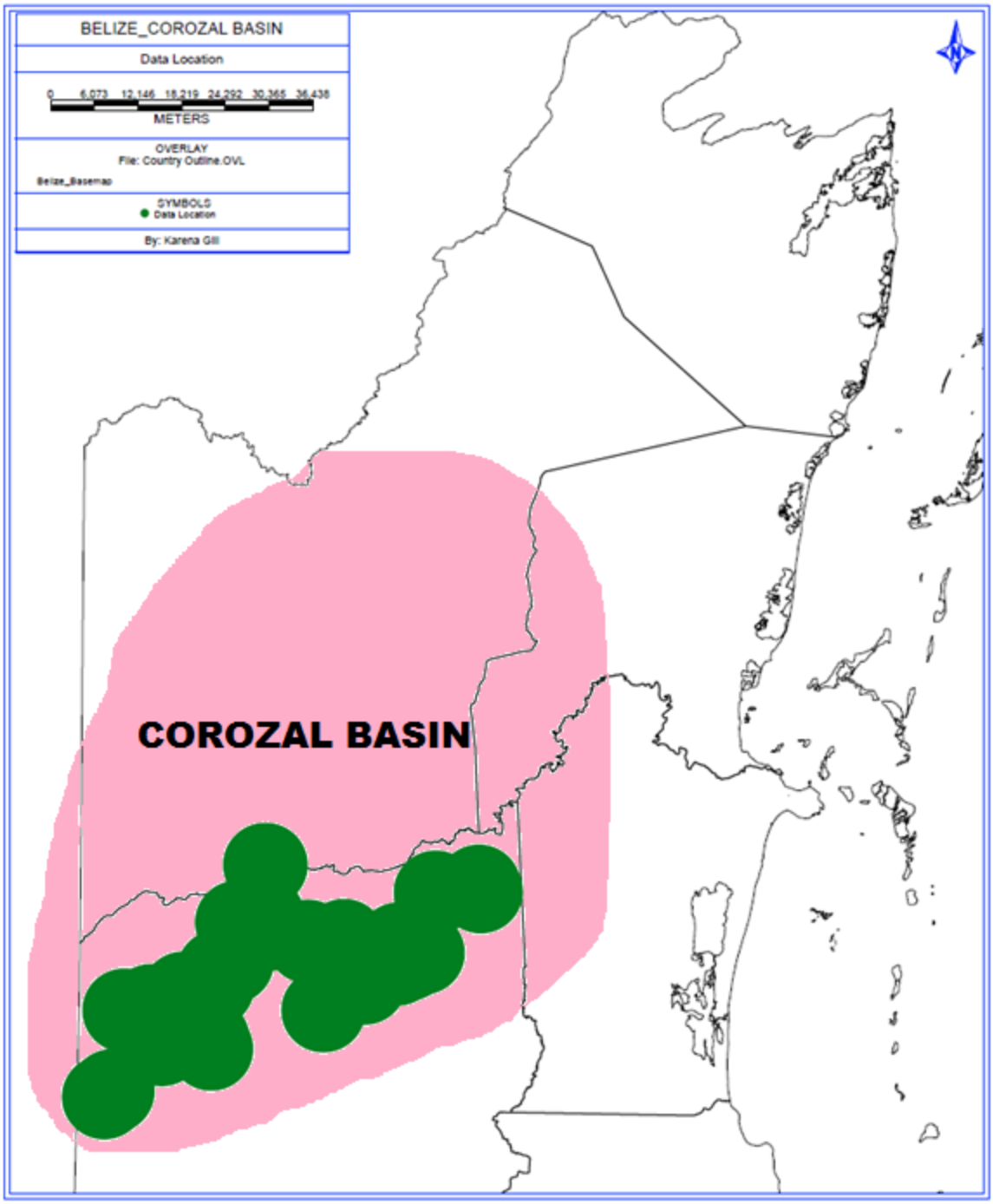

Figure 4. Map of the Corozal basin showing well locations. The green circles represent the general location of the data points used for this study in generating the isopach maps.

3.3. Thin Section Analysis

A detailed petrographic study encompassing over 229 thin sections was carried out using a standard petrogrphic microscope at several magnifications appropriate for the level of detail visible in each. The thin sections received were a standard-size (1 x 1 7/8”), except for one large (2 x 3”) thin section. The thin sections were impregnated during preparation with colored epoxy to indicate porosity and stained with Alizarin Red S before covering to assess the presence or absence of calcite, and potassium ferricyanide to discern between ferroan/nonferroan calcite. The goal was a petrographic study and environmental interpretation of core samples from key intervals throughout the two formations of interest. Well data were also utilized to assist in the corelation and identification of correlative horizons in order to complete a sequence stratigraphy analysis of the formations. Microfacies were defined based on the major petrographic chracteristics, such as relative abundance of major components, rock texture, and matrix or cement using classifications from Wilson (1975) as well as Flügel (2010).

3.3.1 Terminology

Dolostone textures, where depositional textures can be discerned, were described using a modification of the Dunham classification (1962). Where the depositional textures are obliterated, the rock is simply termed dolostone giving textural attributes, including porosity (Choquette and Pray, 1970).

3.4. Strontium Analysis

Since the pioneering work of Peterman et al. (1970), which utilized Sr isotopes as a tracer to monitor the evolution of ancient seawater, strontium isotope stratigraphy (SIS) is now an established chemo-stratigraphic tool (Elderfield, 1986; Veizer et al., 1997; McArthur et al., 2012). The $^{87}Sr/^{86}Sr$ ratio of sea water has changed significantly with

time in response to the input of varying proportions of strontium (Sr) derived from continental crust and upper mantle sources, as moderated and buffered by carbonate recycling (Elderfield, 1986). Because of these fluctuations, the marine strontium-isotope record can be used for stratigraphic correlation and within certain limitations for geochronological estimations (Elderfield, 1986).

Due to the poor state of preservation of fossils in most areas as well as scanty biostratigraphic control, SIS was both appropriate and necessary for dating the ages of the formations in the Corozal basin. One of the apparent advantages of using this method is that it could produce correlations that are global in scale, and it also exceeds the limitations placed on sequences with little to no biostratigraphy or that are non-fossiliferous (Veizer et al., 1997). The ability to use the Phanerozoic seawater strontium isotope curve as a stratigraphic correlation tool depends upon four factors (McArthur, 1994):

1. The state of the preservation of the samples studied;
2. The analytical quality of data;
3. The accuracy of the age model used to calibrate the isotope curve;
4. The slope of the seawater $^{87}Sr/^{86}Sr$ curve at the given time interval.

The analytical method is that given by McArthur et al. (2012). Selected samples were powdered to 200 mesh using agate pestle and mortar. About 100 mg of sample powders were then weighed by a Mettler-Toledo balance in Teflon beakers. Sample powders were treated with ultra-pure ammonium acetate solutions 3 times. After decanting the ammonium acetate solutions, sample powders were washed with ultra-pure water (18.2 megohm-cm) and then dissolved in ultra-pure acetic acids. After

dissolutions of carbonates and dolomite, samples were transferred from Teflon beakers to centrifuge tubes and were centrifuged for several minutes. The clear acetic solutions were then transferred to new Teflon beakers and evaporated to dryness. Samples were then dissolved in 2 N HNO_3 for chromatography column chemistry.

Sr resins from Eichrom were used for column chromatography chemistry. Sr resins were cleaned with ultra-pure water. Clear sample solutions were loaded to columns with 2 N HNO_3, and rinsed with 2 N HNO_3 and 7 N HNO_3. In the end, Sr in the resin was eluted with 0.05 N HNO_3 and dried down on a hotplate.

Sr separates were loaded unto degassed Re filaments and measured by a Finnigan MAT 262 multi-collector thermal ionization mass spectrometer (TIMS) at Auburn University by dynamic mode. Sr isotopic compositions were normalized using $^{86}Sr/^{88}Sr=0.1194$. NIST 987 was used as Sr isotopic standards.

4. STRATIGRAPHY

4.1. Belize's Corozal Basin

Previous studies on Belize and Central America have found several key ideas relating to the evolution of the Corozal basin and its stratigraphy that are explained in this section. Belize forms a part of the North American plate, with the boundary between the North American Plate and the Caribbean plate being the Motagua-Polochic Fault system and the Swan Fracture Zone in the offshore (Morrice, 1988; Rao and Ramanathan, 1990). Regionally, the Corozal basin connects the North Petén Basin of Guatemala and the Yucatán basin of the Caribbean (Whittaker, 1983). Bouguer anomaly maps indicate that the north-northwest normal faults extend into the Paleozoic basement and are only surface expressions of this preexisting trend (Whittaker, 1983). The western part of the basin dips gently north and north-west into the Petén basin, while the eastern part dips very gently east into the Yucatán basin (Whittaker, 1983).

Locally, the Corozal basin is separated by the Northern Boundary Fault from the Maya Block to the south (Morrice, 1988; Rao and Ramanathan, 1990). The basin itself is further separated into western and eastern parts by a high, possibly a continuation of the La Libertad Arch of Guatemala (Whittaker, 1983). The Corozal basin has two significant trends: (a) a large northeast-southwest ridge named Belmopan-Shipstern Ridge flanked in the east and west by sub-basins; and (b) a northwest-southeast fault that bisects the Corozal Basin into two parts – the northern half being the extension of the Yucatán

Platform and the southern half the continuation of the Petén Basin (Morrice, 1988; Rao and Ramanathan, 1990).

An idealized burial history diagram based on historical accounts of formation ages, stratigraphy descriptions (including thickness) and key events such as unconformities within the Corozal basin is shown below (Figure 5). This model was created using the BasinMod program and illustrates the relationship between subsurface depth (m) and age (million years (my)); it provides a general history of the rates of subsidence and major events recorded by the sedimentary record. According to previous work, the depositional record started during Paleozoic with deposition of the Santa Rosa formation. The first erosional event occurs between the Santa Rosa group and the overlying Margaret Creek formation, which was likely related to regional uplift during Middle Jurassic, was formed. The Margaret Creek formation was deposited on this erosional surface as a consequence of this uplift, thus forming a thick clastic sequence. Subsidence of the basin continued into Cretaceous, and the Hillbank sequence was deposited by the end of Early Cretaceous. The Yalbac formation appears to lie conformably above the Hillbank and has a gradational contact. In most areas, the informal upper members of the Yalbac (Y1 and Y2) have been eroded. This is attributed the uplift event near the end of Late Cretaceous. This large unconformity between the Yalbac and the Barton Creek is likely what has incised deeply into the upper Yalbac and in most places in the southern part of the Corozal basin stratigraphically positions the sub-Barton Creek unconformably above the Y3. The Corozal basin shows a rather slow and modest depositional pace throughout Paleozoic and Mesozoic with steady deposition and a few episodes of uplift and erosion. By Late Cretaceous, however, a period of rapid subsidence ensues and the Cenozoic appears to have been a time span

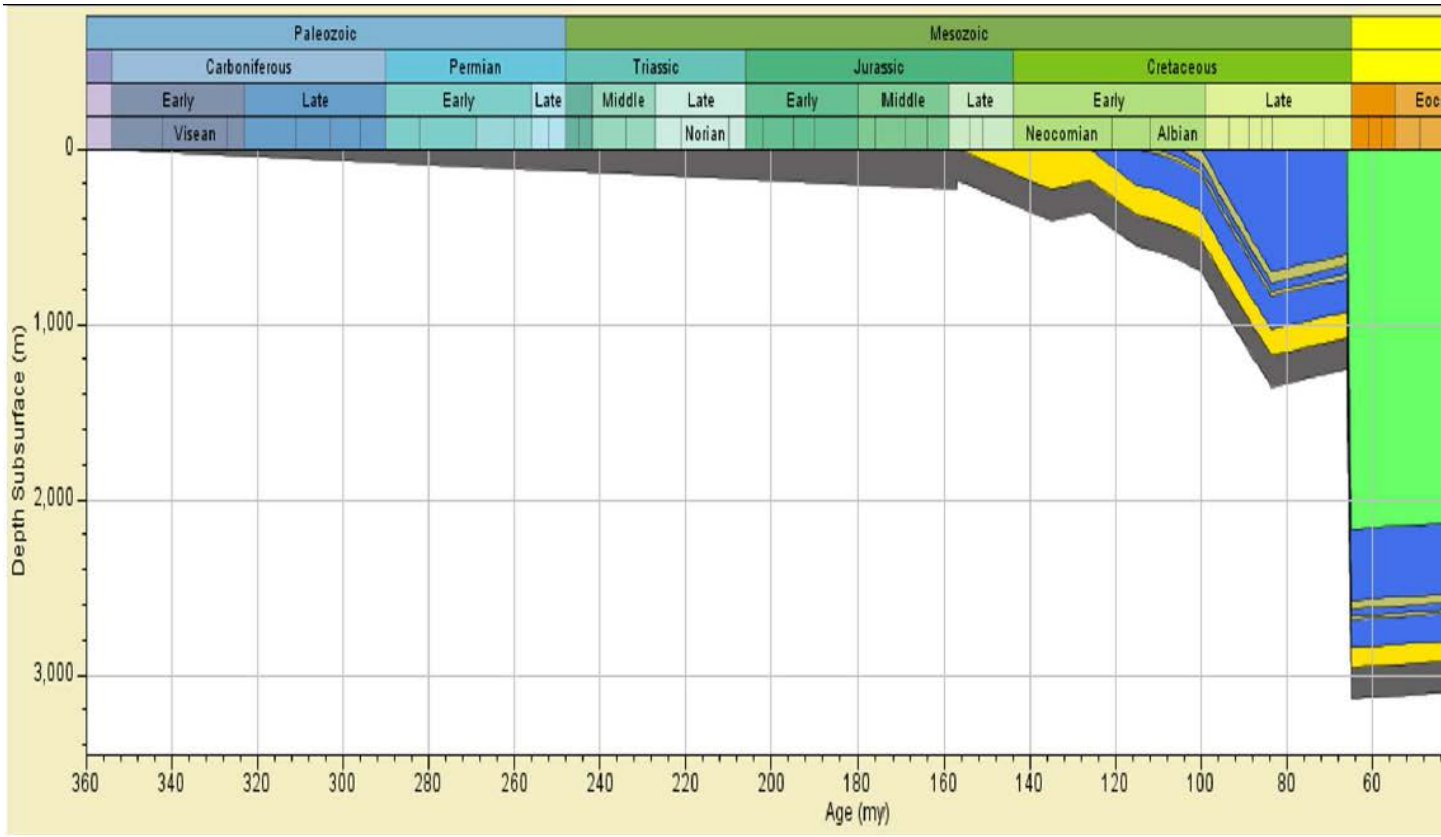

Figure 5. Idealized burial history for the Spanish Lookout area based on historical accounts of ages and stratigraphic descriptions and r events. Data compiled from Flores (1952), Bryson (1975), King et al. (2004), and Petersen et al. (2012).

of very rapid subsidence and deposition of the thickest sequence of strata when compared to the entirety of the basin history.

This was the current understanding of the Corozal basin at the outset of this study and the model that is being tested in the present research.

4.2. Hillbank formation

The Hillbank #1 well was drilled in 1956 as a test for hydrocarbons near the Hillbank lagoon in the Corozal district. The stratigraphy of this well was deemed comparable to the Gulf Yalbac #1 well, which was the first to penetrate a Cretaceous

carbonate and evaporative sequence consisting of limestones and a more basal interbedded anhydrite and dolomite/limestone (Wrestling, 1956). Wrestling (1956) outlined the formations by ages, and names were not assigned informally to these until further exploration wells were drilled in the 1970s and observed a similar stratigraphic sequence. Paleontological age determinations were done in Cuba, but details on the identification were not included in the report, only interpreted ages (Wrestling, 1956). The presence of miliolids and orbitulinas indicate that deposition occurred during Early Cretaceous (Hibbard, 1976).

These Upper Cretaceous porous dolostones in northern Belize pinch out updip in the subsurface southward toward the Maya Mountains as shown in Figure 6 (Hibbard, 1976). Isopach maps of the informal Hillbank members are shown below in Figure 6. The upper Hillbank sandstone increases in thickness to the northwest and shows a slight thickening in the center (Figure 6A). The middle Hillbank dolostone shows a thickening in the western areas (Figure 6B); its thickness increases to the west-northwest and has a zero thickness in the eastern and south-eastern corner of the basin. The lower Hillbank sandstone is the only member that indicates a southern source based on its increasing thickness in that direction (Figure 6C). The more arkosic nature of the constituten microfacies also makes this unit more likely to have been derived from the Maya Mountain granites. The lower Hillbank dolostone shows a general thickening of several hundred meters to the north (Figure 6D). The lower Hillbank dolostone reaches a zero thickness as it abuts the Maya Mountains.

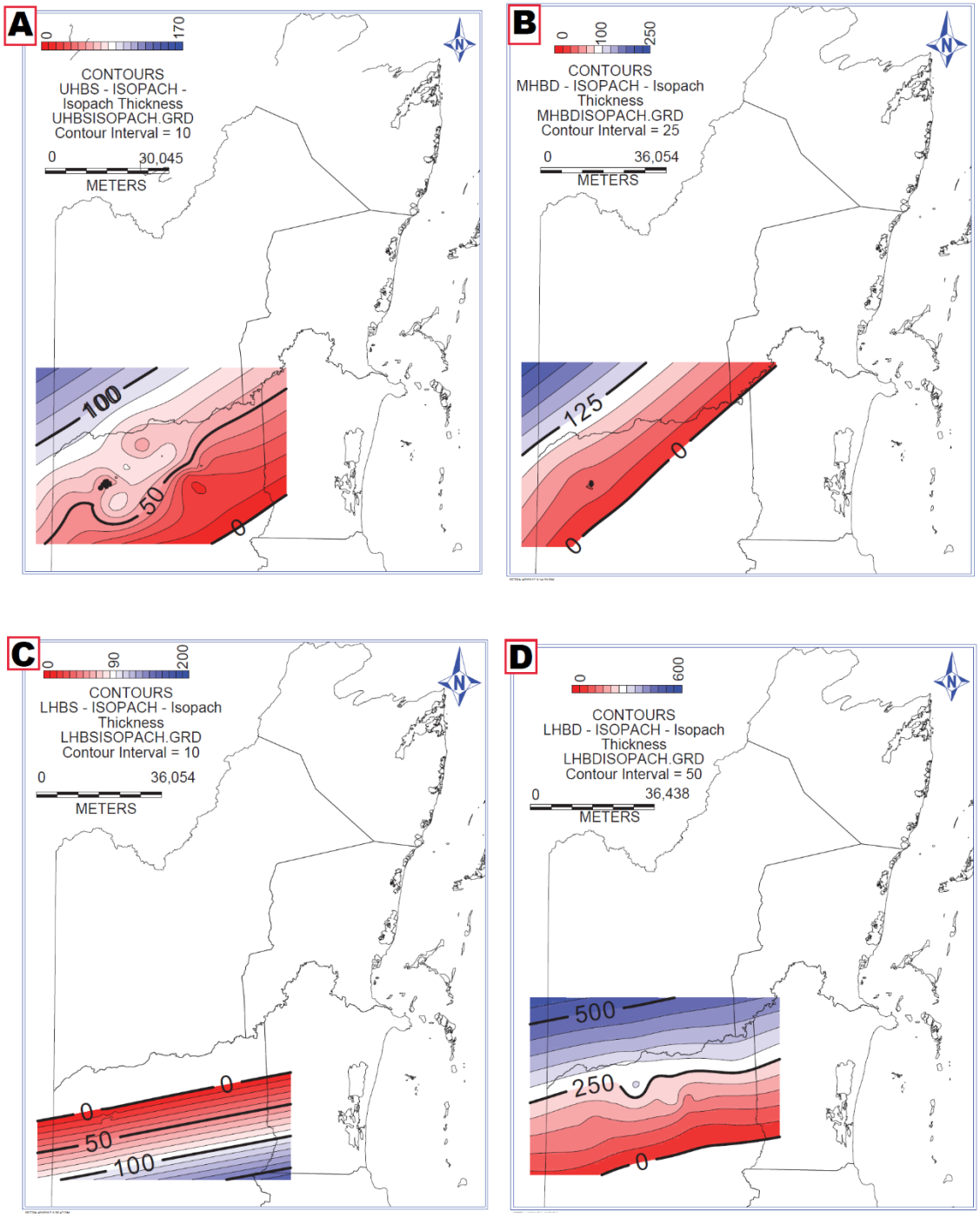

Figure 6. Isopach maps of the four genetic packages of the Hillbank. The upper Hillbank sandstone (A) shows a zero thickness to the southeast and gradually thickens to just over 100 m. The middle Hillbank dolostone (B) follows a similar trend and thickens to over 150 m to the northwest. The lower Hillbank sandstone (C) is the only member that gradually thickens to the southeast to just over 100 m. The lower Hillbank dolostone (D) follows with the previous trend of northwest thickening with a zero thickness towards the south.

4.3. Yalbac formation

The B. H. Gulf Yalbac #1 test well is located 42 kilometers southwest of the Hillbank #1 well. Yalbac #1 was the first well to penetrate the Yalbac formation, a Cretaceous carbonate and evaporative sequence consisting of limestones and a more basal interbedded anhydrite and dolomite/limestone (Wrestling, 1956). Like the Hillbank, the informal name Yalbac was not assigned to these until further exploration wells were drilled in the 1970s and observed a similar stratigraphic sequence.

The Yalbac is divisible into a lower Y3, middle Y2, and upper Y1 informal zones/members based on relative abundances of anhydrite and carbonates (Morrice, 1988; Ramanathan, 1990). The ratio of dolostone to anhydrite is on average 1:2 in Y3, 2:1 in Y2, and 1:9 in Y1 (Ramanathan, 1990). The Yalbac formation ranges greatly in thickness from essentially zero in the eastern part of northern Belize, to over 1500 m.

Historical attempts at biostratigraphic age dating the Yalbac have yielded little success due to scarcity of fossils and lack of well-preserved ones. Ramanathan (1990) attempted to detail the foraminifera assemblage of this area and found benthic species such as *Nummoloculina cf. heimi*, *Quinqueloculina sp*. and other milliolids, which are characteristic of water depths in the range of 0-10 m and bottom temperatures on the order of 21 to 32 C.

Sharing a similar geology with neighboring Guatemala and México, the Yalbac formation conforms to the regional trend in deposition of the carbonates. The three members of the Yalbac formation all thicken to north or northwest (Figure 7). The Y1 member of the Yalbac formation thickens to the NE of the study area and pinches out or

is eroded towards the south approaching the Maya Mountains (Figure 7A). Rapid thickness changes spanning up to hundreds of meters are typically indicative of a prolonged period of exposure, like the stratigraphic break that truncates the Yalbac and incised deeply into the upper members. The middle Yalbac member, Y2, shows a less significant change in thickness throughout the study area (Figure 7B). The Y2 member increases in thickness by tens of meters to the northwest and represents a modest depositional rate. The lowermost Y3 member is the thickest and most widespread member of the Yalbac formation (Figure 7C). Similar to the Y1 member, the Y3 reaches zero thickness the south as it approaches the Maya Mountains and increase by thousands of meters to the north-northwest.

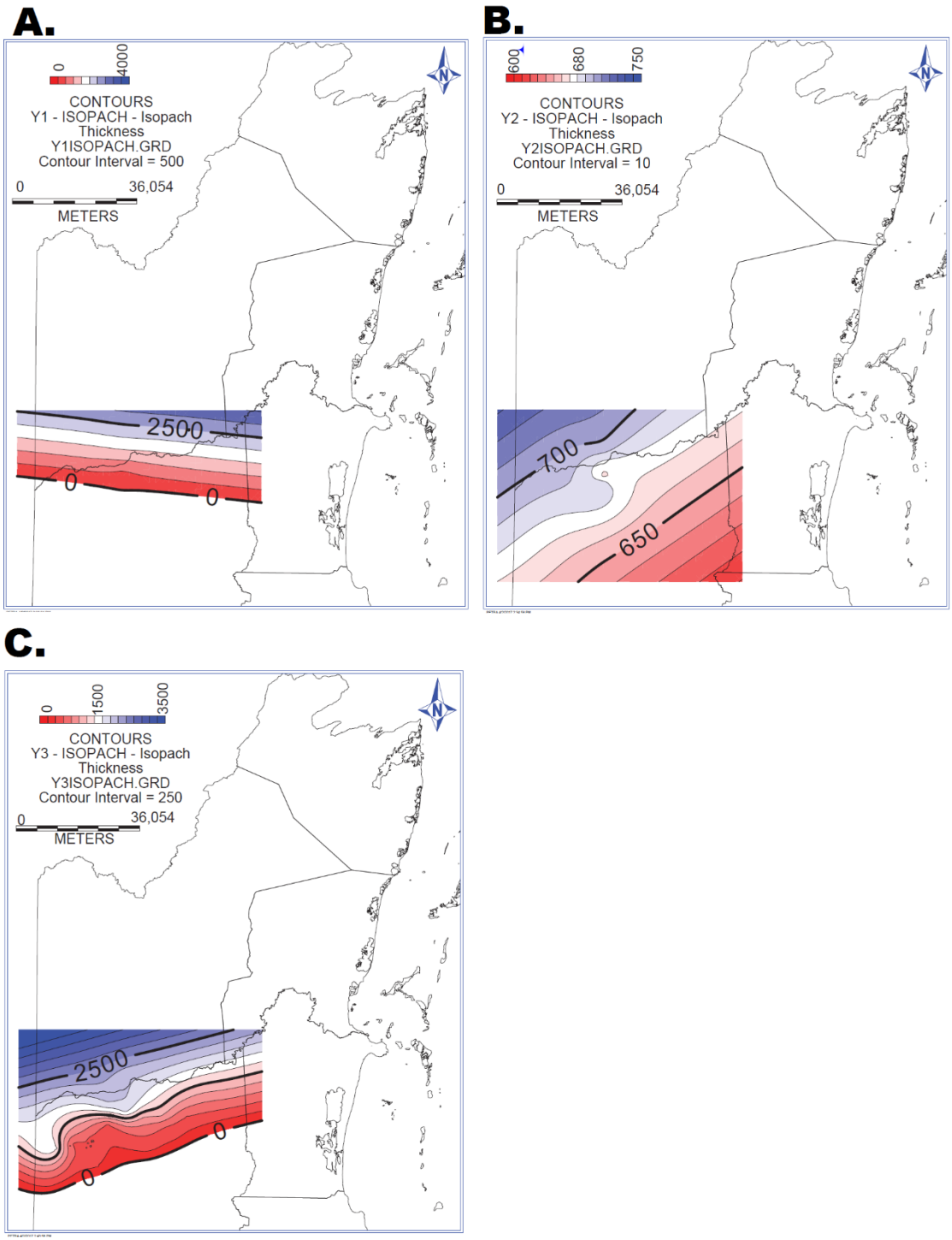

Figure 7. Isopach maps of the Yalbac formation, by informal members The Y1 member (A) shows a zero thickness towards the south and a significant increase to over 2000 m towards the north using the dataset. The Y2 member (B) grossly increases in thickness to the northwest but shows a more modest increase spanning less than 100 m. The Y3 member (C) shows a zero thickness as it approaches the foothills of the Maya Mountains and increases in thickness to the north-northwest to over 2000 m.

5. MICROFACIES ANALYSIS

5.1. Microfacies Description

The following categorization of microfacies are based solely on thin section observations and classifications described by Wilson (1975) and Flügel (2010). The term microfacies is used here because the facies determinations were made using microscopic study of thin sections.

Microfacies 1 (MF1): Bioclastic Packstone/Grainstone with abundant benthic foraminifera or calcareous green algae

Description: Microfacies 1 is dominated by dolomite with anhydrite, gypsum and calcite and has an anhedral, largely nonmimic replacement fabric. Generally, it consists of recrystallized, fine, anhedral (occasionally zoned) dolomite that has replaced a probable skeletal limestone (Figure 8A). The crystalline dolomite also shows extensive interlocking of adjacent crystals. Allochems are diverse and include fragment mollusks and echinoderms together with algae. Commonly, the foraminifer's tests and parts of the matrix are oil-stained, thus accentuating the dark color of the porcelaneous test walls (Figure 8B). Skeletal grains have probably undergone several recrystallization episodes and are now mostly just a remnant outline. Bivalves commonly show neomorphic alteration (inversion) of their originally aragonitic shells. Moldic porosity is also common and show remnants shapes of possibly original grains (Figure 8D). Oöid and pellet grains are more common in this microfacies (Figure 8E/F).

Interpretation: This microfacies represents a restricted inner ramp (shallow lagoon), comparable to standard facies zone (FZ) 7 and 8 of Wilson (1975). FZ7 is a shelf lagoon with open circulation and characterized by dolomitic wackestone with a variety of textures (Figure

27). FZ8 is dominantly a dolomitic bioclatic wackstone and contains pelleted grainstone and coarse lithoclastic wackestone (Figure 27).

MF1 represents deposition in a shelf lagoon, with the predominance of bioclastic shell fragments indicating a shallow subtidal, limited circulation environment with a depth range of 15-30 m (Scholle et al., 1983). Miliolid foraminifera are very common in lagoonal environments (sometimes with elevated salinity) of Mesozoic and Cenozoic restricted inner platforms and inner ramps (Scholle and Ulmer-Scholle, 2003). The alteration here involved dissolution of aragonite, leaving moldic porosity and in some instances re-precipitation (now recrystallized dolomite). This obliterated all relict internal shell structure, so grains are identifiable only on the basis of characteristic shapes (symmetrical shells with distinctive hinge structure). T he numerous foraminifers present, particularly miliolids, have better-preserved wall structure than the mollusks because of their originally high-Mg calcite test composition (Scholle and Ulmer-Scholle, 2003).

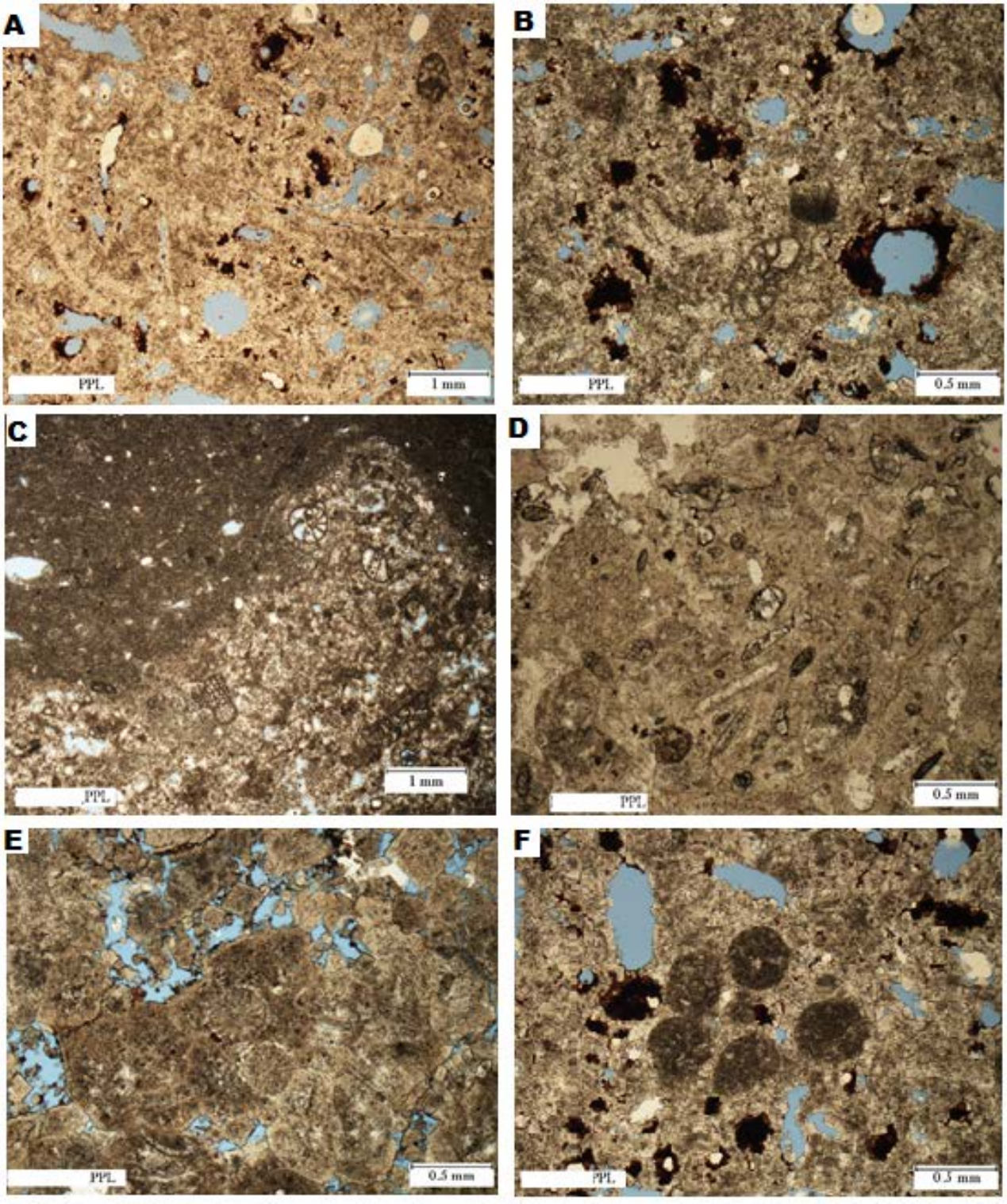

Figure 8. Photomicrographs of microfacies 1. MF1 is typically characterized by a bioclastic packstone with abundant shell fragments and moldic porosity (A). Foraminiferal outlines are common and occasionally well-preserved foraminifera with oil stained tests accentuate the outline of the porcelain wall (B/D). "Clotted" fabric (C) represents probably burrow filled with coarser material and better-preserved foraminifera. Burrows are recognizable in many instances because of the textural contrast between the burrow fill and the surrounding sediment. Relict oöid structures are common, but rarely well preserved as in the case of the radial oöid (E) with other bioclasts such as pellets (F).

Microfacies 2 (MF2): Medium-Coarse Crystalline Dolomite

Description: Microfacies 2 generally grades into microfacies 3 with a gradual decrease from medium-coarse crystalline dolomite, in some places showing a dolomite growth front (Figure 9A). MF2 is characterized by recrystallized dolomite with anhydrite cement. Dolomite crystals size and shape range greatly. These unfossiliferous, medium- to coarse-crystalline dolomites form dense mosaics of subhedral to anhedral crystals with well-defined crystal boundaries and are commonly zoned with dark cloudy cores and a clear rim. Vuggy porosity is common and fractures are present locally. Anhydrite forms a cement in some areas.

Interpretation: This dolomite facies is interpreted to represent an intermediate to late-diagenetic replacement dolomite similarly associated with supratidal (marine sabkha) environment (Wilson, 1975). Replacement dolomite has cloudy cores (initial growth phases rich in host-mineral inclusions or early-formed, metastable precipitates) and clear exteriors (Flügel, 2010). The cloudy cores have been interpreted to reflect mixing zone conditions in which metastable, inclusion-rich dolomite formed (Scholle and Ulmer-Scholle, 2003), and are likely a late-diagenetic, possibly telogenetic (uplift-stage) alteration, which tends to produce hollow crystals due to selective leaching of the cores of these dolomite crystals. A shift to more marine conditions precipitated the more inclusion-free, limpid dolomite outer cores that may, in part, be cements. Compositional variations in dolomite crystals are commonly great enough that selective dissolution is almost the norm in altered dolomites. The inclusion-rich, cloudy dolomite cores are generally more susceptible to leaching than the clear rims.

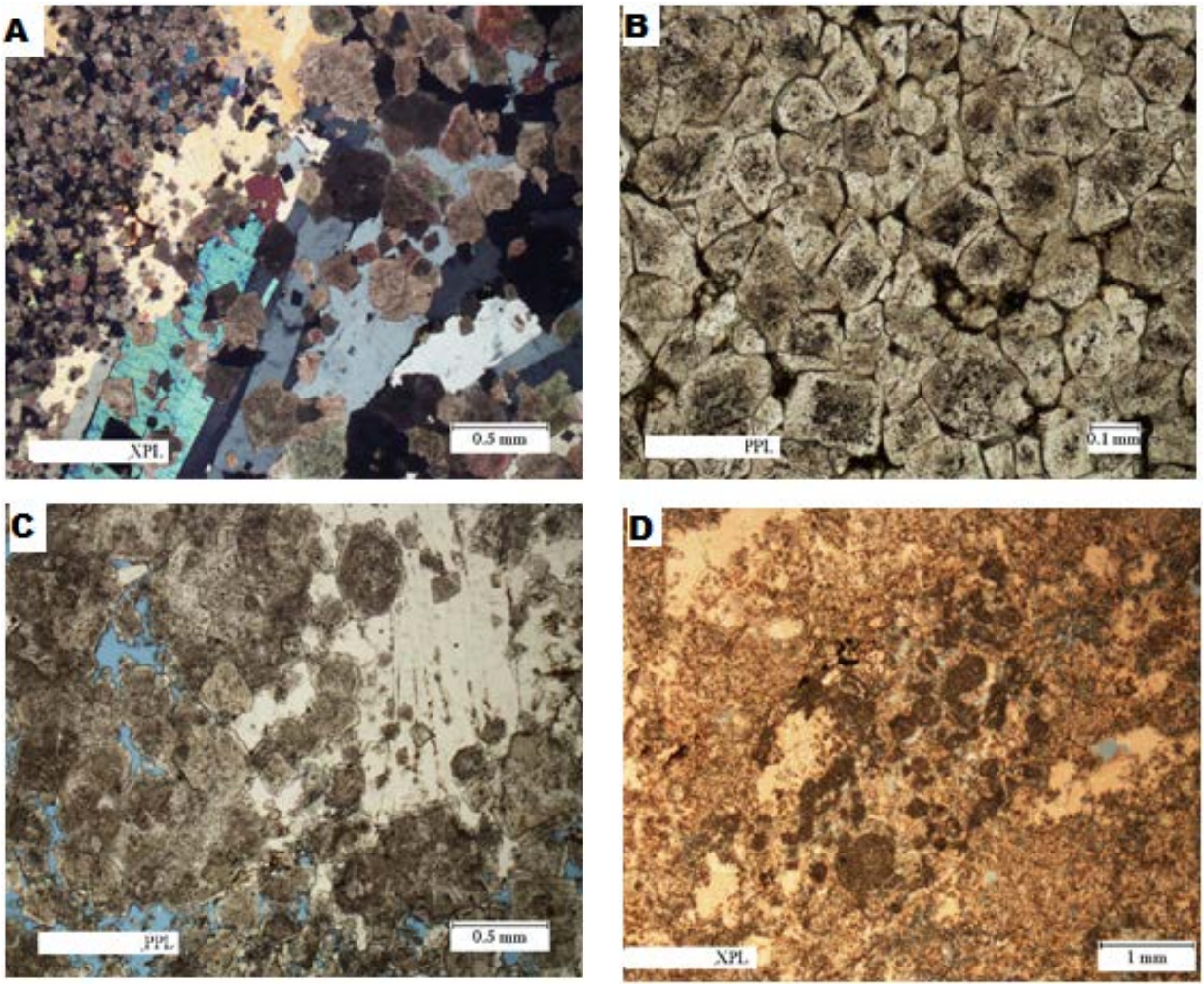

Figure 9. Photomicrographs of microfacies 2. A. Gradational front showing varying sizes in the dolomite crystals. Most of the open pore spaces in this sample have been filled with bladed anhydrite. More typically, MF2 is characterized by largely euhedral dolomite with crystals that have dark cores and limpid rims (B). This is an extremely common fabric in most dolomites. The rhombic outlines and zoning here are characteristics that allow recognition of dolomites. C. Another typical example showing some zoned dolomite with associated anhydrite. Some dolomite crystals have faint appearances of oöltes and possibly marks the boundary of transition with microfacies 1. Dolomite crystals are observed in some places with more clearly visible oöids and pelloids (D).

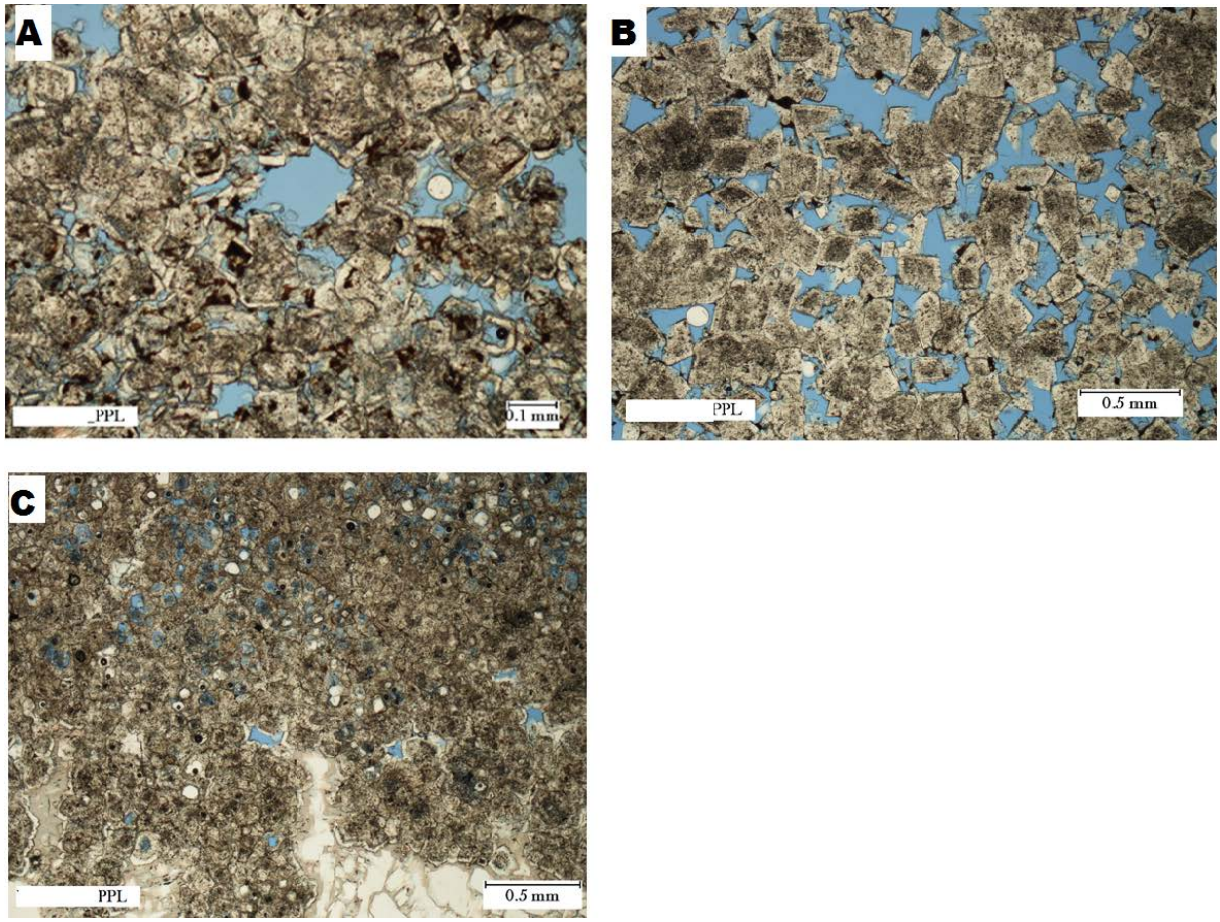

Figure 10. Photomicrographs of rhombic-zoned dolomites in microfacies 2. These rhombic dolomites are typically zoned with dark cores and lighter rims. In some cases, most of the centers have been leached (A) and interparticle porosity is high (B). Some oölitic textures also show the nucleation centers of the dolomite rhombs (C).

Microfacies 3 (MF3): Fine Crystalline Dolomite (Mudstone)

Description: This microfacies consists of a non-laminated unfossiliferous dolomitic mudstone, usually associated with minor anhydrite. Very fine-crystals are dominant with a network of fractures (Figure 11). Some fractures are lined with coarse dolomite crystals with equant anhydrite filling the rest of the pore space (Figure 12C/D). In other areas, anhydrite nodules (0.4mm) are scattered and common. Stylolites are also present and pyrite tends to accumulate in these (Figure 12C). These dense mosaics contain no recognizable allochems.

Numerous fractures radiate away from stylolites. Dolomite and anhydrite crystals fill the wider segments of the fractures.

Interpretation: This finely crystalline dolomite microfacies was likely deposited in a supratidal (marine sabkha) environment. A normal sabkha deposit consists of marine microbially controlled carbonate muds, nodular sulfates, and possible desiccation crusts (Flügel, 2010). The micrite matrix has a very fine crystal size and is likely of physicochemical origin as indicated by the evaporate minerals and complete lack of fossils. The small crystal sizes (<60 μm), are restricted to peritidal environments (Amthor and Friedman, 1991). The fine crystal size is probably a result of an early replacement of precursor of peritidal lime mudstone or of neomorphism of a penecontemporaneous or early diagenetic dolomite (Zenger, 1983; Amthor and Friedman, 1991). The nodular anhydrite represents growth by the displacement of soft sediment after deposition of the dolomite mudstone and should be considered an early diagenetic facies (Scholle and Ulmer-Scholle, 2003). Chemical dissolution takes place in many forms in carbonate rocks, and stylolites are probably the most readily identifiable of them. The stylolite in the micritic matrix is marked by a concentration of insoluble materials along its irregular surface. The surface represents a pressure-induced zone of dissolution with differential grain interpenetration (Scholle and Ulmer-Scholle, 2003). Stylolite formation is associated with thin water films that allow solutes to move away from selected sites during pressure-induced dissolution (Scholle and Ulmer-Scholle, 2003). Although the dolomite clearly occupies the position of a cement, primary dolomite cement can be very difficult to distinguish from dolomite formed by replacement of a precursor calcium carbonate cement.

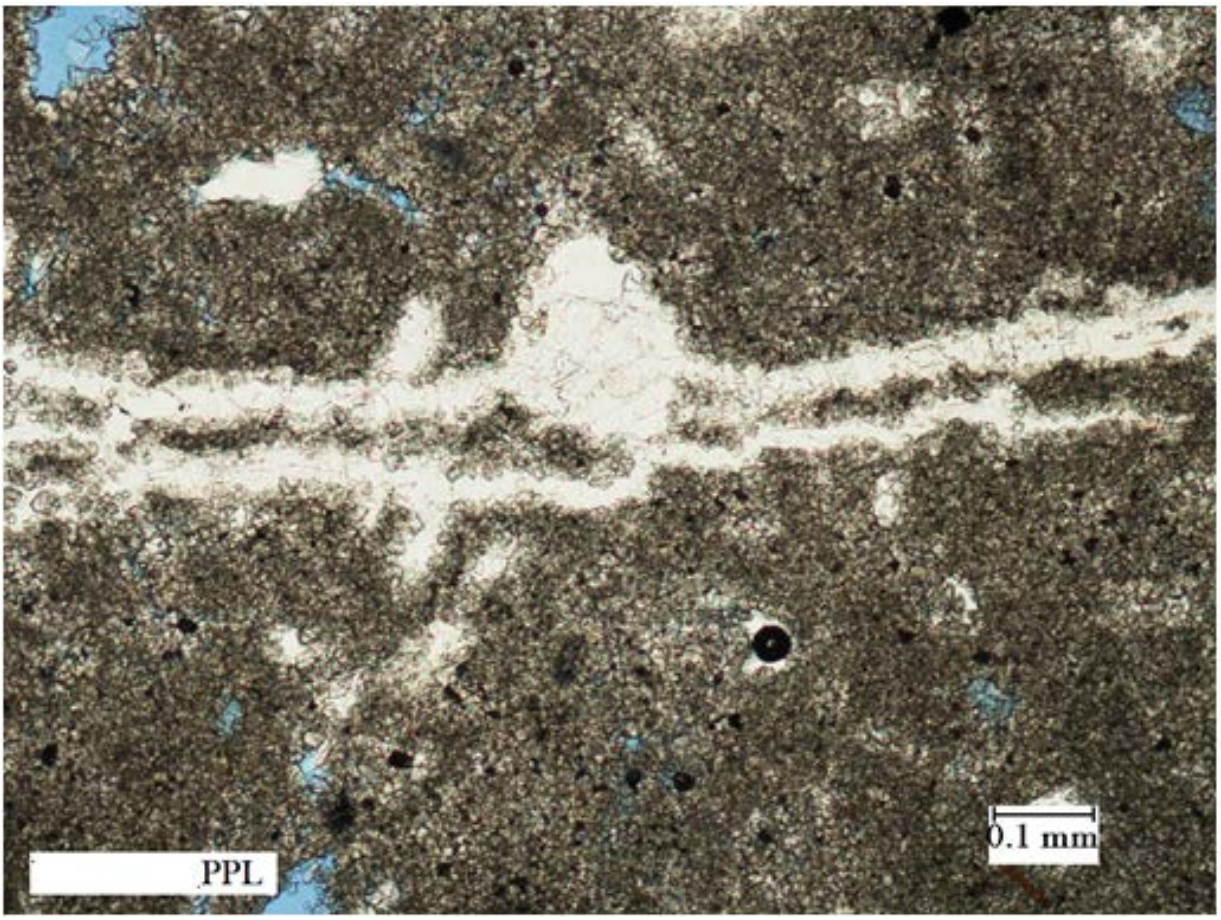

Figure 11. Typical microfacies 3 sample showing fine crystalline dolomite with anhydrite filling fractures.

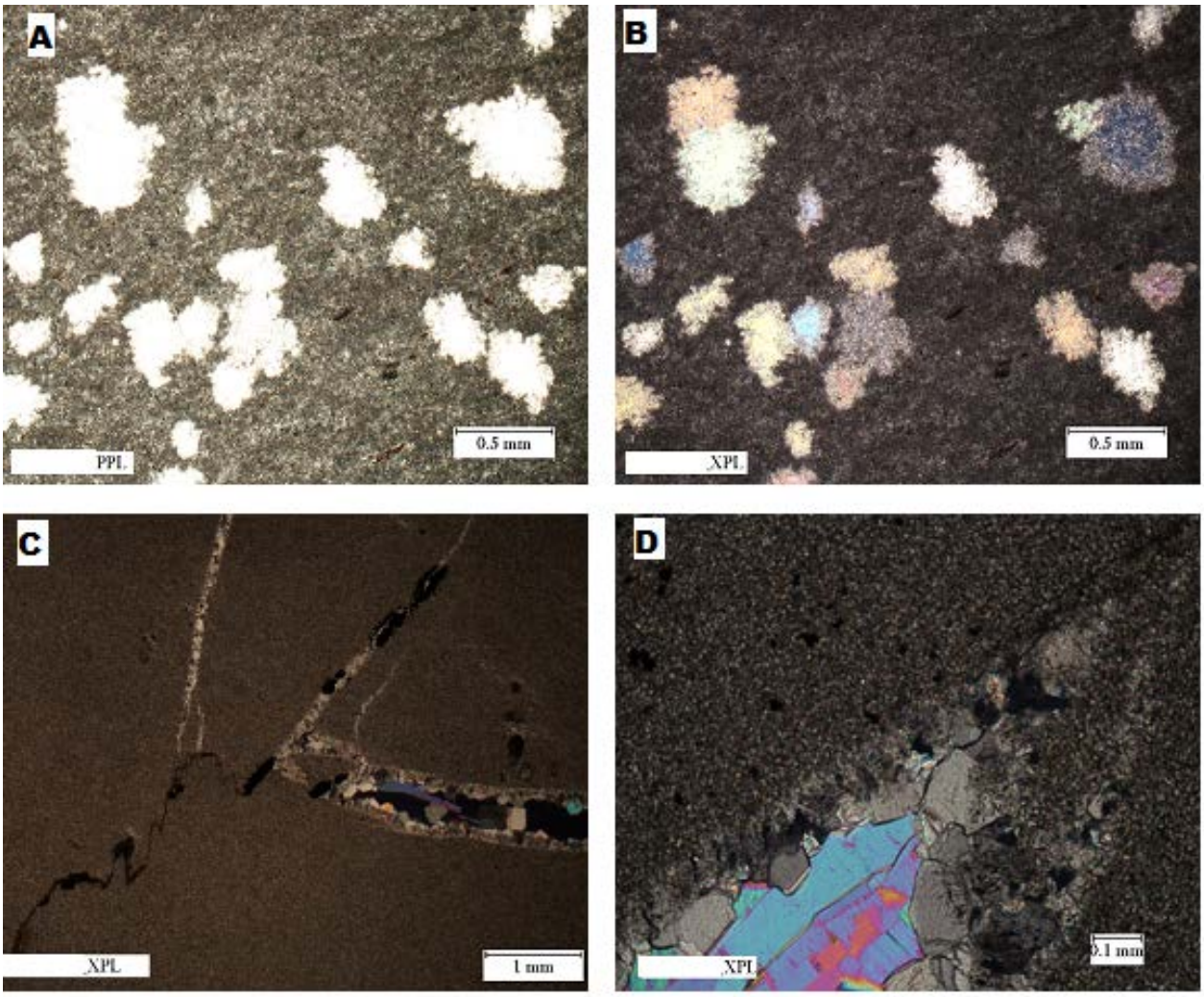

Figure 12. Photomicrographs of microfacies 3 (MF3). MF3 is characterized by mudstone with associated anhydrite occurring as sparse and isolated nodules (A/B). This mudstone is generally composed of fine-crystalline (subhedral) mosaic dolomite, usually forms dense, dark mosaics of interlocking subhedral to anhedral crystals. Fractures occur occasionally within this microfacies and are lined with equant dolomite and subsequently filled with anhydrite (C/D). These fractures typically radiate away from inflection points on a stylolite. Stylolites contain a concentration of pyrite as shown in C.

Microfacies 4 (MF4): Anhydrite

Description: The anhydrite microfacies consists dominantly of pure anhydrite, generally consisting of an aggregate of fibrous crystals. Small-aligned laths are common and usually display a flow-like texture; these crystals vary from parallel and subparallel to a combination of equant, felted, and laths with random and irregular orientations (Figure 13). So-called “chicken-

wire" texture was also observed. In some places, the anhydrite has been hydrated to form secondary gypsum, which contains scattered euhedral dolomite.

Interpretation: Anhydrite deposits are generally indicative of supratidal (marine sabkha) environments (Scholle and Ulmer-Scholle, 2003). These evaporites form a good seal due to the lack of porosity. Gypsum typically replaces anhydrite upon the uplift of evaporate sequences or after removal of overburden sediments (Flügel, 2010). These evaporate deposits are interpreted to have formed originally by evaporation in a marginal-marine environment.

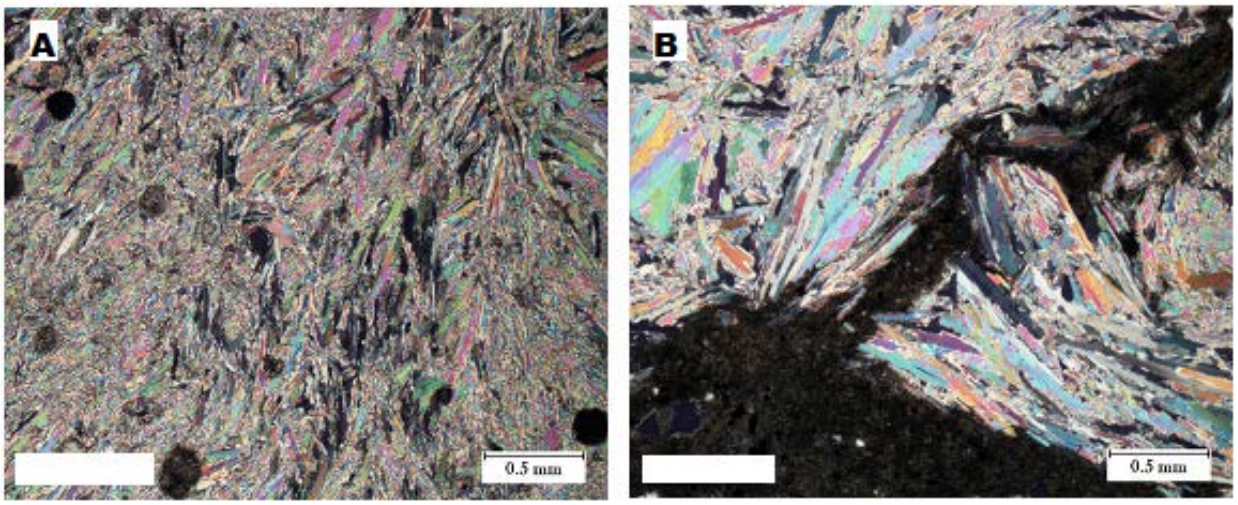

Figure 13. Photomicrographs of microfacies 4: Anhydrite. These samples a representative of the textures and fabrics observed in MF4, including lath (bladed) anhydrite showing a flow-like texture and scattered dolomite (A) and lath anhydrite in contact with shale (B). Acicular to fibrous anhydrite texture dominates MF4.

Microfacies 5 (MF5): Dolomite with Quartz Clasts

Description: This microfacies consists primarily of highly recrystallized dolomite with scattered quartz and feldspar grains. The dolomite is very tightly spaced and shows no visible porosity. Whereas the quartz grains are subangular to angular in nature and range greatly in size from ~0.1mm to over 1mm. Scattered feldspar grains occur as well, and appear to be

highly weathered. Fossils in this microfacies are rare, but a few foraminifera and skeletal grains were observed within the dolomite. Faint remnants of oöid grains also occurred in some areas.

Interpretation: This microfacies is typical of the base of the Yalbac formation and marks a transitional phase from the alternating carbonate clastic sequence of the Hillbank to a pure carbonate system in the Yalbac. The dolomites are likely the result of a restricted lagoonal setting with minor influxes of terrigenous sediments. The depositional regime moves to a marginal marine system with slight terrigenous influence, marked by the presence of the few angular quartz grains. Depositional in MF5 is dominated by carbonate material.

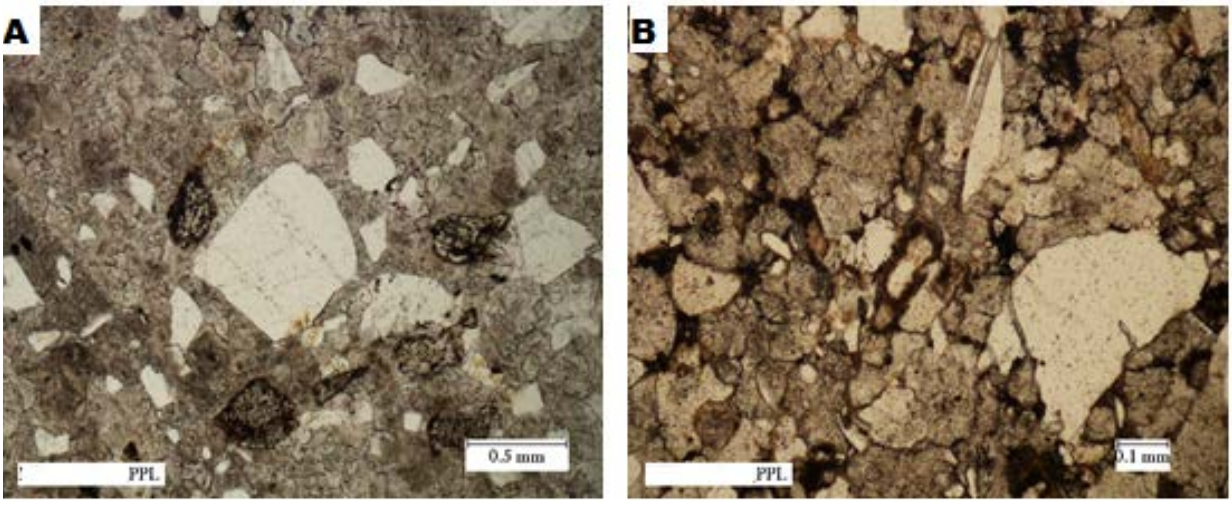

Figure 14. Photomicrographs of microfacies 5. Sample from MF5 typically show highly recrystallized dolomite with scattered quartz and feldspar grains (A). Scattered quartz are angular (B), mostly monocrystalline and undergo slightly undulose extinction, indicating some but not extreme burial and diagenesis from the source. Bitumen fills some of the pore spaces and has stained some crystals mostly along the contact edge.

Microfacies 6 (MF6): Shale

Description: Microfacies 6 consists dominantly of laminated shale and siltstone. This microfacies characteristically is an alternation of dark green shale, with lighter quartz-rich siltstone with common pyrite. Well-segregated laminated beds are common also with micro-

laminations and some silt-filled burrows. Quartz grains are generally fine but can be as large as 1mm in diameter.

Interpretation: This microfacies is interpreted as lacustrine or overbank (floodplain) deposits, which formed in connection with the fluvial channel sands and humid fan deposits of the related clastic facies noted above. These fine laminae are in some places interrupted by large clastic grains, which may be dropstones (for example, see Figure 15A). Bioturbation (tubular, silt-filled burrows) are likely from fresh-water infauna of unknown taxa. Similar, laminated deposits have been interpreted as overbank deposits in the underlying Margaret Creek formation (King and Petruny, 2013).

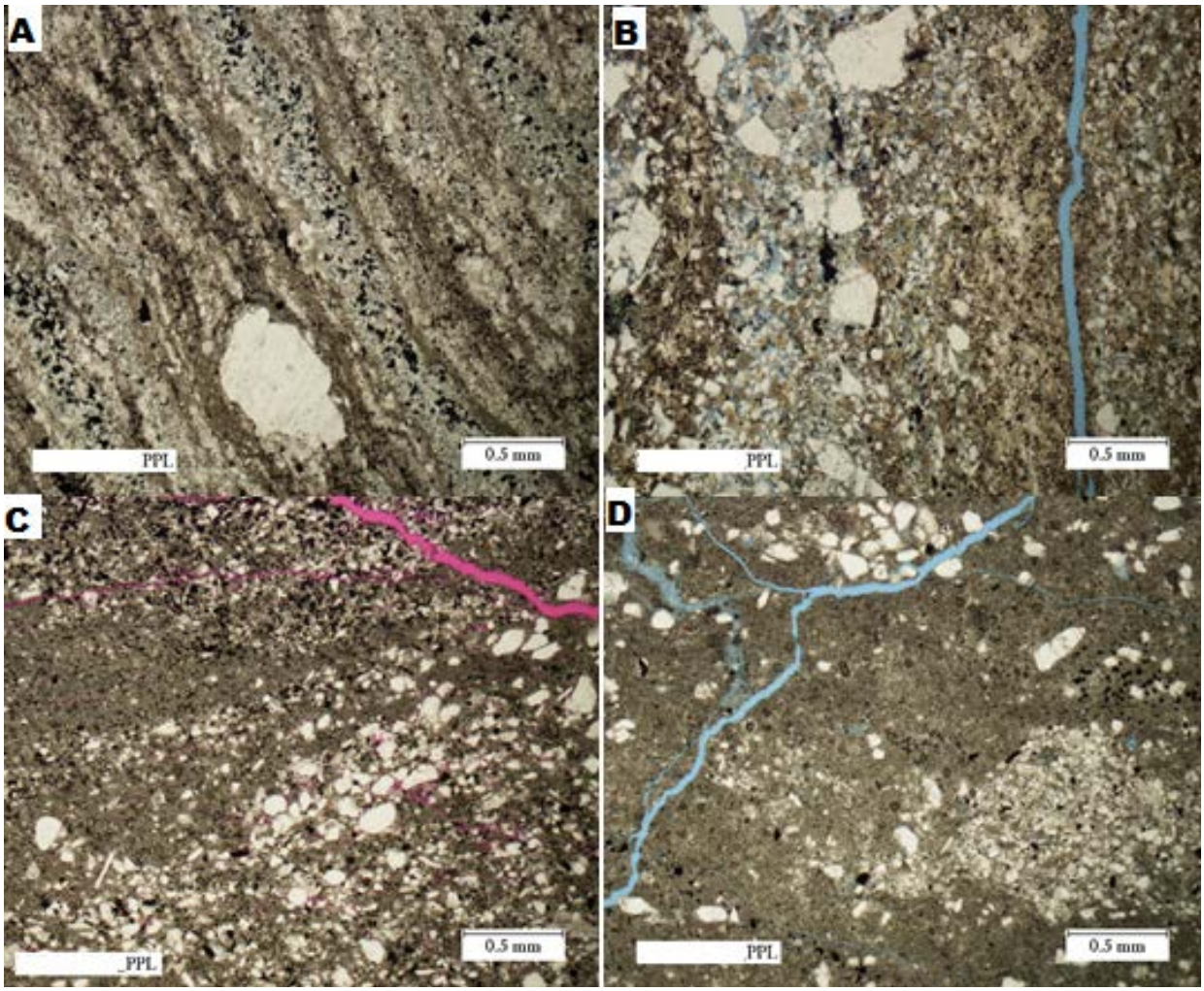

Figure 15. Photomicrographs of microfacies 6. These shales are commonly laminated (A) and rare dropstones can be observed (bottom-center A). Grain size varies and coarser-quartz layers are typically segregated (B/C). Bioturbated areas are infilled with larger clastic grains (D).

Microfacies 7 (MF7): Arkosic Sandstone

Description: This clastic microfacies consists of angular, poorly sorted arkosic sandstone. Dominantly quartz and feldspars grains occur and in some places are associated with dolomite and anhydrite cement; by definition, this microfacies contains more than 25% feldspar grains. Quartz is dominantly monocrystalline and undergoes slightly undulose extinction, but also consists of some polycrystalline grains and dolomite. Highly weathered feldspar grains are common. These weathered feldspars, along with dolomite crystals and in

some areas illite, make up most of the matrix. In some places, pyrite framboids also occur. Interparticle porosity is >25% in some areas.

Interpretation: The texture and mineralogy of MF7 suggest a fluvial transportation of sediment with a relationship to basement uplift, perhaps near a granitic source. The angularity of the grains indicates that transportation was relatively near to the source. Based on the common slightly undulatory quartz grains and relative lack of polycrystalline quartz, the sandstone is likely from a common or plutonic (granitic) provenance (Ulmer-Scholle et al., 2015). Weathering of feldspars (illitization) is common either before or after deposition (Pettijohn et al., 1972), and so gives no conclusive evidence for further interpretation of the depositional environment.

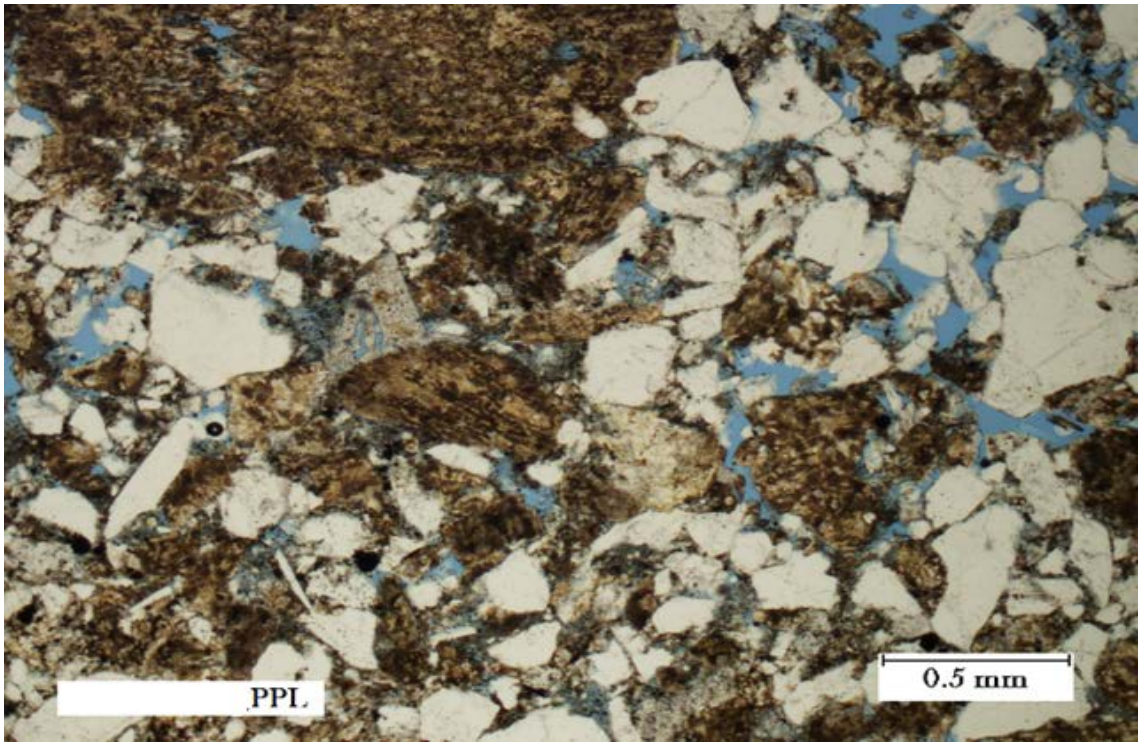

Figure 16. Typical arkosic sandstone consisting microfacies 7. Quartz grains are generally monocrystalline and angular in nature. Feldspar grains are common and characteristically display common weathered texture. Detrital clays make up some of the matrix and fills pore. Interparticle porosity is high.

Microfacies 8 (MF8): Subarkose Sandstone

Description: This microfacies is characterized by angular, poorly sorted quartz grains with minor amounts of feldspars and clays. Quartz is dominantly monocrystalline, but also consists of some polycrystalline grains and occasionally is associated with dolomite. The quartz grains display slightly undulose extinction. Minor amounts of weathered feldspar are present. Porosity is generally high and in some instance anhydrite forms cement between the grains or illite clay rims the grains (Figure 17).

Interpretation: This sand has characteristics consistent with a fluvial channel or humid fan deposit. The petrology is substantially similar to interpreted fluvial and fan facies of the underlying Margaret Creek formation in central Belize (King and Petruny, 2013). In particular, the angular grains and weathered feldspars are common in the Margaret Creek formation. The presence of polycrystalline quartz is not unusual, as they are typically of sandstones but seem less stable and tend to be eliminated (Pettijohn et al., 1972).

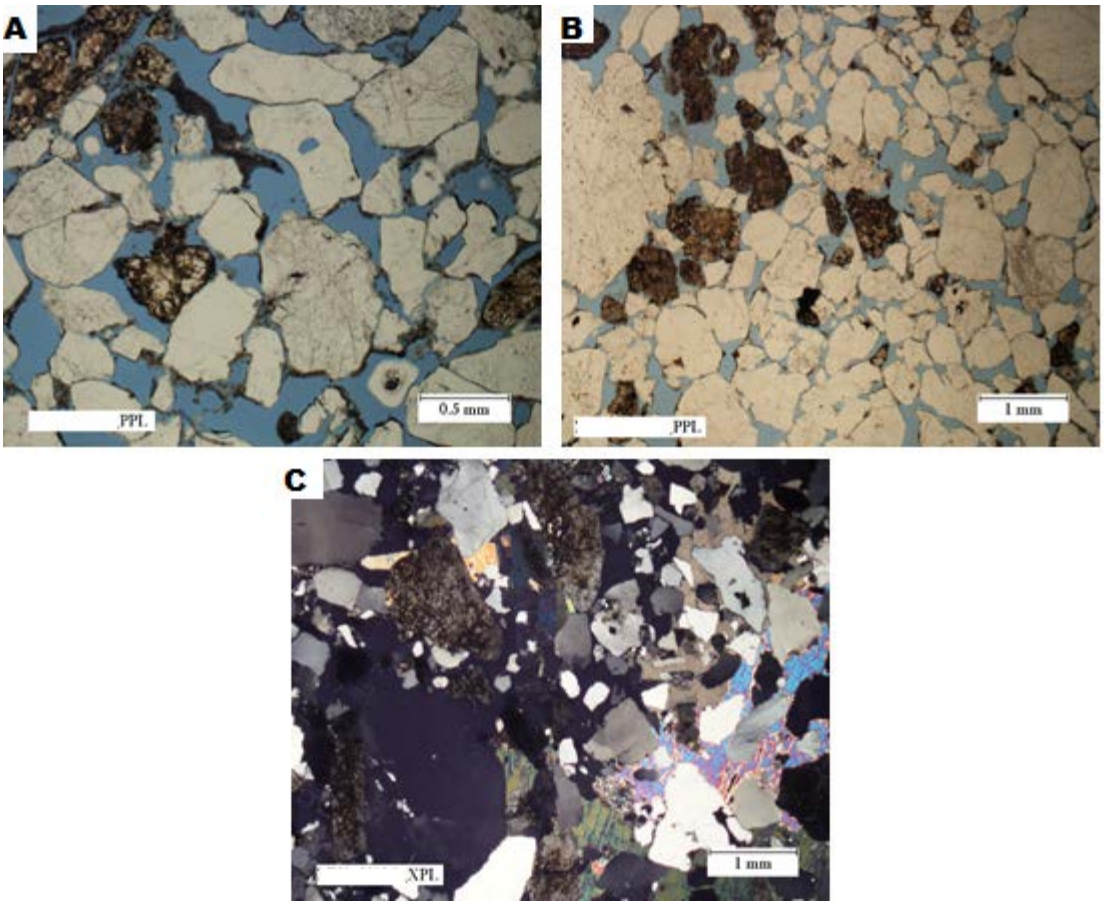

Figure 17. Typical samples of microfacies 8 showing dominantly sub angular to angular quartz grains with minor of weathered feldspars. Illite occasionally forms rims on the grains (A), and anhydrite cement (C) is a common constituent.

Microfacies 9 (MF9): Lithic Arkose Sandstone

Description: This microfacies is characterized by a combination of quartz, feldspars, and several types of lithic fragments (including chert and granite fragments). The quartz grains are mostly monocrystalline, and undergo slightly undulose extinction. Porosity is greatly reduced in this microfacies, and illite generally occurs at the grain boundaries. Feldspars and lithic fragments occur scattered throughout the sample.

Interpretation: Microfacies 9 is interpreted as a humid fan deposit based on its quartz and feldspar content and angularity. The illitic grain boundaries are interpreted to have formed

within the humid fan environment as result of groundwater flushing (Scholle and Spearing, 1982). This fluid circulation in the subsurface during diagenesis is what frequently reacts with the detrital grains resulting in clay cementation (Scholle and Spearing, 1982).

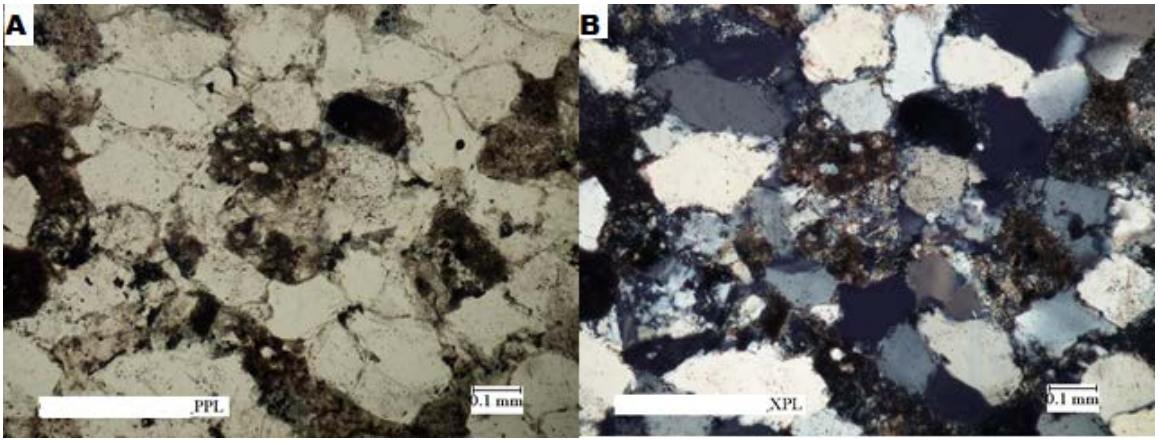

Figure 18. Photomicrographs of microfacies 9. This microfacies' mineralogy is dominantly quartz, feldspar and varying lithic fragments including chert, granitic fragments and opaque clasts.

5.2. Diagenetic Alterations

Pyrite is the most abundant iron sulfide mineral found in carbonate sediments, as well as sandstones (Pettijohn et al., 1972; Scholle and Ulmer-Scholle, 2003). Pyrite is commonly found in the dolomitic microfacies and often associated with fractures/stylolites, likely because of a concentration of organic material and oil in these samples. Framboidal pyrite or pyrite with a raspberry-like morphology are the most common morphology observed, however nodular pyrite also occurs. Framboids are almost perfectly spherical bodies of small, interlocking pyrite crystals (Scholle and Ulmer-Scholle, 2003). These spherical aggregates typically form discrete bodies, but they are also found in clusters or multiple spheroids (Figure 19A). Framboidal pyrite formation has several likely environments. In the observed samples, they are thought to be authigenic in origin and based on the close association of clusters with stylolites, it is interpreted

that they formed in reducing microenvironments associated with decomposing organic matter (Scholle and Ulmer-Scholle, 2003).

Diagenetic alteration of clay minerals is not wide-spread and locally is associated with the feldspathic-rich sandstones. The observed clays appear to be well crystallized and either form a rim around detrital grains or fill pore spaces (Figure 19B). This would seem to indicate that these clays are authigenic in nature and were precipitated from a solution due to the invasion of fresh groundwater (Pettijohn et al., 1972).

Most of the dolomite features and alterations have previously been described with their associated microfacies. However, an additional diagenetic alteration appears to have formed the clear dolomite cement rims, as shown in Figure 19C. While it is difficult to distinguish true dolomite cements from dolomitized precursor calcite cements without additional methods such as cathodoluminescence microscopy (Scholle and Ulmer-Scholle, 2003), here it is interpreted as true dolomite cements. This is partly because of the dominance of rimmed dolomite in previous samples, as well as the general euhedral rhombic nature of the cements (more typical of dolomites, whereas calcite would likely be bladed).

An unusual quartz overgrowth texture was also observed (Figure 19D). While this texture was not common, it is certainly worth mentioning as it likely relates to fluid flow or dissolution within the basin. The quartz overgrowth texture can be attributed to two likely processes: (a) quartz overgrowth crystals may be precipitated as the product of crystallization from a supersaturated pore solution passing over detrital surfaces; or (b) the quartz overgrowth is the final precipitate in the recrystallization process by which an amorphous silica precipitate was locally dissolved and immediately re-precipitated as quartz (Pettijohn et al., 1972). The

isolation of this overgrowth texture would lend favor to the local dissolution and re-precipitation process. Minor glauconite and phosphate minerals were also observed.

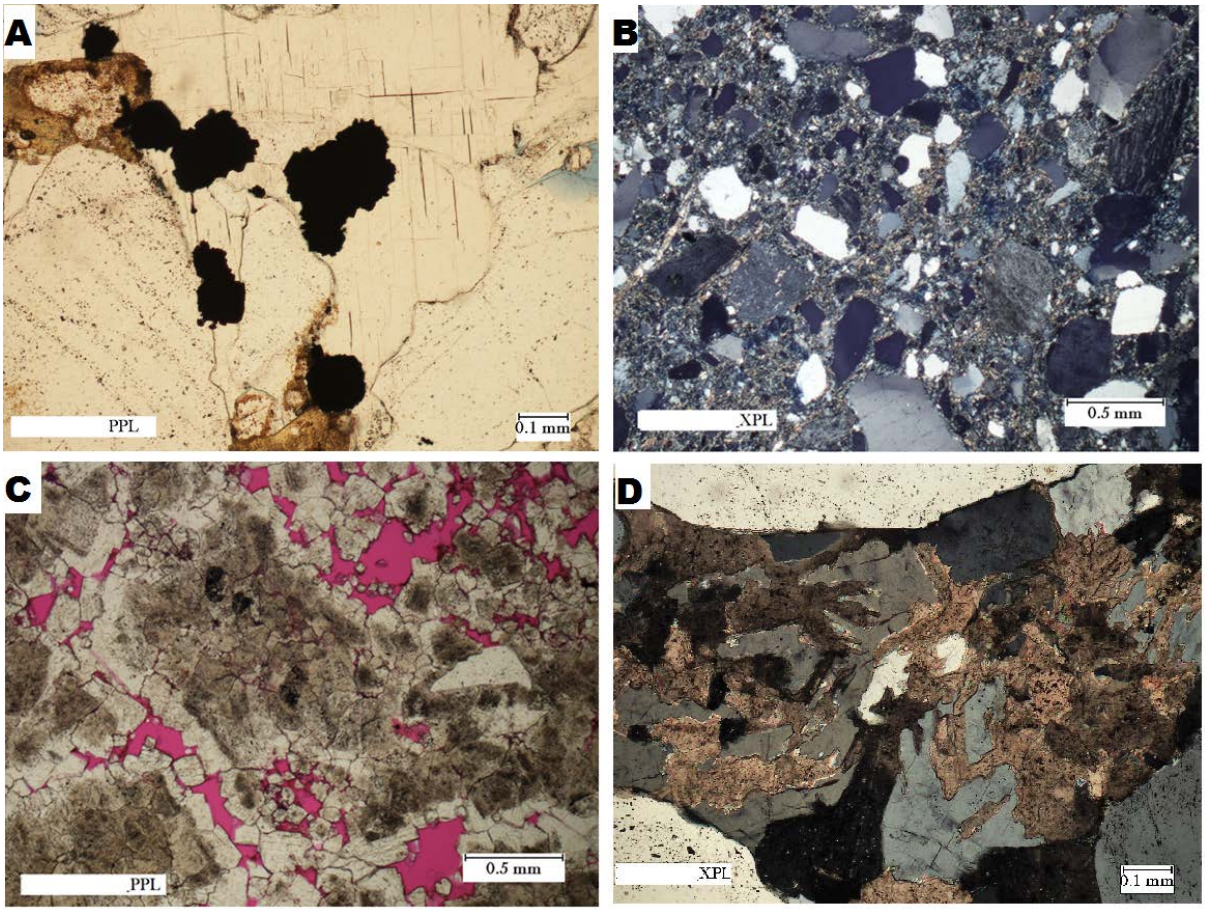

Figure 19. Photomicrographs of diagenetic alteration textures in the Corozal basin.

Anhydrite and gypsum are also common diagenetic minerals found throughout the basin (Figure 20). The occurrence of these minerals as cement is clearly related to evaporite-forming conditions at the time of sedimentation or to movement of hypersaline pore waters from an overlying formation of evaporites (Murray, 1964). The hydration of anhydrite to gypsum occurs readily when exposed to water and explains the alteration rim occurring along the crystal walls (Figure 20B; Deer et al., 1992). Whereas these minerals do not give any further details on the

environment, they do substantiate a sabkha flat sedimentation as their origin is much the same as for dolomite (Pettijohn et al., 1972).

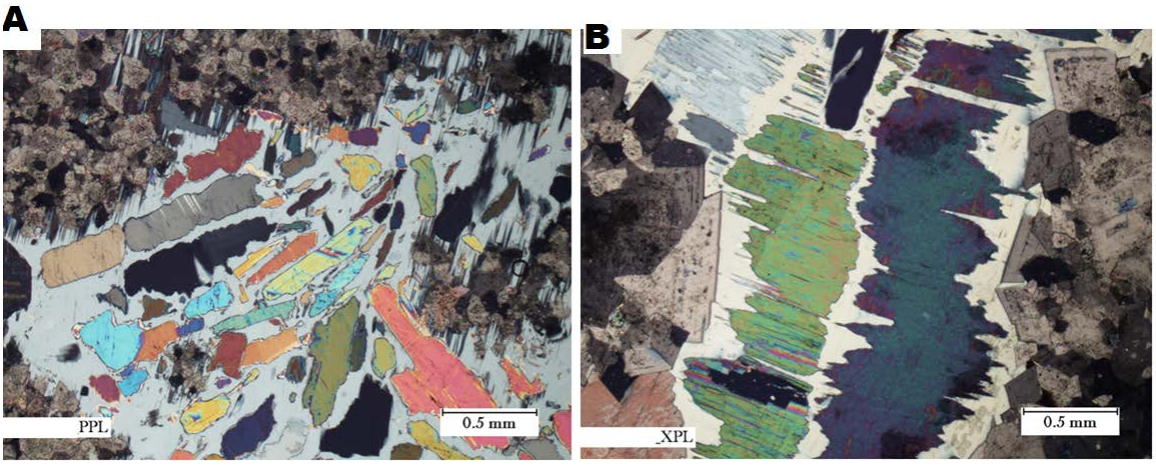

Figure 20. Photomicrographs of anhydrite undergoing the process of hydrating to gypsum.

5.3. Correlation

Following the study of individual thin-sections, each sample was categorized into a microfacies based on the previously outlined descriptions. The display of microfacies distribution were created using cross-sections generated from IHS Petra. The formation tops, including subdivision by informal members, were uploaded from previous interpretation by BNE personnel. The diamond symbols represent the subsurface depth of the thin sections and the color corresponds to its assigned microfacies at that location (see legend, Figure 21). The Yalbac members are characterized by MF1-5. The Hillbank members generally show an alternation between the clastic microfacies (MF6-9) and the carbonates (MF1-4) with MF5 as a carbonate-clastic transitional facies.

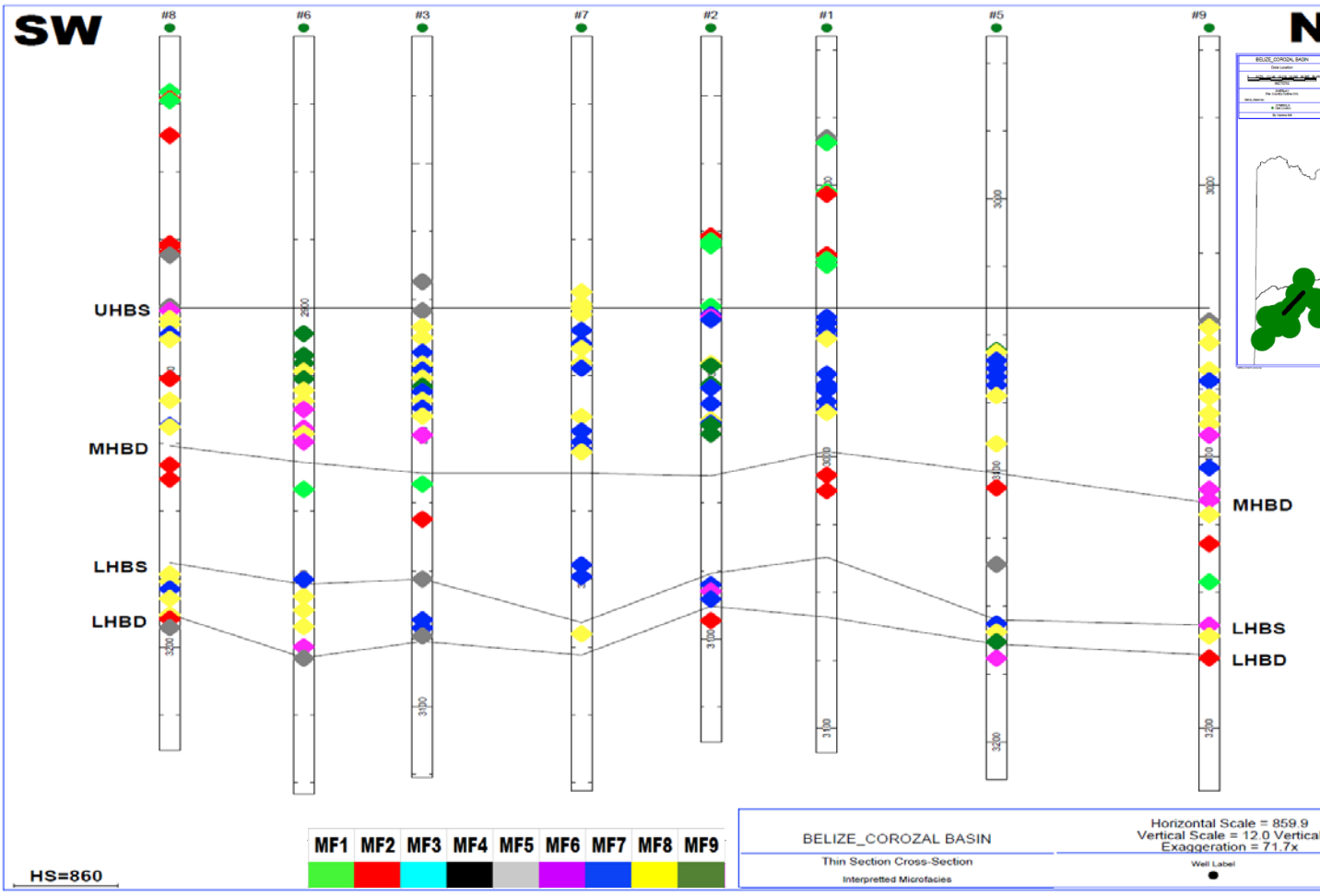

Figure 21. Panel diagram showing microfacies distribution of the Yalbac and Hillbank formations. This cross-section is oriented in a general southwest-northeast direction and the solid black line on the inset map shows its approximate location. Formation tops are labeled and marked by a solid black line, and correlated using a well-well comparison. Datum is the top of the Upper Hillbank sandst Thin section locations are represented by the diamond symbol and colors correspond to the microfacies indicated in the legend.

The BC formation is dominated by MF2 constituting a medium to coarse crystalline dolomite. The Y2 formation also contains mostly MF2, but shows a more cyclical succession with the influence of MF1 and MF3 as well. The Hillbank formation overall shows an alternation between the clastic microfacies (MF6-9) and the carbonates (MF1-4) with MF5 occurring as a transitional zone near the contact between the clastic and carbonate members.

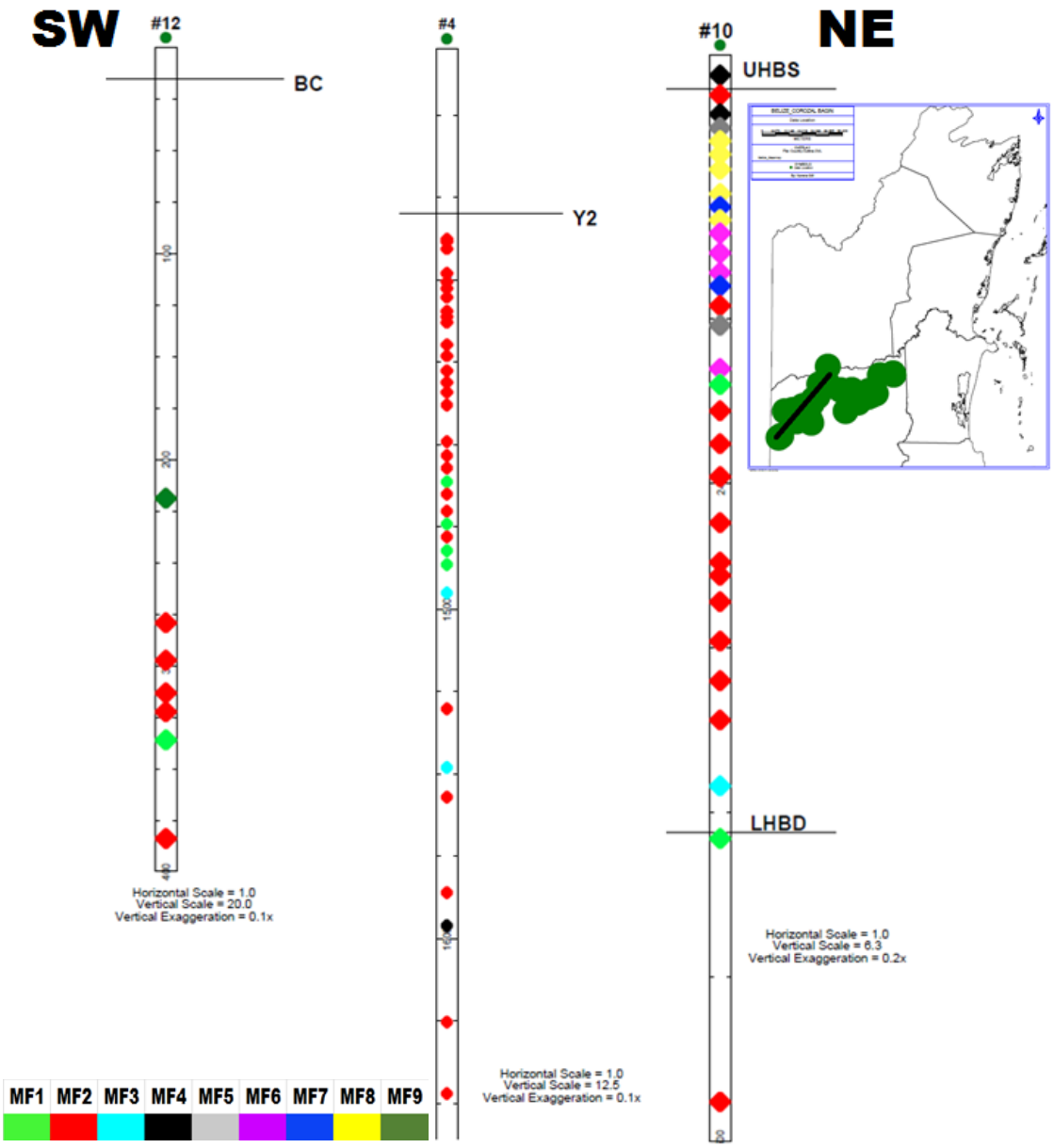

Figure 22. Individual microfacies display of the wells that intersect the BC, Y2 and HB formations. These wells are not drawn to a common scale and positions are not scaled to each other. Each section is displayed using subsurface elevation and there is no common datum. Thin section locations are represented by the diamond symbol and colors correspond to the microfacies indicated in the legend. Formation tops are marked by a solid black line and labelled.

5.4. Interpreted Depositional Environment

The Corozal basin has evolved from a continental to marginal marine clastic environment during Late Jurassic, to a broad restricted carbonate/anhydrite shelf during Cretaceous (Bustamente and Wetzel, 1992). This is supported by the clastic sequences observed in the Hillbank and gradual progression to a carbonate-dominated system with primary dolostone and evaporate-rich rocks in the Yalbac and Barton Creek formations (Figure 23). Whereas there were no petrological samples from the Margaret Creek (MC) formation in this study, a previous study by King and Petruny (2013) describes a comparable petrology to the Hillbank sandstones. The description of the microfacies environments of this study is initiated with the deposition of the LHBD. Following the deposition of the lowermost transitional nonmarine-marine clastics of the MC formation, seas transgressed over the northern Belize shelf, at which time a thick massive dolostone, termed the LHBD of the Hillbank formation was deposited (Hibbard, 1988). The LHBD generally is described as a medium- to coarse-recrystallized dolomite (MF2). However, in some areas, it is rich in silts and shales (MF6) and where closer to the contact with the overlying LHBS, it grades into the transitional MF5 (distinguished by terrigenous clastic grains occurring within the dolomite).

The LHBS is generally an arkosic to subarkosic sandstone with angular poorly sorted quartz and feldspar grains. This member is characterized by two microfacies: MF7 and MF8. The MHBD likely marks a subsidence event in the history of the basin, as the more clastic-influenced systems transgress into a marine system once more. This contact is marked by the transitional MF5 where angular quartz grains are scattered in a dolostone. MF5 is gradually surpassed by a near completely restricted

lagoonal/sabkha environment, with MF3 and MF4 becoming the dominant microfacies. As the basin continued to evolve, an uplift and erosional event led to the deposition of the UHBS, the base of which is defined commonly by finely laminated sediments of MF6. Clastic microfacies alternate throughout this member, primarily a feature of varying degrees of feldspar content. Longman (2009) suggests the likely source for both the UHBS and LHBS is the Maya Mountain granite or granites which are rich in potassium feldspar and low in mica, a finding that is consistent with what is observed in these thin section studies. The Maya Mountain granites are dated mid-Paleozoic (Bateson, 1972). Further investigation into this relationship is needed and analytical age tests can likely define the relationship of the two.

In a continuation of marine sedimentation, the Yalbac formation was deposited conformably over the Hillbank (Hibbard, 1988). The Yalbac consists of interbedded dolostones and dense anhydrites, representing the same cyclic, restricted marine, carbonate-evaporite, depositional conditions that prevailed in the Lower Cretaceous over much of the entire Gulf Coast basin (Hibbard, 1988). This marine transgressive event marks the contact between the UHBS and lowermost Y3 member of the Yalbac formation. Transitional MF5 very commonly occurs near the base of Y3, and this indicates a shift from the clastic system of the UHBS to the marine section of carbonates and evaporates, which are recorded by the stratigraphy in the rest of the basin's depositional history. This carbonate/anhydrite section in the Corozal Basin is interpreted as being deposited in a shallow marine, hypersaline environment, wherein the percent of anhydrite increases shelf-ward to the west (Bustamente and Wetzel, 1992). The carbonate microfacies (MF1-5) are characteristic of the Yalbac members, as well as the overlying Barton Creek formation. MF3 occurs most commonly in the Yalbac, probably

because the extent of dolomitization has obliterated most of the original depositional features of the bioclastic MF1. Oölites are also present in some places and this more clearly indicates the possibility of relatively high energy conditions (Hibbard, 1976). As deposition of Y2 commences, the more anhydritic microfacies (MF3 and MF4) emerge and the uppermost extent of Y2 is predominantly MF3. There were no available thin-sections of the Y1 member of the Yalbac formation (and no available drill core either), so a petrographic study of this member could not be conducted.

Following the restricted and cyclic carbonate-evaporite deposition during Early Cretaceous, shallow open marine shelfal conditions prevailed during the deposition of the limestones of the Barton Creek during Late Cretaceous (Bustamente and Wetzel, 1992; King et al., 2003) and MF3 continued to dominate the Barton Creek stratigraphic record.

These conditions continued through Paleogene when a sequence of shelf limestone and clastics were laid down over northern Belize (Bustamente and Wetzel, 1992). These sediments were deposited over a shallow marine shelf, which occupied all of northern Belize and adjacent areas of México and Guatemala (Hibbard, 1988). These conditions continued through Cenozoic and a sequence of shelf limestones and clastics were laid down over northern Belize (Hibbard, 1988). Deposition ended with regression of the seas from the area during late Paleogene and Pleistocene (Hibbard, 1988).

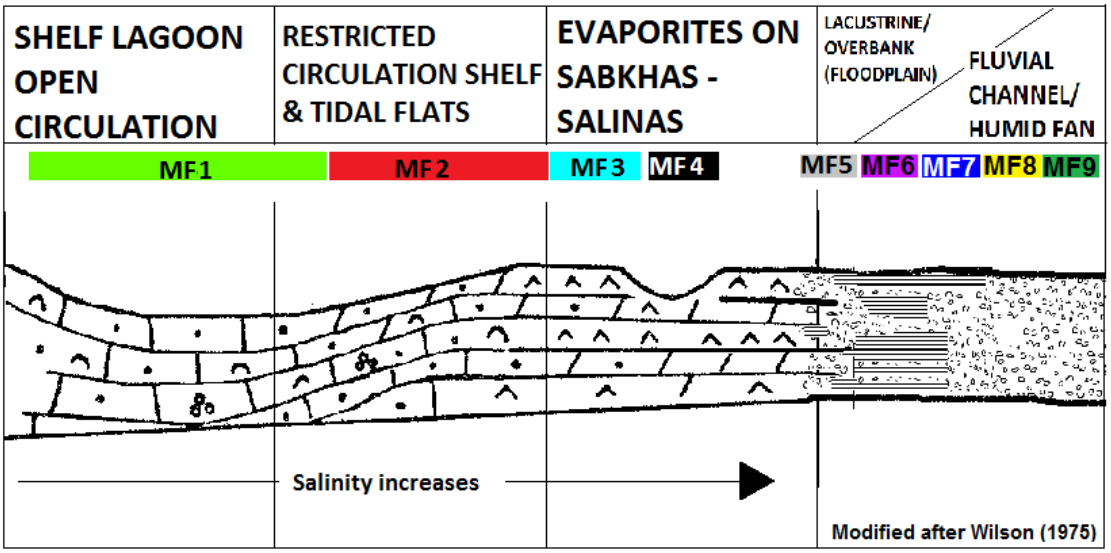

Figure 23. Depositional model of the Hillbank and Yalbac microfacies environments. The Hillbank formation is characterized by fluvial and carbonate facies that transition gradationally into the tidal flat and shallow shelf that characterize the Yalbac formation.

6. STRONTIUM ISOTOPE ANALYSIS

In this study, Sr-isotopic measurements were obtained in order to match with global Sr-isotopic values and obtain a possible numerical age for key stratigraphic intervals in the Corozal basin. Specifically, the carbonates of the Hillbank and Yalbac formations were targeted because these are only known to have inferred ages based on stratigraphic positions and minimal fossil evidence. Being able to correlate these two key formations with the global changes in Sr-isotopic values provides a very important understanding of how the Corozal basin has evolved and its relationship neighboring geology, as well as regionally.

After receipt of Sr-isotopic ratios, the following procedures were followed for analysis of the data. All Sr-isotopic data were normalized to a $^{87}Sr/^{86}Sr$ ratio of 0.1194. The isotopic data was used for correlation, which involved matching a sample $^{87}Sr/^{86}Sr$ to a $^{87}Sr/^{86}Sr$ calibration lines (charts available in Appendix 1) using the Bayesian approach probabilistic program, StronTer (Hercman and Pawlak, 2016). The updated LOWESS Version 5 Fit: 26/03/13 marine Sr-isotope curve was used (Howarth and McArthur, 1997; McArthur et al., 2001) and calculations were done using a single sample, normal distribution curve. The analytical results for sample set 1 are given in Table 2 and Figure 24 shows sample $^{87}Sr/^{86}Sr$ against the derived numerical age. Sample set 2 has analytical delays and the results were not available at the time of publication of this report. However, those results will be published in another separate paper.

Table 2. Isotopic Data for the Corozal Basin. Set 1 (sample numbers 1-22).

Sample Number	Formation	Age/Epoch			Sample 87Sr/86Sr	Standard Deviation	Well_Depth
1	BC	83	Late Cretaceous	**Campanian**	0.707450	0.000014	#14_1530
2	Y1	90		**Turonian**	0.707306	0.000008	#14_1590
3	Y1	90		**Turonian**	0.707276	0.000010	#14_1710
4	Y1	92		**Turonian**	0.707315	0.000010	#14_1950
5	Y1	94		**Cenomanian**	0.707369	0.000008	#14_1970
6	Y2	97		**Cenomanian**	0.707447	0.000009	#14_2000
7	Y2	101	Early Cretaceous	**Albian**	0.707433	0.000008	#14_2210
8	Y3	104		**Albian**	0.707407	0.000009	#14_2960
9	Y3	105		**Albian**	0.707414	0.000013	#14_3440.1
10	Y3	105		**Albian**	0.707402	0.000011	#14_3440.2
11	Y2	109		**Albian**	0.707384	0.000008	#14_2510
12	Y3	123		**Aptian**	0.707355	0.000010	#16_1940
13	Y3	125		**Barremian**	0.707429	0.000019	#16_1980
14	Y2	129		**Barremian**	0.707485	0.000009	#14_2540
15	Y3	133		**Valanginian**	0.707390	0.000011	#16_2050
16	Y3	190	Early Jurassic	**Sinemurian**	0.707368	0.000007	#14_4040
17	Y3	191		**Sinemurian**	0.707392	0.000021	#15_2020
18	Y3	192.5		**Sinemurian**	0.707496	0.000008	#14_4070
19	Y3	195		**Sinemurian**	0.707551	0.000011	#15_1950
20	MHBD	198		**Sinemurian**	0.707623	0.000009	#14_4160
21	LHBD	209	Late Triassic	**Norian**	0.707819	0.000009	#14_4220
22	LHBD	212		**Norian**	0.707881	0.000008	#14_4340

The following discussion is based on the interpreted ages from Sr-isotope analysis and comparison to global sea level from Figure 24 and Figure 25 below. The $^{87}Sr/^{86}Sr$ shows a distinct trend that follows along with the Phanerozoic Sr-isotope curve. Ages used herein are after the international chronostratigraphic chart (Appendix 1: Figure 29). There is a significant break in the stratigraphic record from end-Albian to the beginning of the Sinemurian that spans over 57 million years and separates the

uppermost Y3 member from the lowermost section that is in contact with the Hillbank (Figure 24).

The stratigraphic section of the Corozal Basin in northern Belize starts with the Santa Rosa formation. Reports by Flores (1952) and subsequently Bateson and Hall (1977), determined that this formation is Pennsylvanian to mid-Permian based on indicative fossil taxa (e.g. fusulinids and crinoids). This gives the section a Paleozoic upper limit. The Margaret Creek formation is represented by sandstones, sandy clays, and sandy dolomite streaks that have an inferred likely age of Late Jurassic to Early Cretaceous (Flores, 1952). This formation is completely barren of megascopic fossils with the exception of a few lignite and mollusk fragments and so age determination is solely based on stratigraphic inference because it lies conformably above the Santa Rosa (Flores, 1952; Bateson and Hall, 1977; Ramanathan, 1990). The lateral equivalent of the Margaret Creek formation in the Belize basin and adjacent parts of Guatemala is thought to be the Todos Santos formation (including the San Ricardo formation) (Dixon, 1956; Bryson, 1975; King and Petruny, 2013). Traditionally, these formations have a been interpreted as Lower Jurassic (Oxfordian) to Upper Cretaceous (Hauterivian) based on radiometric dating, analysis of palynomorphs, as well as microfauna and macrofauna observations (Blair, 1988).

Three Sr-isotope samples were taken from the Hillbank dolostones showing it to be Upper Triassic (Norian) to Lower Jurassic (Sinemurian) (Table 2). Providing that the strontium ratios reflect an accurate age of the carbonates, this would then mean that the previous interpretation of the Margaret Creek formation as Lower Jurassic to Upper Cretaceous is incorrect and has to likely be between Early to Middle Triassic. However, in order to definitively ascertain this, it is recommended to sample the Margaret Creek

for any age-indicative microfossils such as palynomorphs. The Hillbank, as well as the overlying Yalbac, have no age-determining fossils that constrained previous age estimates (Bryson, 1975), therefore the present Sr-based age determination is the first such determination for these units in this basin.

The Yalbac grades vertically from the upper Hillbank and consists mostly of dolostones and anhydrite (Bryson, 1975; King et al., 2004). More recent studies have suggested that there is regional evidence that the Hillbank and Yalbac form a single formation (Petersen et al., 2012).

For Sr-analysis, the Yalbac formation was the most sampled interval due to its thickness, as well as economic importance. Eighteen samples were taken throughout this formation; four from the upper Y1, four from the middle Y2 and ten from the lower Y3. Sr-isotope analysis supports a gradational contact between the Hillbank and lowermost Y3 at Sinemurian time. Between 133-190 m.y., there is distinct gap in the Sr-isotope values and this gap apparently represents a substantial stratigraphic break, probably an erosional surface. It is then postulated that the sharp decline in global sea-level (solid red arrows shown in Figure 25) during the balance of Jurassic through to Early Cretaceous allowed for subaerial exposure and erosion within the Y3.

Based on the Sr-age results, the lower Y3 falls with the Hillbank as being Early Jurassic; this forming after a major stratigraphic break. Later, deposition of the Y3 resumes during Early Cretaceous, and subsequently, Y2 and Y1 are deposited continuing during Late Cretaceous. This can possibly be correlated with the Lower Cretaceous basal unconformity of the Cobán A formation, which is present in the South Petén sub-basin as described by Wug et al. (2009). This would mean a greater

expression of that erosional surface in the Corozal basin because a greater amount of stratigraphic section (spanning a longer time period) apparently is missing.

An alternate way of expressing the stratigraphy is to say that the Jurassic beds of dolostone (a few 10s of feet thick), which so far have been interpreted as the base of Y3, are in fact the upper beds of the Hillbank, i.e, these beds are a continuation of the cyclical Hillbank carbonate and clastic sequence (an Upper Hillbank dolostone above the Upper Hillbank sandstone). That means the newly discovered break corresponds to the Hillbank-Yalbac unconformity. This alternate view makes sense because the upper dolomitic package can possibly be another carbonate sequence deposited as marine transgression ensued and covered the UHBS.

In terms of the stratigraphic sequence, this means that the Hillbank and Yalbac would not share a gradational contact (as reported in all previous work), but instead a significant break in the stratigraphic record separating these two formations exists. If the stratigraphic break is not an unconformity, rather than erosion due to subaerial exposure, perhaps the Hillbank and Yalbac are separated by a maximum flooding surface expressed as a condensed section. Condensed sections are generally characterized by slow rates of sediment accumulation that preserve relatively long geologic timespans (“An Online Guide to Sequence Stratigraphy,” 2016). Because such as surface is usually characterized by the presence of the rare authigenic minerals such as pyrite, glauconite and phosphate, a detailed core study might help to shed some light on the exact nature of this stratigraphic break (and possible formation contact).

The lowermost Barton Creek formation shows a Sr-based age of 83 m.y. (Campanian), which coincides with the upper limit of previous studies (Flores, 1952; Bryson, 1975; Ramanathan, 1990). Previous workers concluded that Barton Creek was

Campanian to Maastrichtian based on the presence of *Dyciclina sp*. in association with Miliolids*, Valvulina*, and calcareous tubes. The Barton Creek formation comprises all the limestones and dolomitic limestones and marls occurring above the Yalbac formation and is likely to be the equivalent to part of the Coban and the upper part of the Campur Formation (Bryson, 1975). Bryson (1975) reported a clearly defined unconformity between the Yalbac and overlying Barton Creek formation. This is likely the result of the global sea-level fall shown at ~90 m.y. (Figure 25) that separates the Y1 member from the overlying BC. Specifically, it is likely the result of subaerial exposure of the Yalbac formation before deposition of the Barton Creek formation.

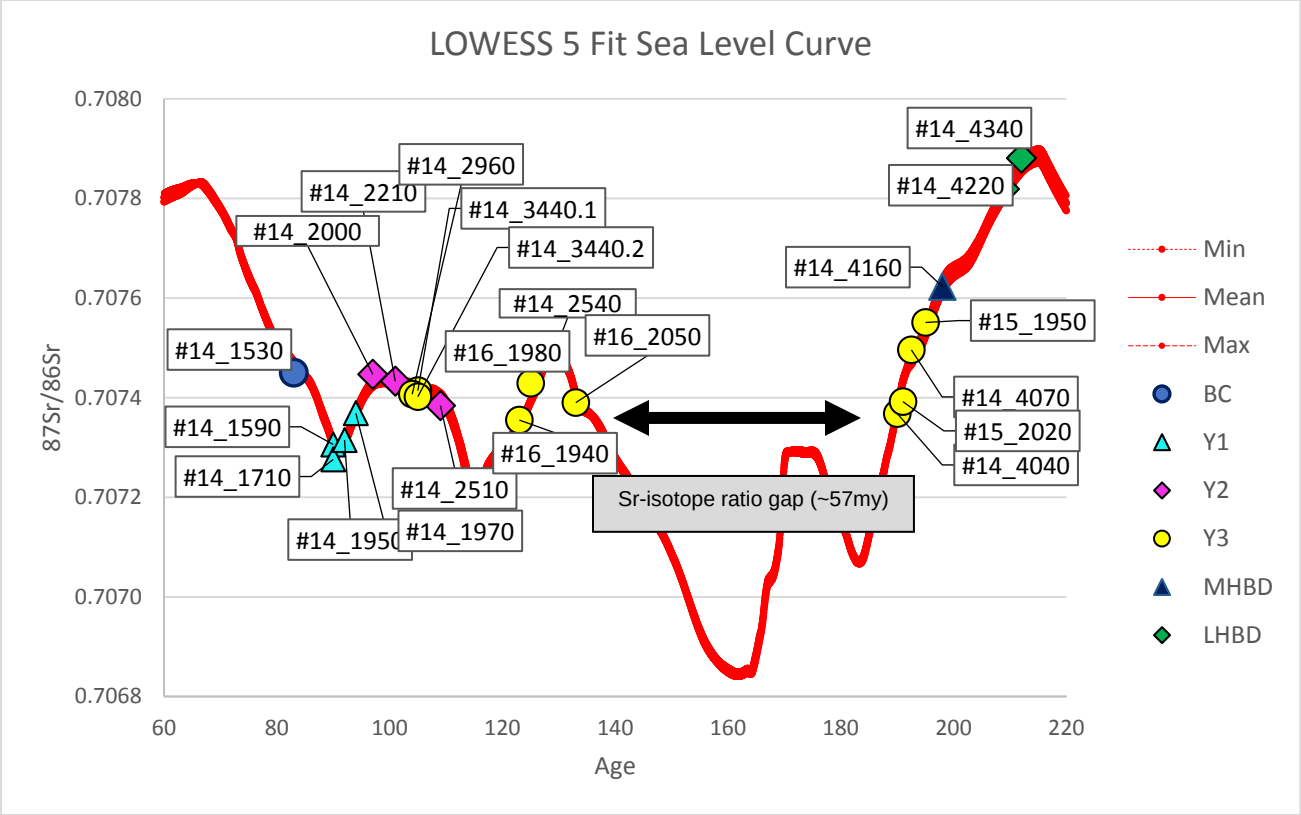

Figure 24. Strontium isotope ratio values for the Corozal basin plotted on the LOWESS 5 Fit Sea Level Curve (after Howarth and MacArthur (1997), and their additional look-up table version 5: 09/04/13).

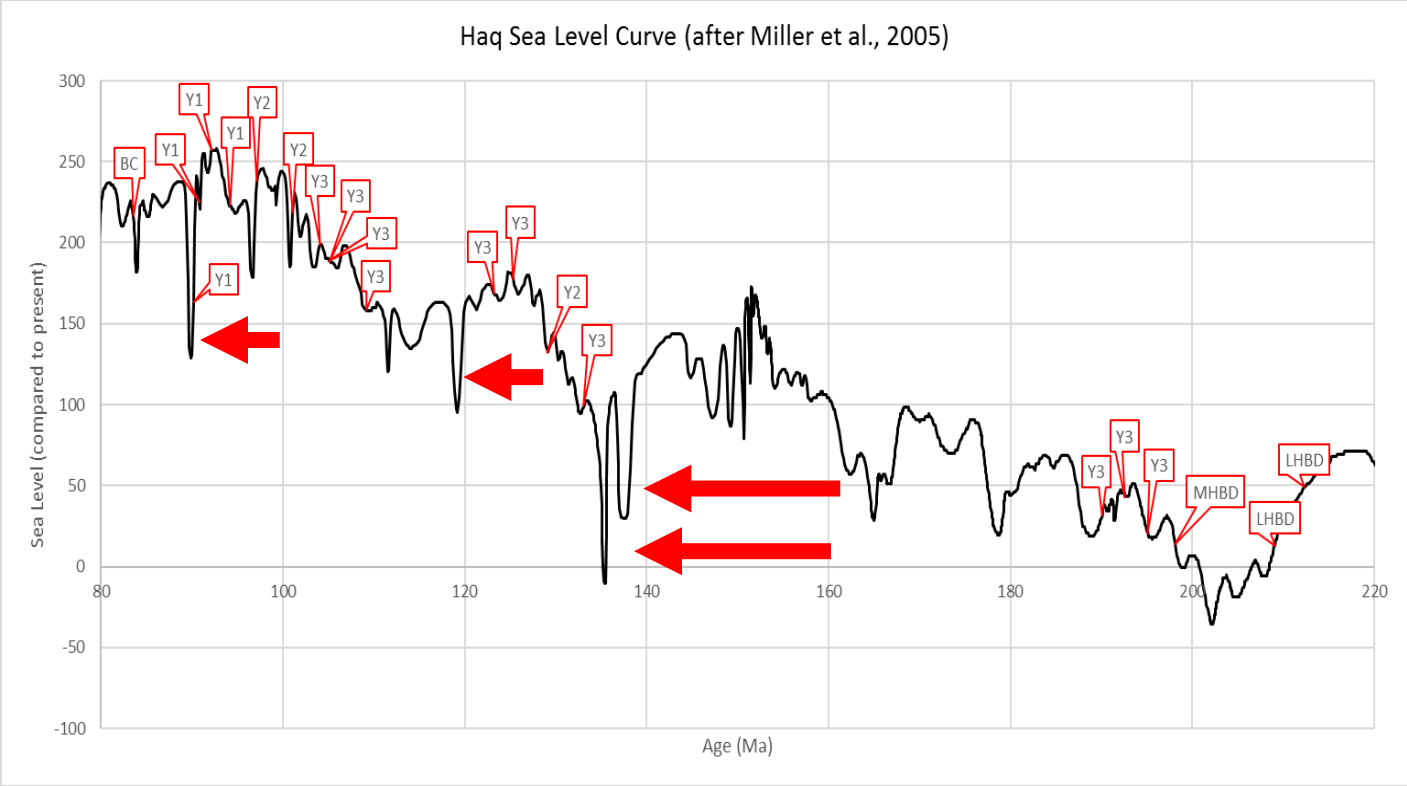

Figure 25. Haq sea-level curve (Miller, 2005) with interpreted ages from Sr-isotope analysis showing the age distribution of the formations in the Corozal basin. If the lack of Sr-isotope values are indicative of an unconformity during the Mesozoic, the solid red arrows indicate the largest drops in sea level that are most likely to affect the stratigraphic record of the Corozal basin and result in an unconformity.

Based on the above interpretation of depositional history of the Corozal basin, the following modified stratigraphic column (Figure 26) is proposed to accurately reflect Sr-isotope age values. Key changes include a break within Y3 separating the upper part of the Y3 from the basal Y3 beds and the HB.

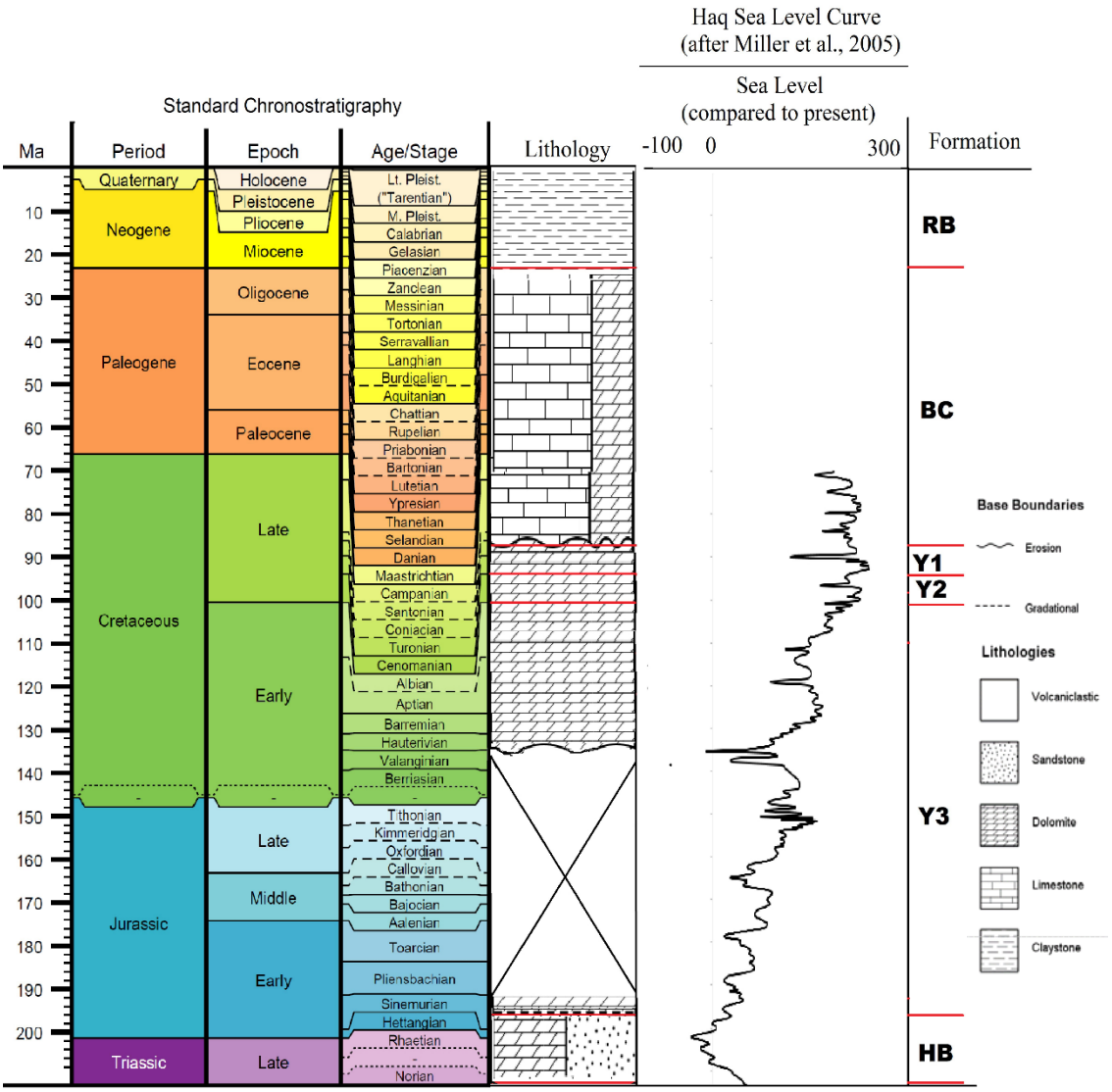

Figure 26. Modified stratigraphic column of the Corozal basin based on interpreted ages from Sr-isotope values. Gross lithology is displayed alongside ages and a mean sea-level curve. Formation boundaries are interpreted based on Sr-isotope values and marked with a solid red line. The lithology legend shows percent of rock type.

7. CONCLUSIONS

Petrographic analysis revealed nine distinct microfacies that comprise the Hillbank and Yalbac formations of the Corozal basin in northern Belize. These microfacies include shallow water carbonates, sabkha evaporates, and continental clastics (fluvial, humid fan, and lacustrine).

The Hillbank consists of an alternating cycle of clastics (MF6-9) and carbonates (MF1-3), and including a carbonate-clastic transitional facies (MF5). The Yalbac formation represents an overall marine transgression and a later shift to a marginal marine environment in which sabkha and lagoonal facies eventually dominate (MF1-4).

Isotopic analysis of well-preserved chippings provide a Sr-based numerical age solution for the carbonate stratigraphy of the Corozal Basin. Variations in $^{87}Sr/^{86}Sr$ have a strong correlation to the global standard for the Phanerozoic Sr-ratio curve over two parts of the curve – Late Cretaceous and Early Jurassic to Late Triassic. There is a gap of about 57 million years within the Y3 member, which was not previously known.

It is proposed that the strata below this gap, namely the Hillbank carbonates as well as the lower part of the Y3 member of the Yalbac formation, may be in fact Lower Jurassic to Upper Triassic strata. There is Sr-based evidence, presented here, for a stratigraphic break spanning 110 to 190 million years within the Y3 member.

Owing to the apparent correlation between a substantial global sea level fall during Early Cretaceous, we suggest that this event may be at least partially responsible for this remarkable and previously unknown erosional surface within the Corozal basin. Alternatively, this break is possible the result of a maximum flooding surface, expressed as a condensed section.

8. REFERENCES

Amthor, J. E., and G. M. Friedman, 1991, Dolomite-rock textures and secondary porosity development in Ellenburger Group carbonates (Lower Ordovician), west Texas and southeastern New Mexico: Sedimentology, v. 38, no. 2, p. 343–362, doi:10.1111/j.1365-3091.1991.tb01264.x.

An Online Guide to Sequence Stratigraphy, 2016: <http://strata.uga.edu/sequence/surfaces.html>.

Bateson, J. H., 1972, New Interpretation of Geology of Maya Mountains, British Honduras: GEOLOGICAL NOTES: American Association of Petroleum Geologists Bulletin, v. 56, no. 5, p. 963.

Bateson, J. H., and I. H. S. Hall, 1977, The Geology of the Maya Mountains, Belize: Institute of Geological Science, Overseas Memoir, v. 3, p. 1–43.

Bishop, W. F., 1980, Petroleum geology of northern Central America: Journal of Petroleum Geology, v. 3, no. 1, p. 3–59.

Blair, T. C., 1988, Mixed Siliciclastic-Carbonate Marine and Continental Syn-Rift Sedimentation, Upper Jurassic-Lowermost Cretaceous Todos Santos and San Ricardo Formations, Western Chiapas, Mexico: SEPM Journal of Sedimentary Research, v. 58, doi:10.1306/212F8E09-2B24-11D7-8648000102C1865D.

Bryson, R. S., 1975, Stratigraphic Problems of Northern Belize: Belmopan, Belize, 1-22 p.

Bustamente, C., and M. G. Wetzel, 1992, Petroleum assessment of the OPL-1 block, Corozal Basin, Belize, Geology & Petroleum Office, Belmopan, Belize.

Choquette, P. W., and L. C. Pray, 1970, Geologic nomenclature and classification of porosity in sedimentary carbonates.: p. 207–250, doi:10.1306/5D25C98B-16C1-11D7-8645000102C1865D.

Cornec, J. H., 2003, Geology Map of Belize at the scale of 1:250,000: Geology & Petroleum Office, Belmopan, Belize.

Cornec, J. H., 1985, Note on the provisional geological map of Belize at the scale of 1:250,000: Geology & Petroleum Office, Belmopan, Belize.

Cornec, J. H., 1986, Provisional geological map of Belize at the scale of 1:250,000: Geology & Petroleum Office, Belmopan, Belize.

Deer, W. A., R. A. Howie, and J. Zussman, 1992, An Introduction to the Rock-Forming Minerals: 696 p., doi:0-582-30094-0.

Dixon, C. G., 1956, Geology of southern British Honduras with notes on adjacent areas, Geology & Petroleum Office, Belmopan, Belize.

Elderfield, H., 1986, Strontium isotope stratigraphy: Palaeogeography, Palaeoclimatology, Palaeoecology, v. 57, no. 1, p. 71–90, doi:10.1016/0031-0182(86)90007-6.

Erhardt, S., P. Hochreuther, and M. Schütz, 2017, Open TopoMaps: <https://opentopomap.org> (accessed January 1, 2017).

Flores, G., 1952, Summary report of the preliminary geological studies of the area north of 17° North Latitude, British Honduras: Geology & Petroleum Office, Belmopan, Belize, 1-71 p.

Flügel, E., 2010, Microfacies of Carbonate Rocks: Analysis, Interpretation and Application: 976 p., doi:10.1007/978-3-642-03796-2.

Geology and Petroleum Department, 2013, Geophysical & Well Data: <http://estpu.gov.bz/index.php/geology-petroleum/gpd-geophysical-well-data> (accessed January 1, 2017).

Harr, N., 1972, Well report Rancho Dolores 1: Belize, British Honduras, Geology & Petroleum Office, Belmopan, Belize, 1-37 p.

Hercman, H., and J. Pawlak, 2016, StronTer: Tools for Probabilistic Methods in Strontium Isotope Stratigraphy: The Journal of Geology, v. 124, no. 2, p. 267–275, doi:10.1086/684789.

Hibbard, D. E., 1976, Geology and oil potential of the Anschutz Overseas licenses northern Belize - Central America: Geology & Petroleum Office, Belmopan, Belize, 1-14 p.

Hibbard, D. E., 1988, Geology and petroleum potential of the Seahawk Group license area, Northern Belize - Central America: Geology & Petroleum Office, Belmopan, Belize, 1-21 p.

Howarth, R., and J. McArthur, 1997, Statistics for strontium isotope stratigraphy: a robust LOWESS fit to the marine Sr-isotope curve for 0 to 206 Ma, with look-up table for derivation of numeric age: The Journal of Geology, v. 105, no. 4, p. 441–456, doi:10.1086/515938.

International Commission on Stratigraphy, 2016, International Chronostratigraphic Chart: www.stratigraphy.org, v. 12.

Kim, Y., R. W. Clayton, and F. Keppie, 2011, Evidence of a collision between the Yucatán Block and Mexico in the Miocene: Geophysical Journal International, v. 187, no. 2, p. 989–1000, doi:10.1111/j.1365-246X.2011.05191.x.

King Jr., D. T., and L. Petruny, 2012a, Belize - Onshore stratigraphy and renewed onshore petroleum exploration activity north of the 17th Parallel: Abstracts: Annual Meeting - American Association of Petroleum Geologists, v. 2012, p. 1–3.

King Jr., D. T., and L. Petruny, 2012b, Northern Belize's onshore petroleum stratigraphy, structures, and oil seeps: Gulf Coast Association of Geological Societies Transactions, v. 62, p. 227–242.

King Jr., D. T., and L. W. Petruny, 2003, Stratigraphy and sedimentology of coarse impactoclastic breccia units within the Cretaceous-Tertiary boundary section, Albion Island, Belize: 6th ESF-impact workshop "Impact makers in the stratigraphic record," p. 203–228.

King Jr., D. T., and L. W. Petruny, 2014, Stratigraphy of the Barton Creek Formation, Corozal Basin, Northern Belize: Gulf Coast Association of Geological Societies

Transactions, v. 6, p. 215–228.

King Jr., D. T., and L. W. Petruny, 2013, Stratigraphy of the Margaret Creek Formation, Corozal Basin, Northern Belize: Gulf Coast Association of Geological Societies Transactions, v. 63, p. 275–283.

King Jr., D. T., L. W. Petruny, and K. O. Pope, 2003, Shallow-marine facies of the Orange Walk Group, Miocene-Pliocene, northern Belize (Central America); Transactions of the 53rd annual convention; 50th GCSSEPM anniversary: 53rd annual convention, 50th GCSSEPM anniversary, Baton Rouge, LA, United States, Oct. 22-24, 2003, v. 53, p. 384–397.

Limes, L. L., 1979, The Petroleum Geology of Northern Belize (Formerly British Honduras): New Orleans, Louisiana, 1-29 p.

Longman, M., 2009, Study of Core from the Hill Bank Formation in Mike Usher #11 Well, Spanish Lookout Field, Belize: Belize Natural Energy, Spanish Lookout, Internal Report, 26 p.

McArthur, J. M., 1994, Recent trends in strontium isotope stratigraphy: Terra Nova, v. 6, no. 4, p. 331–358, doi:10.1111/j.1365-3121.1994.tb00507.x.

McArthur, J. M., R. J. Howarth, and T. R. Bailey, 2001, Strontium isotope stratigraphy: LOWESS version 3: best fit to the marine Sr-isotope curve for 0-509 Ma and accompanying look-up table for deriving numerical age: The Journal of Geology, v. 109, no. 2, p. 155–170, doi:10.1086/319243.

McArthur, J. M., R. J. Howarth, and G. A. Shields, 2012, Strontium Isotope Stratigraphy:

Felix M. Gradstein, James G. Ogg, Mark Schmitz and Gabi Ogg, 127-144 p., doi:10.1016/B978-0-444-59425-9.00007-X.

Miller, K. G., 2005, The Phanerozoic Record of Global Sea-Level Change: Science, v. 310, no. 5752, p. 1293–1298, doi:10.1126/science.1116412.

Morrice, S., 1988, Petroleum Prospects of the Exeter Morrice License Blocks Onshore Belize, Central America: Denver, Colorado, Geology & Petroleum Office, Belmopan, Belize, 41 p.

Murray, R. C., 1964, Origin and diagenesis of gypsum and anhydrite: Journal of Sedimentary Research, v. 34, no. 3, p. 512–523, doi:10.1306/74D710D2-2B21-11D7-8648000102C1865D.

NACSN, 2005, North American Stratigraphic Code: (North American Commission on Stratigraphic Nomenclature), American Association of Petroleum Geologists Bulletin, v. 89, no. 11, p. 1547–1591.

Nair, K. M., 1988, Thin Section Petrolgraphic Studies in Corozal Basin; N. Belize: Geology & Petroleum Office, Belmopan, Belize, 1-43 p.

New World Oil and Gas Plc, 2012, Evaluation of the Prospectivity and Work Program in the Blue Creek Concession, onshore NW Belize, Danica Jutland licences 1/09 & 2/09, onshore Denmark, & Danica Resources licence 1/08, onshore/offshore Denmark: Houston, Texas, 1-65 p.

Ower, L. H., 1928, Geology of British Honduras: The Journal of Geology, v. 36, no. 6, Geology & Petroleum Office, Belmopan, Belize, p. 494–509.

Peterman, Z. E., C. E. Hedge, and H. A. Tourtelot, 1970, Isotopic composition of strontium in sea water throughout Phanerozoic time: Geochimica et Cosmochimica Acta, v. 34, no. 1, p. 105–120, doi:10.1016/0016-7037(70)90154-7.

Petersen, H. I., B. Holland, H. P. Nytoft, A. Cho, S. Piasecki, J. de la Cruz, and J. H. Cornec, 2012, Geochemistry of crude oils, seepage oils and source rocks from Belize and Guatemala: Indications of carbonate-sourced petroleum systems: Journal of Petroleum Geology, v. 35, no. 2, p. 127–163, doi:10.1111/j.1747-5457.2012.00523.x.

Pettijohn, F. J., P. E. Potter, and R. Siever, 1972, Sand and Sandstone: Berlin-Herdelberg-New York, Springer, 618 p.

Pindell, J. L., and L. Kennan, 2009, Tectonic evolution of the Gulf of Mexico, Caribbean and northern South America in the mantle reference frame: an update: Geological Society, London, Special Publications, v. 328, no. 1, p. 1–55, doi:10.1144/SP328.1.

Purdy, E. G., E. Gischler, and A. J. Lomando, 2003, The Belize margin revisited. 2. Origin of Holocene antecedent topography: International Journal of Earth Sciences, v. 92, no. 4, p. 552–572, doi:10.1007/s00531-003-0325-z.

Purrazzella, P. F., 1992, Final Results Petrograhic Analysis of Selected Cuttings Samples Multiple Wells, Yalbac Formation, Belize: Tulsa, Oklahoma, 1-67 p.

Ramanathan, R., 1990, Foraminiferal Micropaleontological Report on Belize: Geology & Petroleum Office, Belmopan, Belize.

Rao, R. P., and R. Ramanathan, 1990, Tectonics and Petrolelm Potential of Belize:

Transactions of the twelfth Caribbean Geological Conference, edited by DK LaRue and G. Draper., Geology & Petroleum Office, Belmopan, Belize, p. 520–527.

Salvador, A. (ed.), 1994, International stratigraphic guide: a guide to stratigraphic classification, terminology, and procedure. No. 30: Geological Society of America, 214 p.

Scholle, P. A., D. G. Bebout, and C. H. Moore (eds.), 1983, Carbonate Depositional Environments: American Association of Petroleum Geologists Memoir 33: Tulsa, Oklahoma, American Association of Petroleum Geologists.

Scholle, P. A., and D. Spearing (eds.), 1982, Sandstone Depositional Environment: American Association of Petroleum Geologists Memoir 31: Tulsa, Oklahoma, American Association of Petroleum Geologists, 410 p.

Scholle, P. A., and D. S. Ulmer-Scholle, 2003, A Color Guide to the Petrography of Carbonate Rocks: Grains, textures, porosity, diagenesis: 460 p., doi:10.1306/m77973.

Sherman, J., 1992, Well Report: Eagle #2 Horizontal Drilling Joint Venture, Geology & Petroleum Office, Belmopan, Belize.

Ulmer-Scholle, D. S., P. A. Scholle, J. Schieber, and R. J. Raine, 2015, A Color Guide to the Petrography of Sandstones (AAPG Memoir 109): AAPG, 509 p.

Veizer, J. et al., 1997, Strontium isotope stratigraphy: Potential resolution and event correlation: Palaeogeography, Palaeoclimatology, Palaeoecology, v. 132, no. 1–4, p. 65–77, doi:10.1016/S0031-0182(97)00054-0.

Whittaker, R. C., 1983, The Hydrocarbon Potential of Belize: Submitted for MSc. Petroleum Geology, Imperial College, Geology & Petroleum Office, Belmopan, Belize, 1-27 p.

Wilson, J. L., 1975, Carbonate Facies in Geologic History: Berlin-Herdelberg-New York, Springer Science & Business Media, 471 p.

Wrestling, R. E., 1956, Well Report: Hillbank 1: Geology & Petroleum Office, Belmopan, Belize, 45 p.

Wug, L. A., R. M. Matias, C. A. de Leon, and J. S. de la Cruz, 2009, The Coban Formation in the Peten Basin, Guatemala: Energy and mineral potential of the Central American-Caribbean regions, v. 16, no. 1899, p. 115–121.

Zenger, D. H., 1983, Burial dolomitization in the Lost Burro Formation (Devonian), east-central California, and the significance of late diagenetic dolomitization: p. 519–522, doi:10.1130/0091-7613(1983)11<519:BDITLB>2.0.CO.

9. APPENDIX 1

The following materials were referenced within this study and contain important additional information. The standard facies belt outline by Wilson (1975) was used as an outline for the description of microfacies (Figure 26). The International

Chronostratigraphic Chart (Figure 27) was used for age referencing, e.g., as to stage names.

Idealized sequence of Standard Facies Belts (from Wilson, 1975)

re-drawn by Nassir Alnaji (2002)

Belt	BASIN	OPEN SEA SHELF	DEEP SHELF MARGIN	FORESLOPE	ORGANIC BUILD UP	WINNOWED EDGE SANDS	SHELF LAGOON OPEN CIRCULATION	RESTRICTED CIRULATION SHELF & TIDAL FLATS	EVAPORITES ON SABKHAS - SALINAS
	1	2	3	4	5	6	7	8	9
Diagrammatic cross section & Facies Number	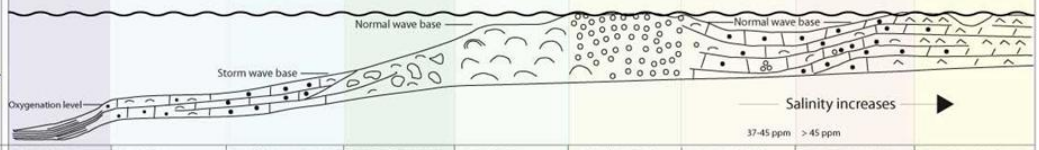								
Facies	a) Fine Clastics b) Carbonates c) Evaporites	a) Carbonates b) Shale	Toe of Slope carbonates	a) Bedded fine grain & slumps b) Foreset debris & lime sands c) Lime mud mases	a) Boundstone b) Crust on accumulations of debris lime mud; bindstone c) Bafflestone	a) Shoal lime sands b) Islands w. dune sands	a) Lime snad bodies b) Wackestone-mudstone areas, bioherms c) Areas of clastics	a) Bioclastic wackestone, lagoons and bays b) litho-bioclastic sands in tidal channels c) Lime mud-tide flats d) Fine clastic units	a) Nodular anhydirte & dolomite on salt flats. b) Laminated evaporites in ponds
Lithology	Dark shale or silt, thin limestones (starved basin); evaporite fill w. salt	Very fossiliferous lime-stone interbedded with marls; well segregated beds.	Fine grain limestone; cherty in some cases.	Variable, depending on water energy upslope; sedimentary breccia and lime sands	Massive limestone-dolomite	Calcarenitic-oolite lime sand or dolomite	Variable carbonate and clastics	Generally dolomite and dolomitic limestone	Irregularly laminated dolomite and anhydrite, may grade to red beds
Color	Dark brown, black, red	Gray, green, red, brown	Dark to light	Dark to light	Light	Light	Dark to light	Light	Red, yellow, brown
Grain type and depositoinal texture	Lime mudstone,; fine calcisiltites	Bioclastic and whole fossil wackestone; some calcisiltites	Mostly lime mudstone with some calcisiltites	Lime silt and bioclastic wackestone-packstone; lithoclastics of varying sizes	Boundstones and pockets of grainstone; packstone	Grainstones well sorted rounded	Great variety of textures, grainstone to mudstone	Clotted, pelleted mudstone & grainstone; laminated mudstone; coarse lithoclastic wackestone in channels	
Bedding and sedimentary structure	Very even mm lami-nations; rhythmic bedding; ripple cross lamination	Thoroughly burrowed; thin to medium; wavy to nodular beds; bedding surfaces show diastems	Lamination may be minor; often massive beds; lenses of graded sediment; lithoclasts & exotic blocks. Rhythmic beds	Slump in soft sedi-ments; sofeset bedding; slope bioherms; exotic blocks	Massive org. structure or open framework with roofed cavities; Lamination contrary to gravity	Medium to large scale crossbedding; festoons common	Burrowing traces very prominent	Birdseye, stromatolites, mm lamination, graded bedding, dolomite crusts on flats. Cross-bedded sand in channels	Anhydrite after gypsum; nodular, rosettes, chickenwire, and blades; irregular lamination; carbonate caliche
Terrigenous clastics admixed or interbedded	Quartz silt & shale; fine grain siltstone; cherty	Quartz silt, siltstone, & shale; well segregated beds	Some shales, silt, & fine grained siltstone	Some shales, silt, & fine grained siltstone	None	Only some quartz sand admixed	Clastics and carbonates in well segregated beds	Clastics and carbonates in well segregated beds	Windblown, land derived admixtures; clastics may be very important units
Biota	Exclusively nektonic-pelagic fauna preserved in abundance on bedding planes	Very diverse shelly fauna preserving both infauna & epifauna	Bioclastic detritus derived principally from upslope	Colonies of whole fossil organisms & bioclastic debris	Major frame building colonies with ramose forms in pockets; in situ communities dwelling in certain niches	Worn and abraided coquinas of forms living at or on slope; few indigenous organisms	Open marine fauna lacking; mollusca, sponges, forams, algae abundant; patch reefs present	Very limited fauna, mainly gastropods, algae, certain foraminfirera & ostracods	Almost no indigenous fauna, except for stromatolitic algae

Figure 27. Idealized sequence of standard facies belts (from Wilson, 1975).

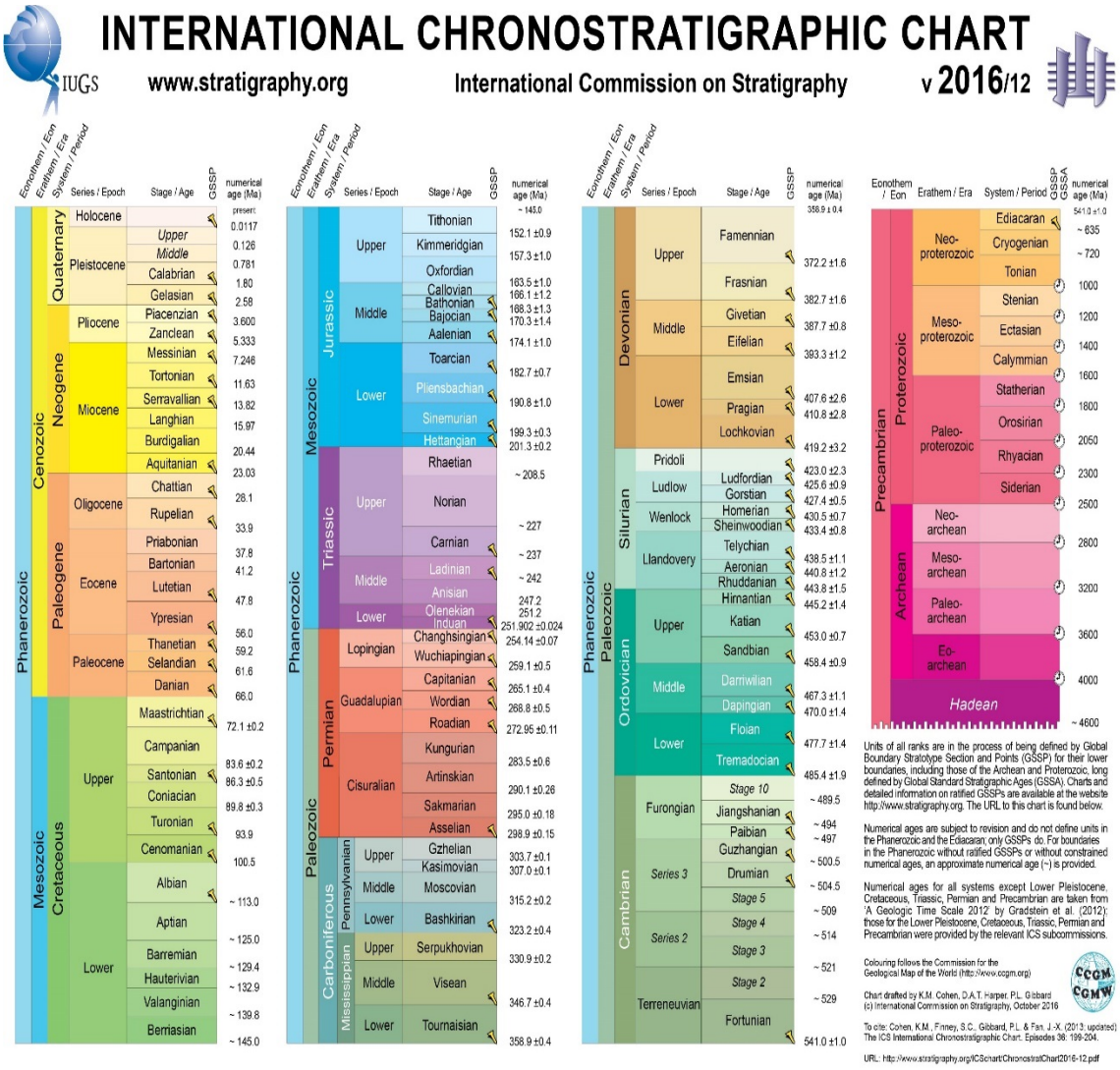

Figure 28. International Chronostratigraphic Chart (2016) used for age referencing.

The following figures are the matched $^{87}Sr/^{86}Sr$ ratios for each sample compared to the $^{87}Sr/^{86}Sr$ calibration lines using the Bayesian approach probabilistic program, StronTer (Hercman and Pawlak, 2016). The updated LOWESS Version 5 Fit: 26/03/13 marine Sr-isotope curve (red lines) was used (Howarth and McArthur, 1997; McArthur et al., 2001) and calculations were done using a single sample, normal distribution curve. The solid blue line represents the analytical $^{87}Sr/^{86}Sr$ value, while the dashed blue lines above and below represent the standard error associated with each sample. The age range as well as probability for each match is also displayed. There is one graph per sample analyzed in the present project.

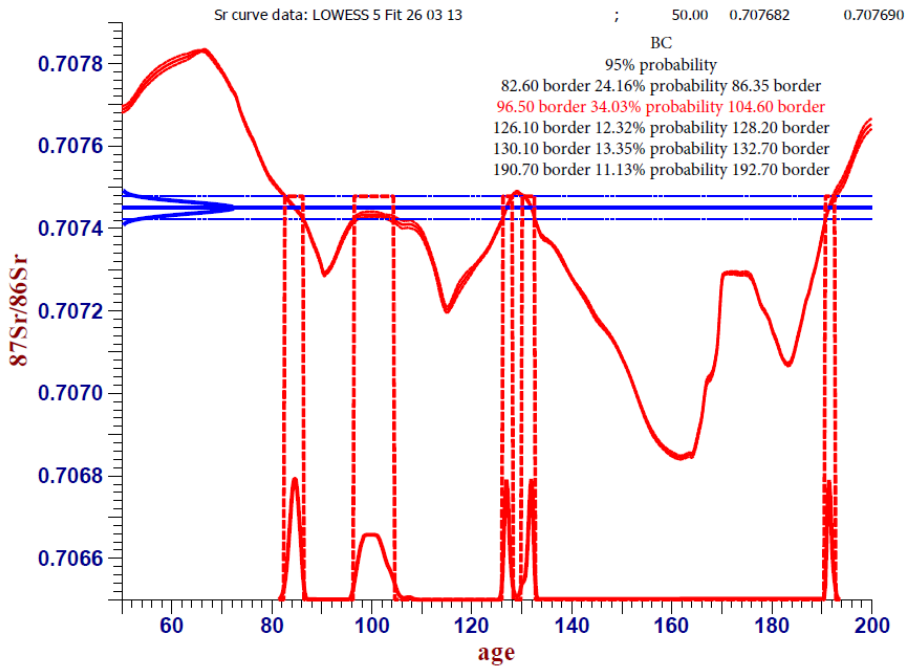

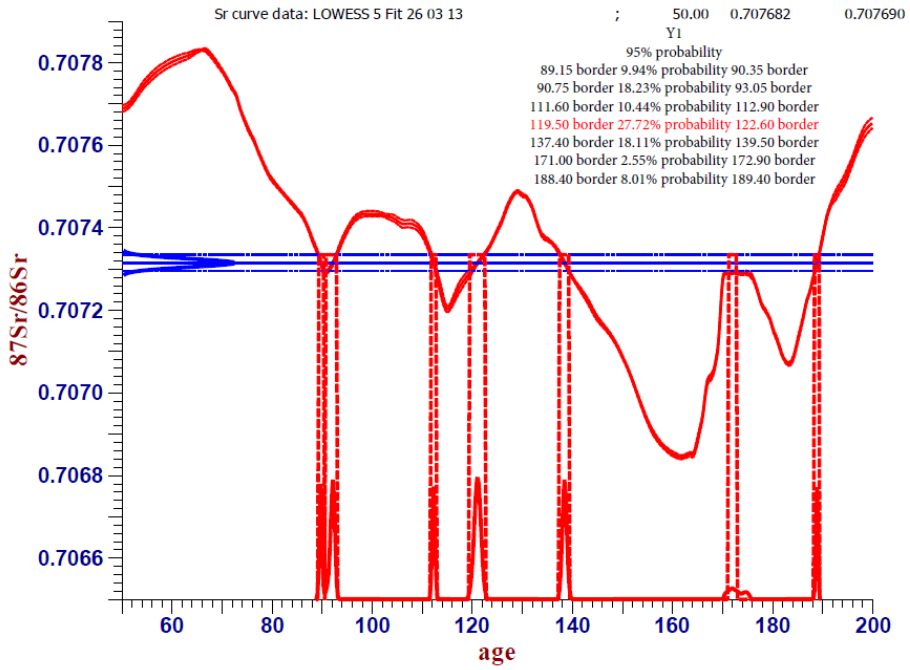
Sr curve data: LOWESS 5 Fit 26 03 13 ; 50.00 0.707682 0.707690
Y1
95% probability
89.15 border 9.94% probability 90.35 border
90.75 border 18.23% probability 93.05 border
111.60 border 10.44% probability 112.90 border
119.50 border 27.72% probability 122.60 border
137.40 border 18.11% probability 139.50 border
171.00 border 2.55% probability 172.90 border
188.40 border 8.01% probability 189.40 border
87Sr/86Sr
0.7078
0.7076
0.7074
0.7072
0.7070
0.7068
0.7066
60
80
100
120
140
160
180
200
age

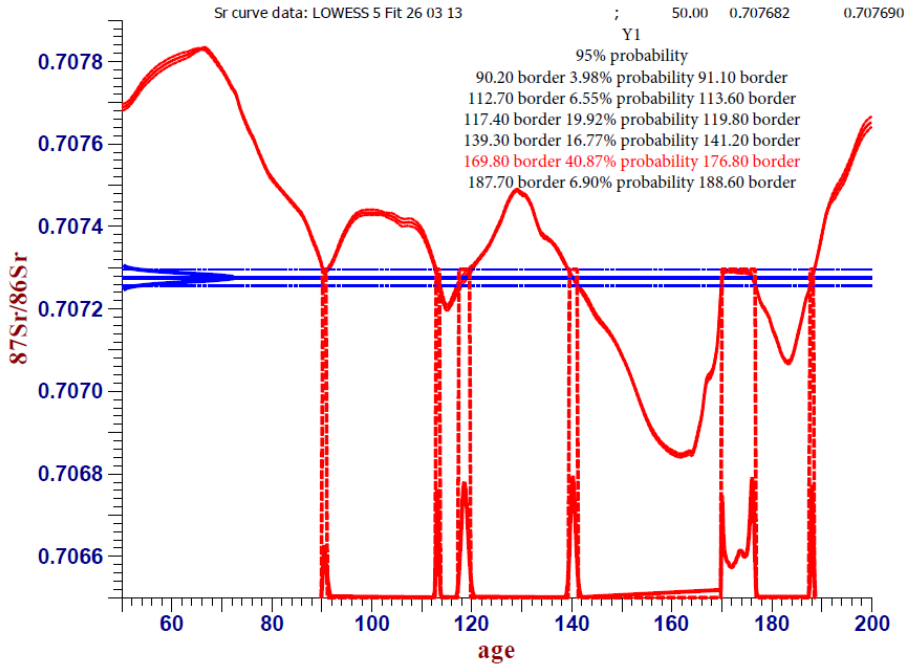
Sr curve data: LOWESS 5 Fit 26 03 13 ; 50.00 0.707682 0.707690
Y1
95% probability
90.20 border 3.98% probability 91.10 border
112.70 border 6.55% probability 113.60 border
117.40 border 19.92% probability 119.80 border
139.30 border 16.77% probability 141.20 border
169.80 border 40.87% probability 176.80 border
187.70 border 6.90% probability 188.60 border
87Sr/86Sr
0.7078
0.7076
0.7074
0.7072
0.7070
0.7068
0.7066
60
80
100
120
140
160
180
200
age

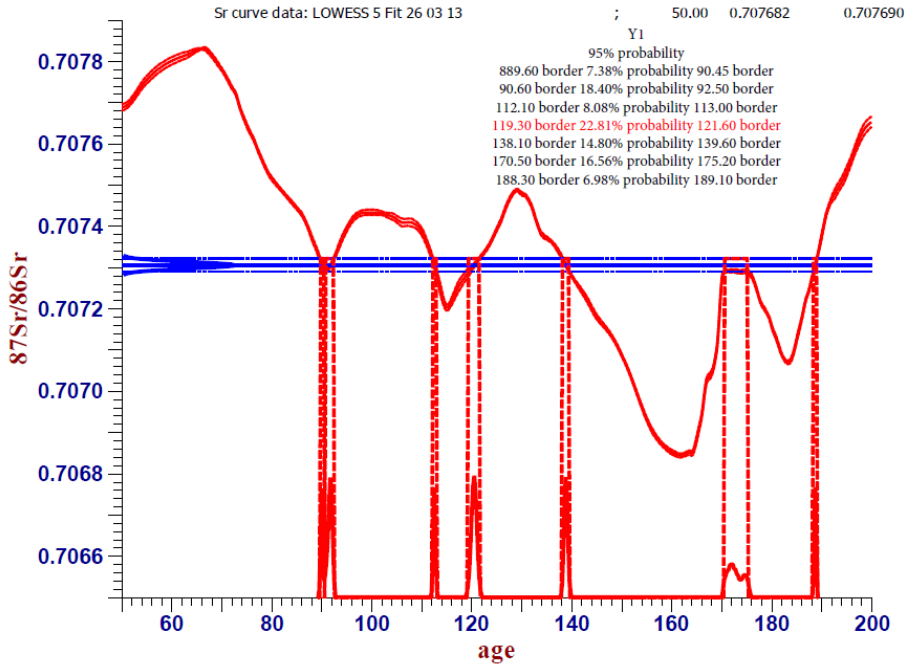
Sr curve data: LOWESS 5 Fit 26 03 13 ; 50.00 0.707682 0.707690
Y1
95% probability
889.60 border 7.38% probability 90.45 border
90.60 border 18.40% probability 92.50 border
112.10 border 8.08% probability 113.00 border
119.30 border 22.81% probability 121.60 border
138.10 border 14.80% probability 139.60 border
170.50 border 16.56% probability 175.20 border
188.30 border 6.98% probability 189.10 border
87Sr/86Sr
0.7078
0.7076
0.7074
0.7072
0.7070
0.7068
0.7066
60
80
100
120
140
160
180
200
age

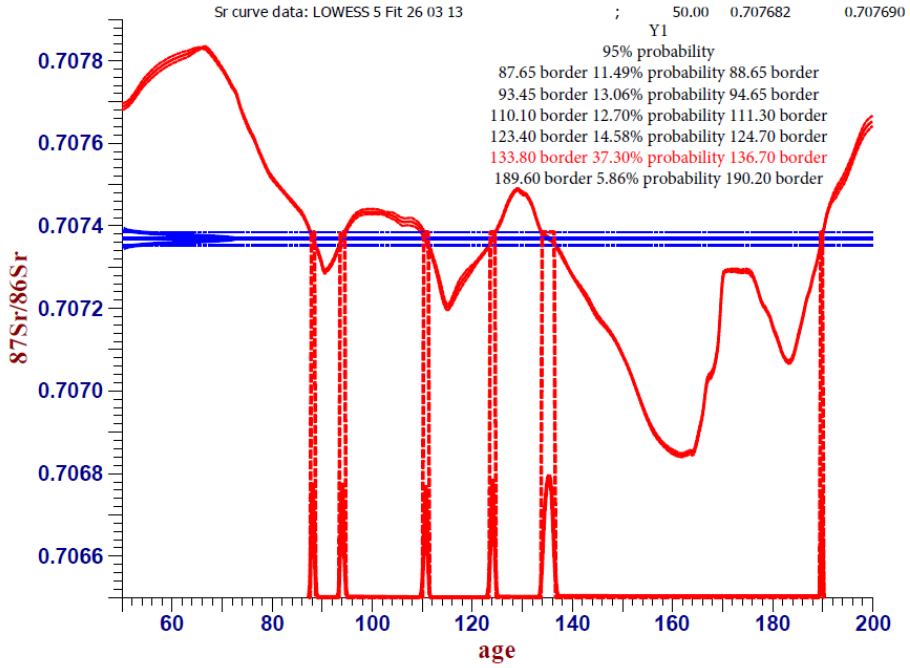
Sr curve data: LOWESS 5 Fit 26 03 13 ; 50.00 0.707682 0.707690
Y1
95% probability
87.65 border 11.49% probability 88.65 border
93.45 border 13.06% probability 94.65 border
110.10 border 12.70% probability 111.30 border
123.40 border 14.58% probability 124.70 border
133.80 border 37.30% probability 136.70 border
189.60 border 5.86% probability 190.20 border
87Sr/86Sr
0.7078
0.7076
0.7074
0.7072
0.7070
0.7068
0.7066
60
80
100
120
140
160
180
200
age

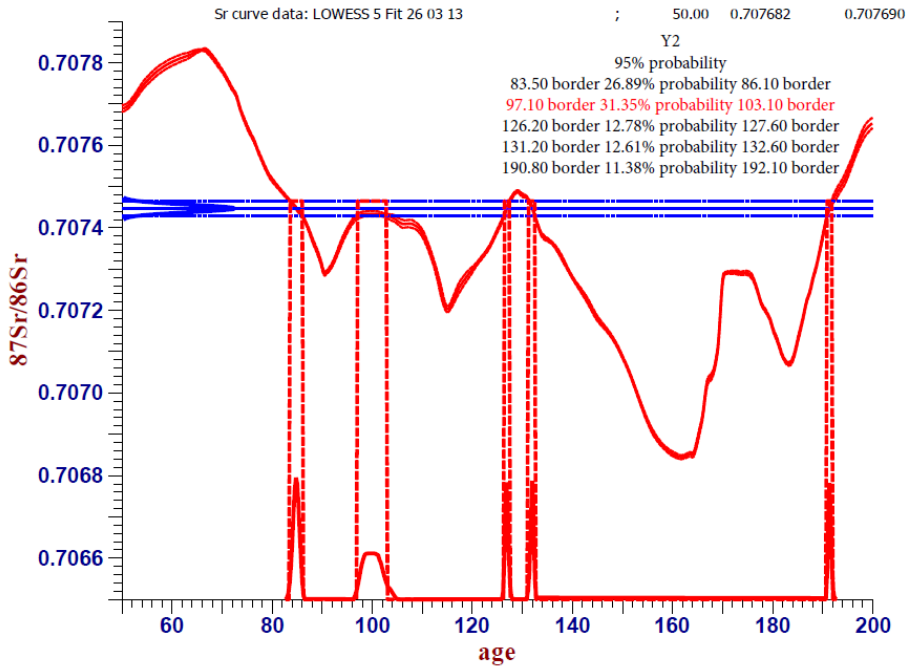
Sr curve data: LOWESS 5 Fit 26 03 13 ; 50.00 0.707682 0.707690
Y2
95% probability
83.50 border 26.89% probability 86.10 border
97.10 border 31.35% probability 103.10 border
126.20 border 12.78% probability 127.60 border
131.20 border 12.61% probability 132.60 border
190.80 border 11.38% probability 192.10 border
87Sr/86Sr
0.7078
0.7076
0.7074
0.7072
0.7070
0.7068
0.7066
60
80
100
120
140
160
180
200
age

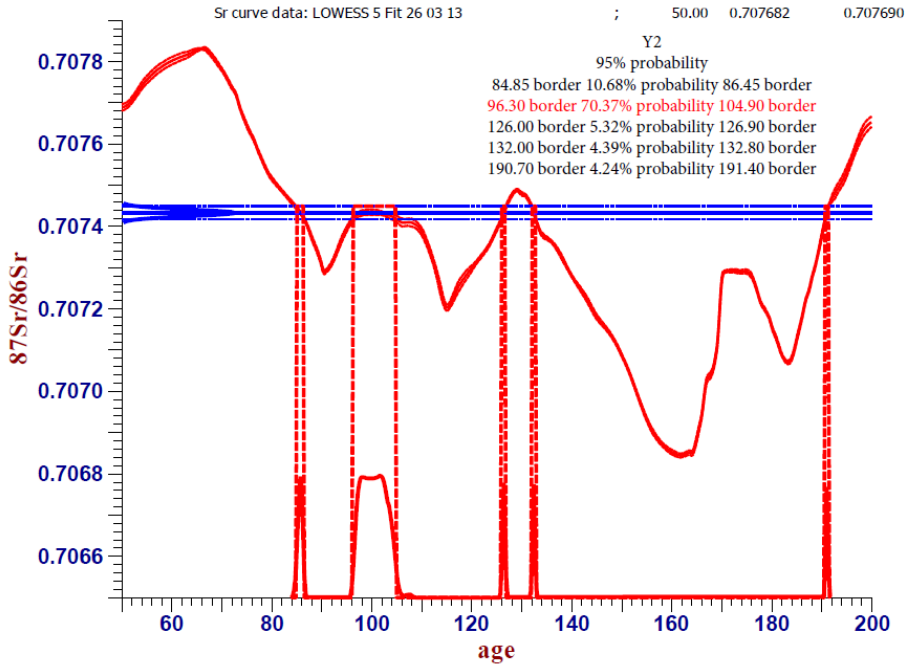
Sr curve data: LOWESS 5 Fit 26 03 13 ; 50.00 0.707682 0.707690
Y2
95% probability
84.85 border 10.68% probability 86.45 border
96.30 border 70.37% probability 104.90 border
126.00 border 5.32% probability 126.90 border
132.00 border 4.39% probability 132.80 border
190.70 border 4.24% probability 191.40 border
87Sr/86Sr
0.7078
0.7076
0.7074
0.7072
0.7070
0.7068
0.7066
60
80
100
120
140
160
180
200
age

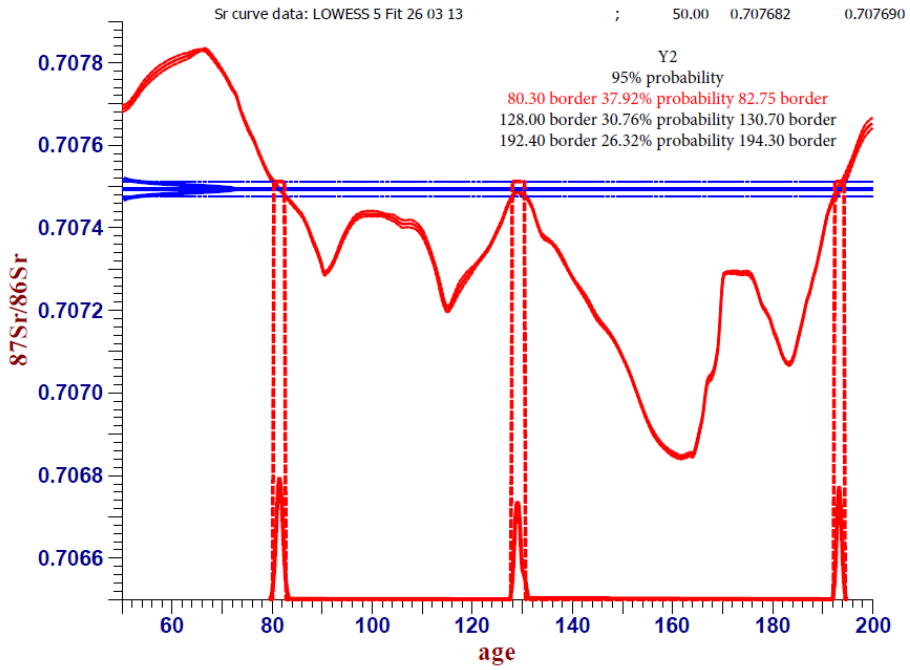
Sr curve data: LOWESS 5 Fit 26 03 13 ; 50.00 0.707682 0.707690
Y2
95% probability
80.30 border 37.92% probability 82.75 border
128.00 border 30.76% probability 130.70 border
192.40 border 26.32% probability 194.30 border
87Sr/86Sr
0.7078
0.7076
0.7074
0.7072
0.7070
0.7068
0.7066
60
80
100
120
140
160
180
200
age

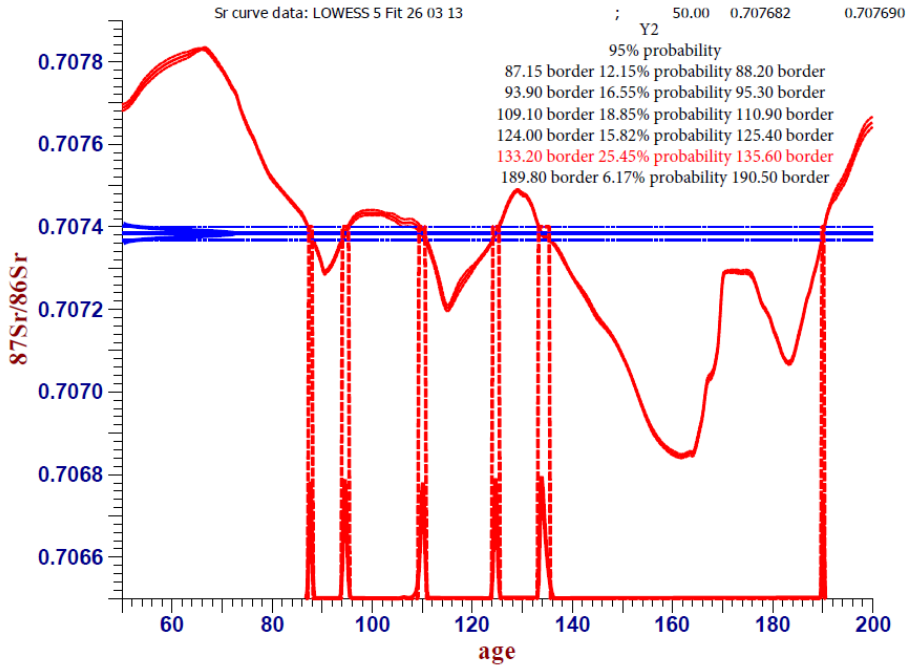
Sr curve data: LOWESS 5 Fit 26 03 13 ; 50.00 0.707682 0.707690
Y2
95% probability
87.15 border 12.15% probability 88.20 border
93.90 border 16.55% probability 95.30 border
109.10 border 18.85% probability 110.90 border
124.00 border 15.82% probability 125.40 border
133.20 border 25.45% probability 135.60 border
189.80 border 6.17% probability 190.50 border
87Sr/86Sr
0.7078
0.7076
0.7074
0.7072
0.7070
0.7068
0.7066
60
80
100
120
140
160
180
200
age

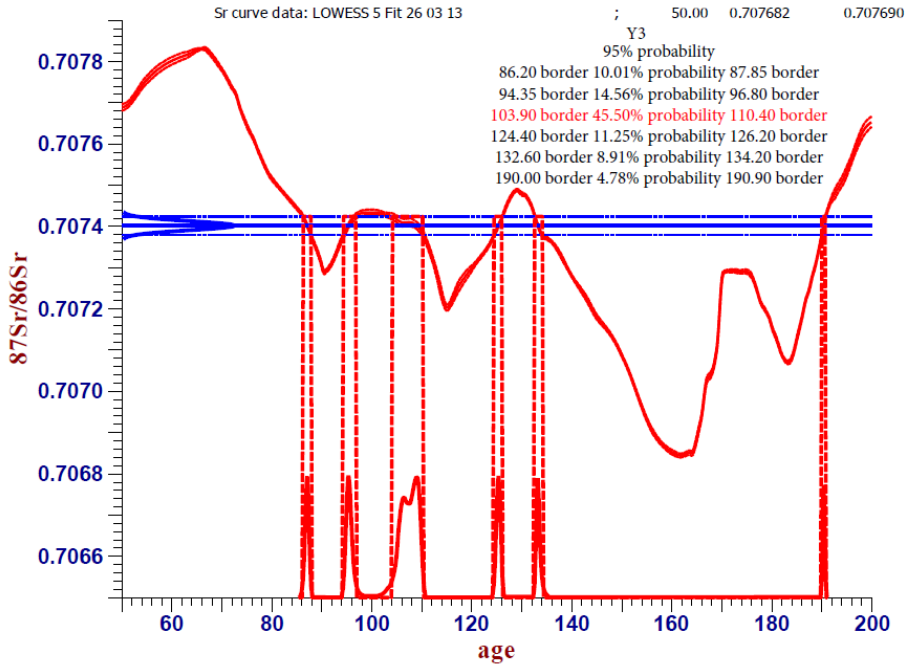
Sr curve data: LOWESS 5 Fit 26 03 13 ; 50.00 0.707682 0.707690
Y3
95% probability
86.20 border 10.01% probability 87.85 border
94.35 border 14.56% probability 96.80 border
103.90 border 45.50% probability 110.40 border
124.40 border 11.25% probability 126.20 border
132.60 border 8.91% probability 134.20 border
190.00 border 4.78% probability 190.90 border
87Sr/86Sr
0.7078
0.7076
0.7074
0.7072
0.7070
0.7068
0.7066
60
80
100
120
140
160
180
200
age

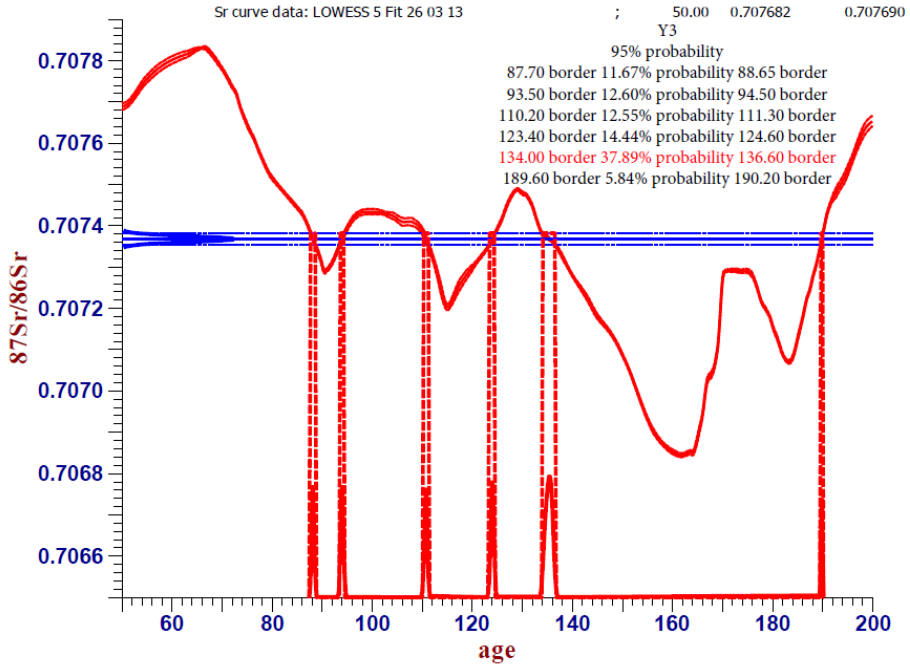
Sr curve data: LOWESS 5 Fit 26 03 13 ; 50.00 0.707682 0.707690
Y3
95% probability
87.70 border 11.67% probability 88.65 border
93.50 border 12.60% probability 94.50 border
110.20 border 12.55% probability 111.30 border
123.40 border 14.44% probability 124.60 border
134.00 border 37.89% probability 136.60 border
189.60 border 5.84% probability 190.20 border
87Sr/86Sr
0.7078
0.7076
0.7074
0.7072
0.7070
0.7068
0.7066
60
80
100
120
140
160
180
200
age

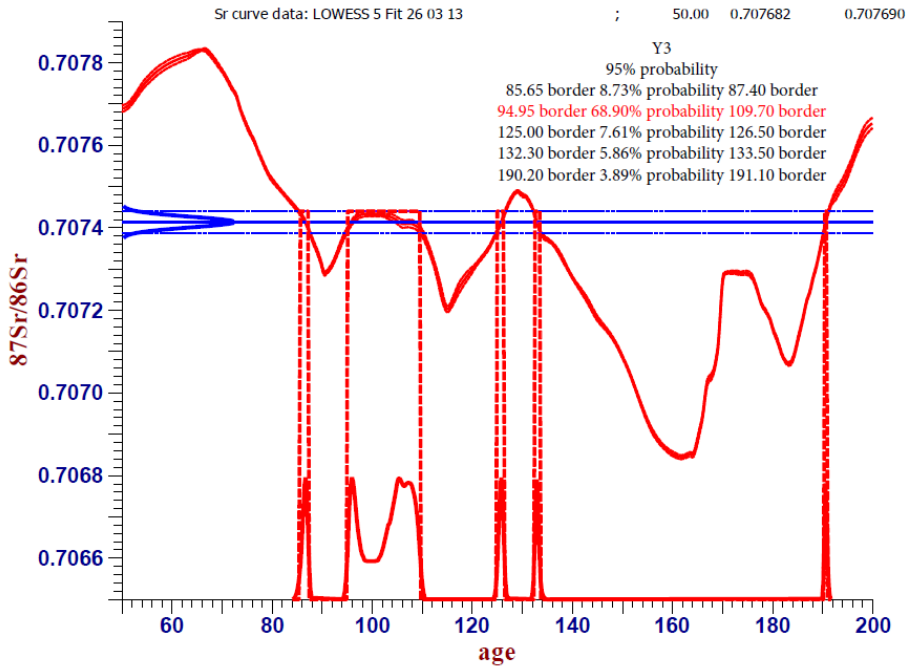
Sr curve data: LOWESS 5 Fit 26 03 13 ; 50.00 0.707682 0.707690
Y3
95% probability
85.65 border 8.73% probability 87.40 border
94.95 border 68.90% probability 109.70 border
125.00 border 7.61% probability 126.50 border
132.30 border 5.86% probability 133.50 border
190.20 border 3.89% probability 191.10 border
87Sr/86Sr
0.7078
0.7076
0.7074
0.7072
0.7070
0.7068
0.7066
60
80
100
120
140
160
180
200
age

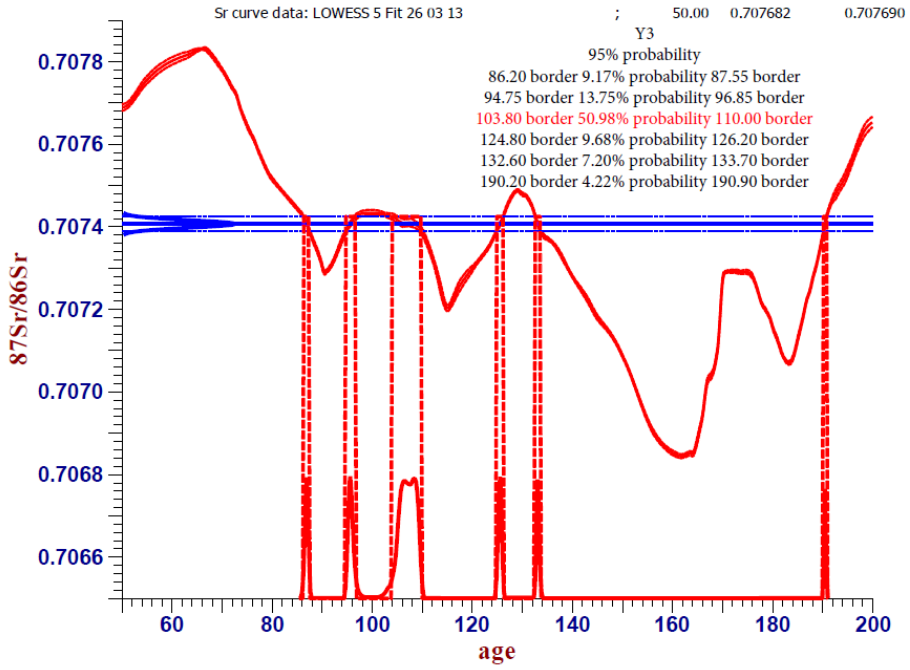
Sr curve data: LOWESS 5 Fit 26 03 13 ; 50.00 0.707682 0.707690
Y3
95% probability
86.20 border 9.17% probability 87.55 border
94.75 border 13.75% probability 96.85 border
103.80 border 50.98% probability 110.00 border
124.80 border 9.68% probability 126.20 border
132.60 border 7.20% probability 133.70 border
190.20 border 4.22% probability 190.90 border
87Sr/86Sr
0.7078
0.7076
0.7074
0.7072
0.7070
0.7068
0.7066
60
80
100
120
140
160
180
200
age

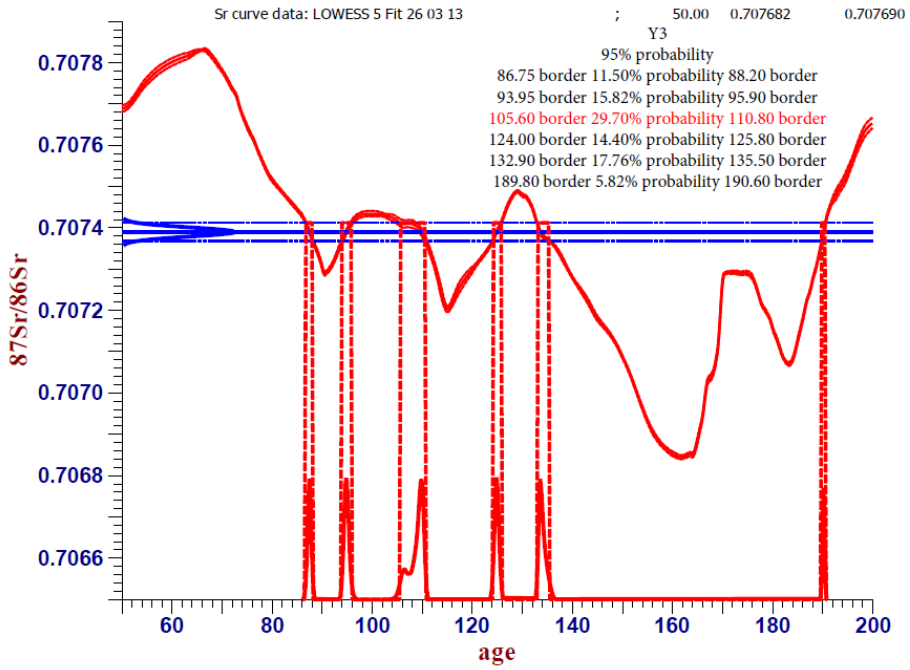
Sr curve data: LOWESS 5 Fit 26 03 13 ; 50.00 0.707682 0.707690
Y3
95% probability
86.75 border 11.50% probability 88.20 border
93.95 border 15.82% probability 95.90 border
105.60 border 29.70% probability 110.80 border
124.00 border 14.40% probability 125.80 border
132.90 border 17.76% probability 135.50 border
189.80 border 5.82% probability 190.60 border
87Sr/86Sr
0.7078
0.7076
0.7074
0.7072
0.7070
0.7068
0.7066
60
80
100
120
140
160
180
200
age

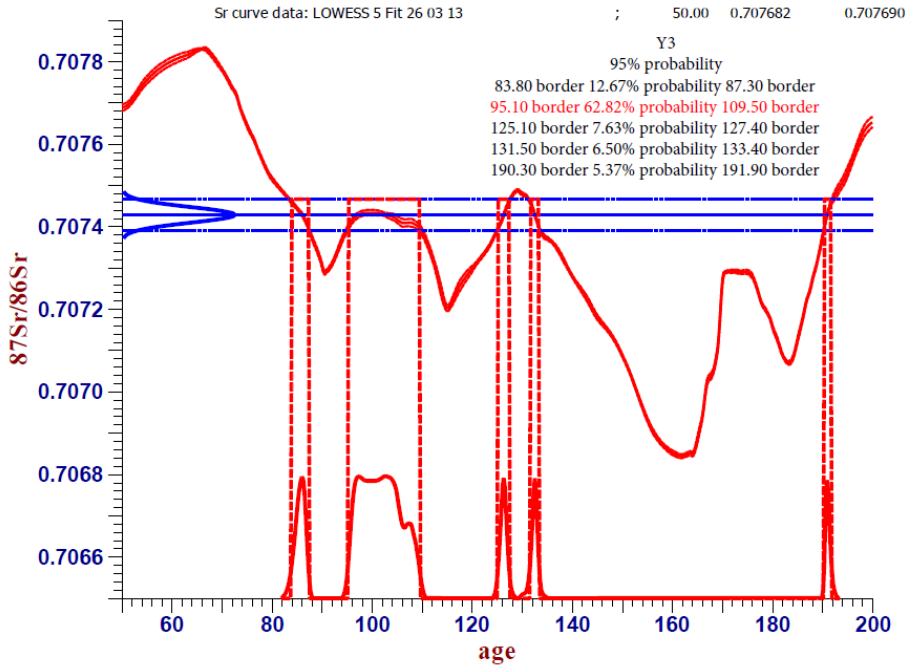
Sr curve data: LOWESS 5 Fit 26 03 13 ; 50.00 0.707682 0.707690
Y3
95% probability
83.80 border 12.67% probability 87.30 border
95.10 border 62.82% probability 109.50 border
125.10 border 7.63% probability 127.40 border
131.50 border 6.50% probability 133.40 border
190.30 border 5.37% probability 191.90 border
87Sr/86Sr
0.7078
0.7076
0.7074
0.7072
0.7070
0.7068
0.7066
60
80
100
120
140
160
180
200
age

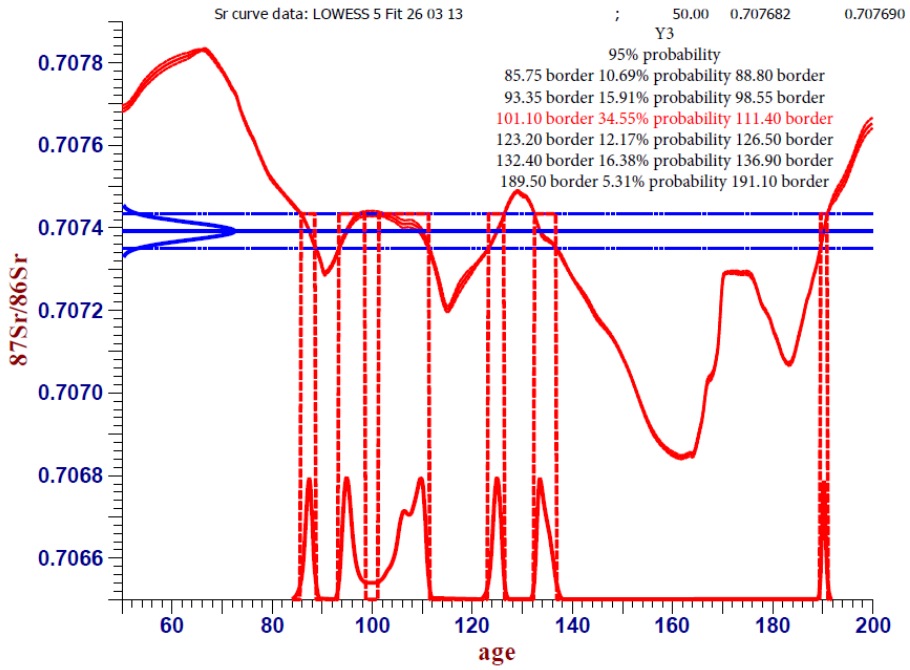
Sr curve data: LOWESS 5 Fit 26 03 13 ; 50.00 0.707682 0.707690
Y3
95% probability
85.75 border 10.69% probability 88.80 border
93.35 border 15.91% probability 98.55 border
101.10 border 34.55% probability 111.40 border
123.20 border 12.17% probability 126.50 border
132.40 border 16.38% probability 136.90 border
189.50 border 5.31% probability 191.10 border
87Sr/86Sr
0.7078
0.7076
0.7074
0.7072
0.7070
0.7068
0.7066
60
80
100
120
140
160
180
200
age

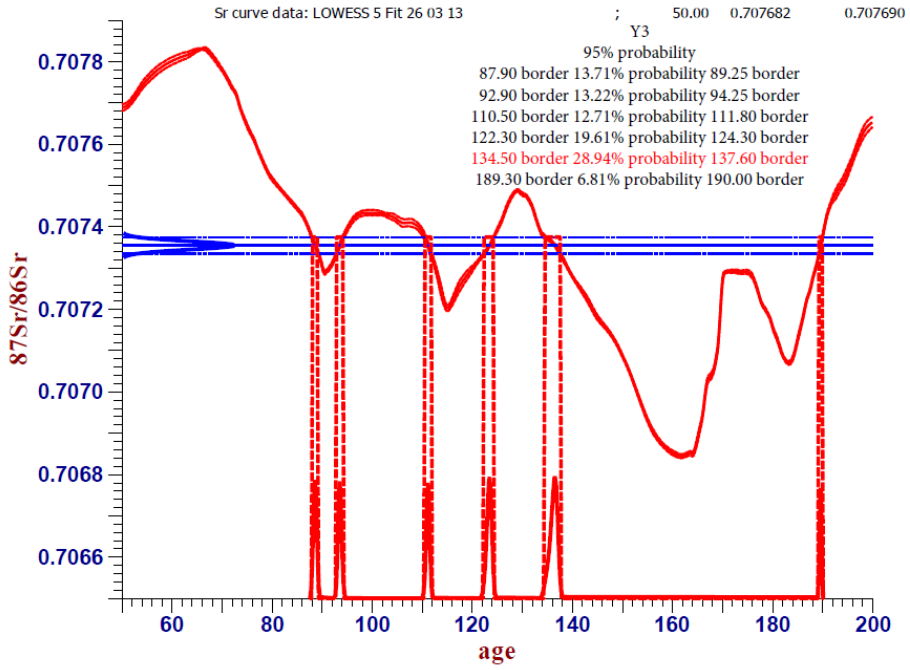
Sr curve data: LOWESS 5 Fit 26 03 13 ; 50.00 0.707682 0.707690
Y3
95% probability
87.90 border 13.71% probability 89.25 border
92.90 border 13.22% probability 94.25 border
110.50 border 12.71% probability 111.80 border
122.30 border 19.61% probability 124.30 border
134.50 border 28.94% probability 137.60 border
189.30 border 6.81% probability 190.00 border
87Sr/86Sr
0.7078
0.7076
0.7074
0.7072
0.7070
0.7068
0.7066
60
80
100
120
140
160
180
200
age

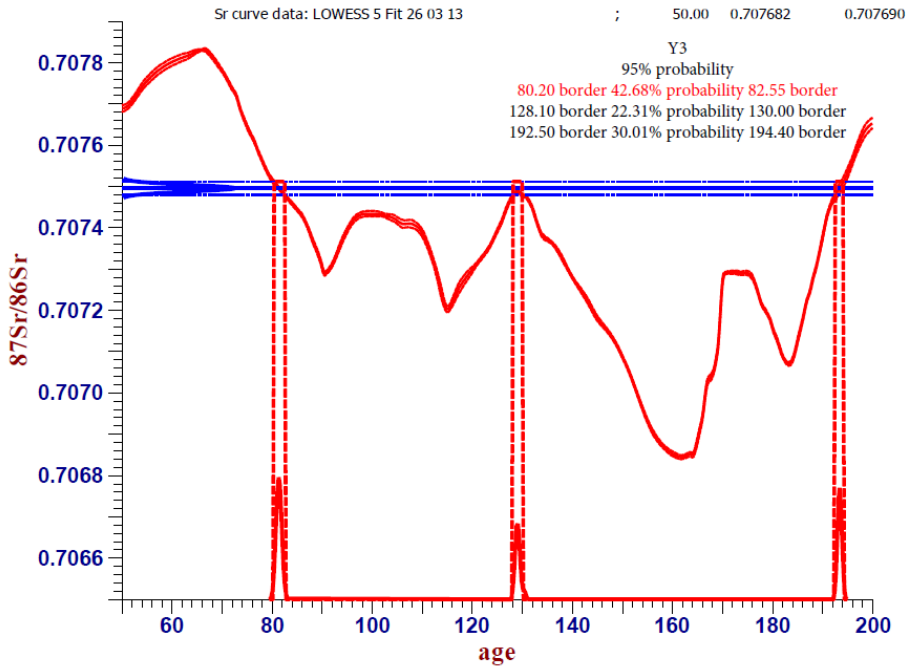
Sr curve data: LOWESS 5 Fit 26 03 13 ; 50.00 0.707682 0.707690
Y3
95% probability
80.20 border 42.68% probability 82.55 border
128.10 border 22.31% probability 130.00 border
192.50 border 30.01% probability 194.40 border
87Sr/86Sr
0.7078
0.7076
0.7074
0.7072
0.7070
0.7068
0.7066
60
80
100
120
140
160
180
200
age

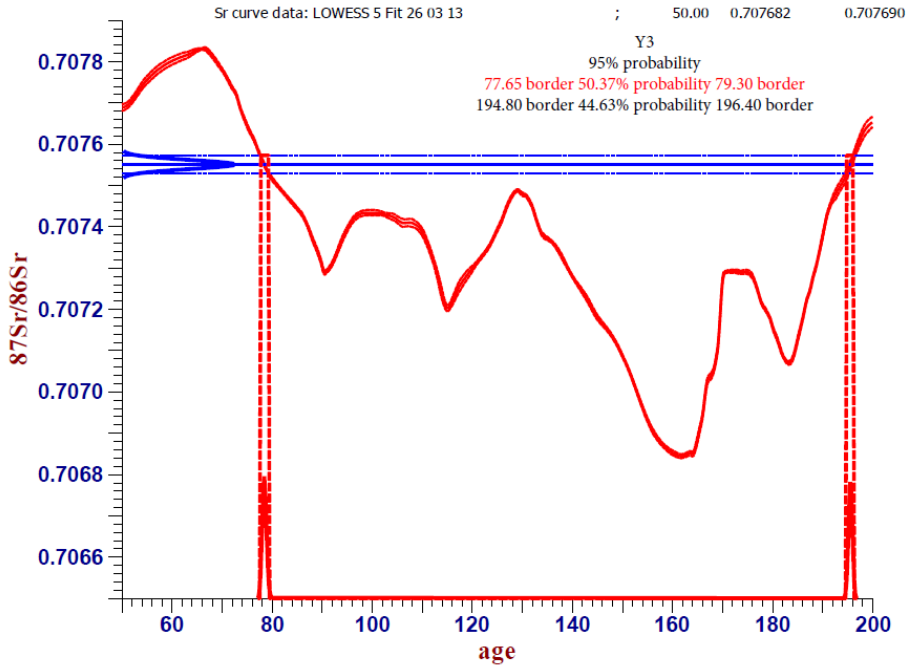
Sr curve data: LOWESS 5 Fit 26 03 13 ; 50.00 0.707682 0.707690
Y3
95% probability
77.65 border 50.37% probability 79.30 border
194.80 border 44.63% probability 196.40 border
87Sr/86Sr
0.7078
0.7076
0.7074
0.7072
0.7070
0.7068
0.7066
60
80
100
120
140
160
180
200
age

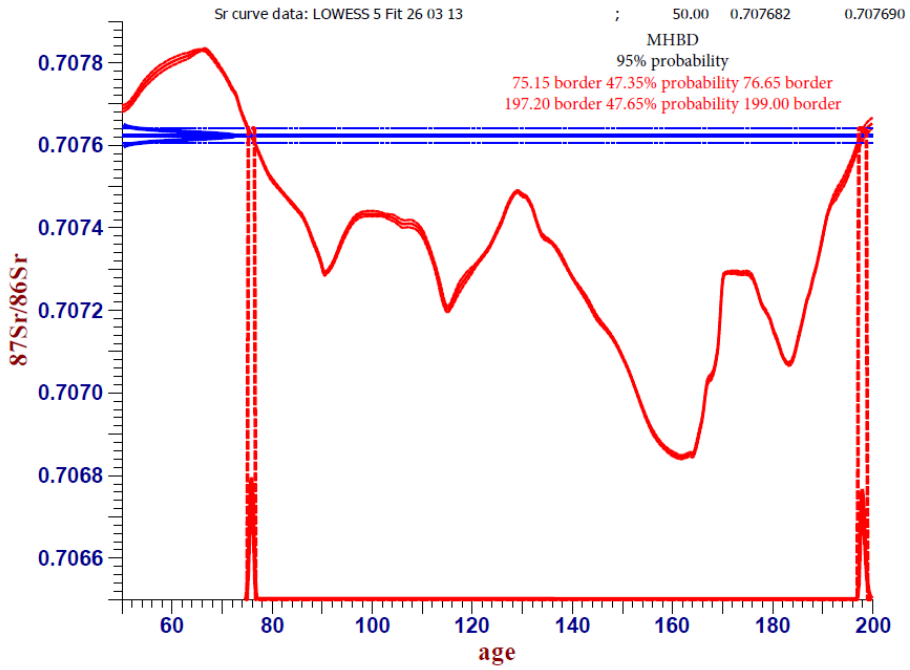
Sr curve data: LOWESS 5 Fit 26 03 13 ; 50.00 0.707682 0.707690
MHBD
95% probability
75.15 border 47.35% probability 76.65 border
197.20 border 47.65% probability 199.00 border
87Sr/86Sr
0.7078
0.7076
0.7074
0.7072
0.7070
0.7068
0.7066
60
80
100
120
140
160
180
200
age

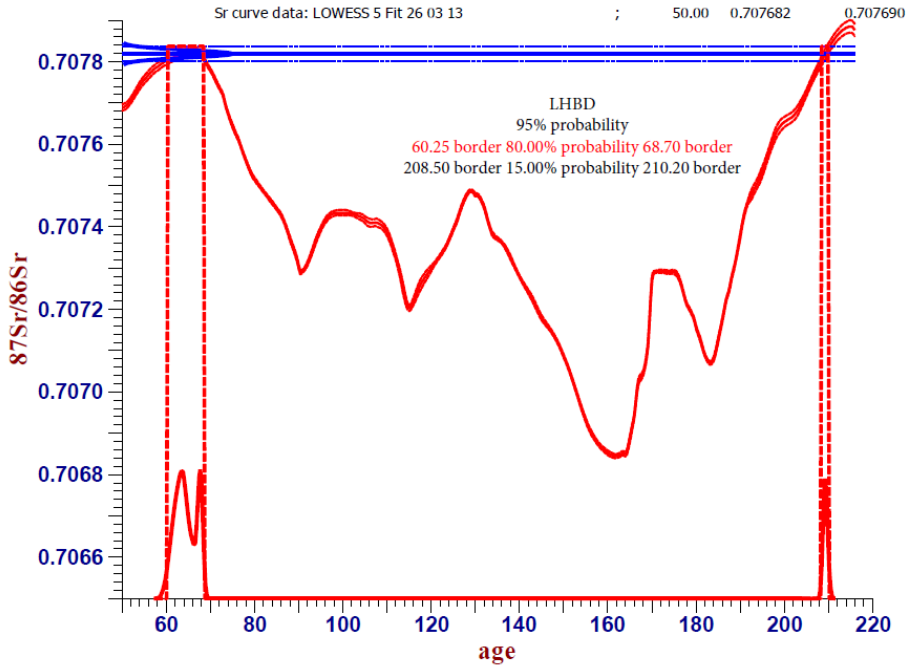
Sr curve data: LOWESS 5 Fit 26 03 13 ; 50.00 0.707682 0.707690
LHBD
95% probability
60.25 border 80.00% probability 68.70 border
208.50 border 15.00% probability 210.20 border
87Sr/86Sr
0.7078
0.7076
0.7074
0.7072
0.7070
0.7068
0.7066
60
80
100
120
140
160
180
200
220
age

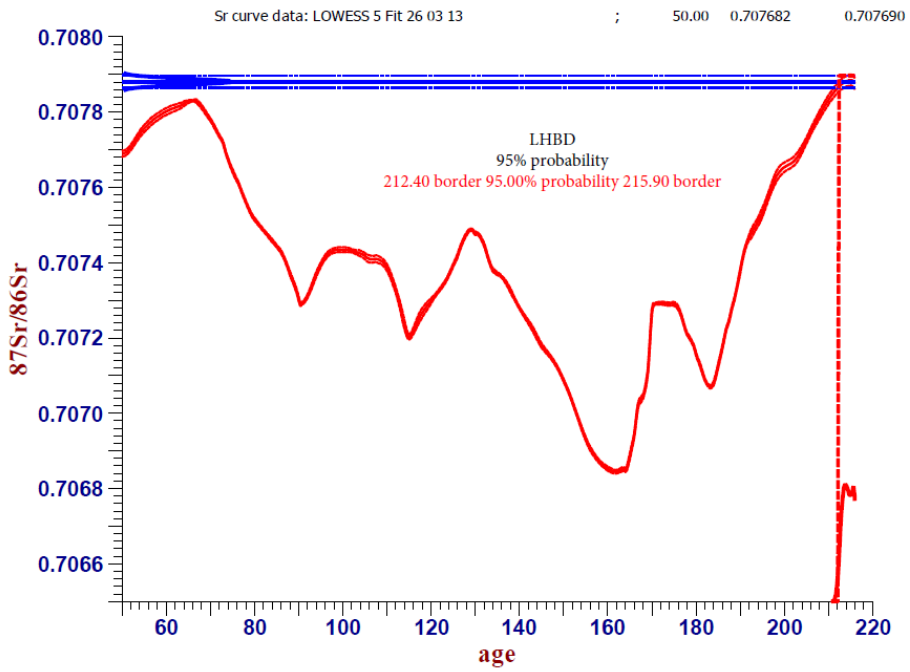
Sr curve data: LOWESS 5 Fit 26 03 13 ; 50.00 0.707682 0.707690
LHBD
95% probability
212.40 border 95.00% probability 215.90 border
87Sr/86Sr
0.7080
0.7078
0.7076
0.7074
0.7072
0.7070
0.7068
0.7066
60
80
100
120
140
160
180
200
220
age